

Aus dem Institut für Schlaganfall und Demenzforschung
der Ludwig-Maximilians-Universität München
Direktorin: Prof. Dr. Martin Dichgans

The role of blood components in microcirculatory dysfunction after subarachnoid hemorrhage

Dissertation
zum Erwerb des Doktorgrades der Medizin
an der Medizinischen Fakultät der
Ludwig-Maximilians-Universität zu München

vorgelegt von

Hanhan Liu
aus
Changsha, Hunan, P.R.China

2018

Mit Genehmigung der Medizinischen Fakultät
der Universität München

Berichterstatter: Prof.Dr. Nikolaus Plesnila

Mitberichterstatter: Prof.Dr. Stefan Zausinger
Prof.Dr. Hans-Walter Pflister
PD Dr. Rupert Egensperger

Mitbetreuung durch die
promovierten Mitarbeiterin: Kathrin Nehr Korn, Ph.D.

Dekan: Prof. Dr. Reinhard Hickel

Tag der mündlichen Prüfung: 20.12.2018

Contents

1.	Introduction	3
1.1	Clinical features.....	3
1.1.1	Epidemiology.....	3
1.1.2	Etiology.....	4
1.1.3	Symptoms.....	5
1.1.4	Complications	6
1.1.5	Diagnosis	6
1.1.6	Therapy	8
1.2	Animal models.....	11
1.3	Pathophysiology	12
1.3.1	Early brain injury	12
1.3.2	Inflammation	15
1.3.3	Delayed cerebral ischemia	17
1.3.4	Dysfunction of the cerebral microcirculation	18
1.3.5	Microthrombosis	19
1.3.6	Mircovasospasm	20
1.3.7	Hemolysis	21
2.	Methods and Materials	26
2.1	Materials	26
2.1.1	Equipment	26
2.1.2	Software	27
2.1.3	Consumables	27
2.1.4	Chemicals	29
2.1.5	Antibodies	30
2.1.6	Buffers and solutions	30
2.2	Methods	32
2.2.1	Randomization and blinding.....	32
2.2.2	Animals.....	32
2.2.3	Filament perforation SAH model	32
2.2.4	Cisterna magna injection (CMI) model	35
2.2.5	Two-photon microscopy	37

2.2.6	Tissue harvesting	38
2.2.7	Experimental protocols	39
2.2.8	Quantification of two photon microscopy images	45
3.	Results	47
3.1	Clazosentan experiment	47
3.1.1	Physiological monitoring.....	47
3.1.2	Microvasospasms of the pial arterioles during imaging	50
3.2	Cisterna magna injection	51
3.2.1	Establishment of CMI model	51
3.2.2	Comparison between CMI and perforation model.....	55
3.3	Deferoxamine experiment.....	58
3.3.1	Physiological monitoring.....	58
3.3.2	Vessel quantification and hemodynamic changes.....	60
3.3.3	Characteristic of blood distribution and investigation of erythrocytes and leukocytes after SAH	62
4.	Discussion	66
4.1	Comprehensive summary of the results.....	66
4.2	Clazosentan does not relieve microvasospasm in EBI after SAH.....	68
4.3	Distribution and characteristic of extravasated blood and non-perfused vessels in perforation SAH model.....	70
4.4	Cisterna magna injection model.....	72
4.5	Deferoxamine relieves microvasospasm in EBI after SAH	73
4.6	Conclusion.....	75
5.	References.....	76
6.	List of Abbreviations.....	90
7.	Acknowledgements.....	92
8.	Publication.....	93
9.	Curriculum Vitae	94

1. Introduction

1.1 Clinical features

1.1.1 Epidemiology

Subarachnoid hemorrhage (SAH), as the name implies, is a disease caused by the extravasation of blood into the subarachnoid space which is located between the arachnoid mater and the pia mater. SAH is a sub-type of stroke and accounts for about 4.4% -9.2%¹⁻³ of all strokes. Although the incidence of SAH varies from region to region, the worldwide incidence rate is about 10.5 cases per 100,000 person-years. SAH is a devastating neurosurgical emergency which has an in-hospital mortality ranging from 18% to 30%⁴⁻⁶. Although the diagnosis and treatment of SAH have improved in recent years, our understanding of the pathophysiological processes is still limited. Thus until now, no effective therapy is available to decrease the high mortality and disability rates. Since most patients need long-term medical rehabilitation after SAH, it is a substantial economic burden to health care systems. In Germany, the average overall direct cost for SAH treatment in the first year after the bleeding is 39,075 € per patient⁷. Considering the fact that SAH affects mainly working individuals (median age 55) and at least 20% of survivors are unable to regain functional independence^{8,9}, the indirect socioeconomic burden of SAH makes up a great impact on national economics. An incidence-based study in the US in 1992 estimated that the one-year productivity loss due to aneurysmal subarachnoid hemorrhage is about 1,550 billion\$ (in 2018 US dollars)¹⁰.

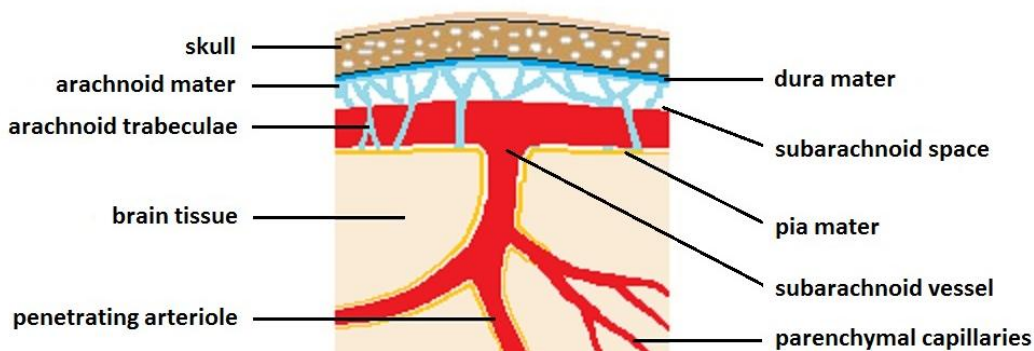


Figure 1

1.1.2 Etiology

The cause of SAH varies. It can be caused by brain trauma, cerebral vascular malformation, intracranial surgery, central nervous system tumors, pituitary apoplexy, cerebral amyloid angiopathy and else¹¹⁻¹⁵. Among non-traumatic SAH, about 85%¹⁶ of all bleedings are caused by a spontaneous rupture of an intracranial aneurysm. An aneurysm is an expansion or bulging in the arterial wall due to a weakening of the vessel wall. The incidence of intracranial aneurysm in the general population is about 3.2%¹⁷. Intracranial aneurysms occur more frequently at vessel bifurcations such as the circle of Willis¹⁸. Intracranial blood vessels have a thick internal elastic lamina but little elastin fibers and smooth muscle cells, which make them prone to develop aneurysms. The specific pathophysiological mechanism of aneurysm formation is unclear. It has been suggested that the formation of intracranial aneurysms depends on the degree of vessel wall inflammation, collagen and/or elastin construction and hemodynamic stress due to cardiovascular risk factors^{19 20}.

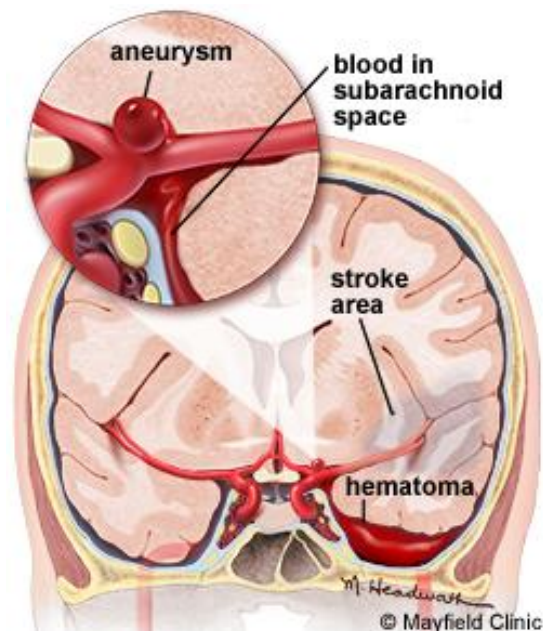


Figure 2

About 20% of aneurysmal SAH patients have a family history of aneurysm or SAH, but the exact genetic factors that cause the formation of intracranial aneurysms are still unclear²¹. Age, female sex and genetic factors are irreversible risk factors for SAH

whereas reversible risk factors include cigarette smoking, hypertension, cocaine use, and heavy alcohol abuse²².

1.1.3 Symptoms

Approximately 10%-43% of aneurysmal SAH patients experience sentinel headache, which is possibly caused by enlarging aneurysms or minor bleedings preceding the large bleeding. It may occur one to three weeks before the rupture of an aneurysm²³²⁴. 50% of patients with aneurysmal SAH have instantaneous serious headache, often being described as the worst headache in life. Most patients experience nausea (91%), vomiting (70%) and physical exertion (50%) together with the onset of headache.²⁵ Headache after SAH is thought to be caused by increased intracranial pressure (ICP), local distention and stretching of intracranial vessel or irritation of adjacent sensory nerves by subarachnoid blood (meningeal irritation)²⁶. 35% of patients have neck stiffness several hours after the bleeding due to an inflammatory response to blood in the subarachnoid space²⁷.

Impaired consciousness or complete unconsciousness affects around 34%-67% of SAH patients. Half of patients experience neurological abnormalities such as a change of the mental state or focal neurological deficits which may indicate the location of the ruptured aneurysm. For example, a third cranial nerve palsy can be a sign for the rupture of a posterior communicating artery aneurysm²⁷²⁸. Seizures occur in 10%-26% of patients during or shortly after SAH and are a risk factor for late seizures and related with poor outcome²⁹³⁰.

3% of patients complain about blurred vision or floating shadows due to vitreous hemorrhage (Terson's syndrome)³¹. The generally accepted mechanism is that a sudden increase of ICP after SAH induces swelling of the optic disc and occludes the retinal venous system, thereby leading to intraocular hemorrhage³². Intraocular hemorrhage is often found in patients with impaired consciousness³¹.

Systemic symptoms like chest pain, palpitation and dyspnea can be symptoms of severe hypertension or hypoxemia. Electrocardiographic changes can be found in 75%

of SAH patients without a previously diagnosed heart disease³³. About 0.7% of patients without previous hypertension had cardiac arrest at onset of SAH, but half of the survivors regain self-care ability³⁴.

1.1.4 Complications

Rebleeding is an acute and serious complication with an incidence of 8%-23% during the first 72 hours, with most of them happening within the first 6 hours after the initial bleeding. Rebleedings are associated with a poor prognosis: 20%-60% of patients with rebleedings die³⁵. The clinical manifestation of a rebleeding is the exacerbation or reappearance of previous symptoms such as sudden severe headache, nausea and vomiting, disturbance of consciousness and convulsions.

Within the first three days, about 30% of SAH patients develop an acute obstructive hydrocephalus due to the formation of a blood clot in the cerebrospinal fluid circulation²⁷. Patients who develop a gradual reduction of consciousness or a sudden neurological decline should be examined for hydrocephalus. The clinical presentation of a hydrocephalus starts with the reduction of consciousness and eye symptoms such as downward deviation and/or small and unreactive pupils. In serious cases, patient can develop severe headache, nausea and coma³⁶.

Delayed cerebral ischemia (DCI) is defined as newly appearing cerebral ischemia or an infarction several days after SAH, which cannot be attributed to other identified causes. Approximately 30% of SAH patients will develop DCI three to 14 days after the onset of aneurysmal rupture³⁷. DCI is more likely to happen in patients who have a large amount of arterial bleeding and/or long duration of initial unconsciousness³⁸³⁹. Symptoms of DCI are focal neurological deficit like hemiparesis, aphasia and decreased consciousness that can progress due to infarction. It is related with poor clinical outcome for SAH patients⁴⁰.

1.1.5 Diagnosis

Patients who have a classic clinical presentation of SAH with sudden severe headache, vomiting and meningeal irritation should be considered to suffer from subarachnoid

hemorrhage. Subarachnoid hemorrhage can be confirmed when extravasated blood is found in the subarachnoid space on computed tomography (CT) scan⁴¹. Various studies show that the sensitivity of a non-contrast head CT with at least third-generation scanners in the hands of an experienced radiologist can reach almost 100% within 6 hours of headache onset⁴². The sensitivity drops to 95% after 6 hours and less than 90% after 24 hours⁴³. Apart from the quality of the CT and the radiologist, patients who have only small amounts of extravasated blood or a hematocrit below 30% can have a negative CT scan. Another diagnostic approach is to examine the cerebrospinal fluid for the hemoglobin breakdown product bilirubin six to twelve hours after onset of headache⁴¹. It is absolutely necessary to perform a lumbar puncture in every patient who presents with sudden headache and has a negative CT scan²⁷.

Compared to CT imaging, magnetic resonance imaging (MRI) is similarly sensitive, but not the first choice in the acute phase after SAH, because CT imaging is faster and more cost-efficient. Since the blood signal intensity on CT scan decreases with time, MRI is more sensitive for detecting blood between four and 14 days after the initial bleeding⁴⁴.

CT angiography is very sensitive for the detection of aneurysm larger than three to four mm⁴⁵. It is recommended by the American Heart Association for suspected SAH patients with non-diagnostic non-contrast head CT scan⁴⁶. With angiography, the number of aneurysm and the adjacent anatomical configuration can be detected, which helps doctors to make a better treatment decision. Meanwhile, patients who are unfit to undergo lumbar puncture can benefit from angiography⁴².

However, with obscure clinical features and/or improper examination method, 12% of SAH patients are misdiagnosed. Misdiagnosis is often associated with a high mortality and disability rate⁴⁷. The differential diagnoses for SAH are, e.g. hypertensive encephalopathy, meningitis, encephalitis, pituitary apoplexy, mass lesion and else⁴².

1.1.6 Therapy

As soon as the diagnosis of SAH is confirmed, symptomatic treatment as well as etiologic treatment aiming at obliterating the aneurysm should be given.

For general management, patient should be placed in an elevated-head bed for better cerebrospinal fluid (CSF) drainage. Continuous observation of vital signs, electrocardiographic changes and neurological symptoms are necessary. If patients have difficulty in eating, regular food intake can be guaranteed by using a nasogastric tube. Establishment of a continuous intravenous access is mandatory. Blood electrolyte imbalance and hypo- or hyperglycemia should be corrected, but infusion of large amount of hypotonic fluids is not recommended. Analgesia is often needed to comfort the patient⁴². The common agreement for treatment of hypertension is that blood pressure should be controlled until the ruptured aneurysm is obliterated⁴⁶.

Patients who have a large hematoma might need extensive hemi-craniectomy to allow expansion of the brain⁴⁸. Subdural hematomas should be removed when they are life-threatening⁴⁹.

Before the final diagnosis of SAH, short-term antifibrinolytics can be given to prevent rebleeding. According to a prospective randomized study, immediate administration of tranexamic acid can also reduce early rebleeding in SAH patients⁵⁰. As soon as a ruptured aneurysm is confirmed by angiography, experienced specialists' opinion should be considered in choosing surgical clipping or endovascular coiling to obliterate the aneurysm⁴⁶. Patient who received endovascular coiling need follow-up cerebrovascular imaging since a compaction of the coil or a recanalization of the aneurysm may occur after surgery.

Hydrocephalus is more common in patients with massive hemorrhage in the perimesencephalic cisterns or with intraventricular blood. After the initial CT scan, persistent observation of drowsy patients with dilated ventricles is important since spontaneous recovery may happen in up to 50% of patients²⁷. If patients develop a symptomatic hydrocephalus, external ventricular drainage is achieved by putting a

drainage catheter through a burr hole. Patients with drainage have a risk of developing ventriculitis, especially if the catheter remains in place over three days⁵¹. In any case a strict protocol for handling the drain is necessary. Lumbar drainage may also be considered in patients who have a low risk of cerebral herniation⁴⁶. About 26% of SAH patients develop a chronic hydrocephalus and need ventricular shunting surgery⁵².

Though management of seizures after SAH is disputed, immediate prophylactic anticonvulsant agents are usually used after SAH. Patients with preexisting convulsive conditions and those who suffered from cerebral infarction, intractable hypertension or intracerebral hematoma, long-term use of anticonvulsant agents are usually considered⁴⁶.

DCI with large artery vasospasm is a primary important contributor to death and disability in SAH patients. Thus, constant monitoring of cerebral hemodynamics by using transcranial Doppler sonography is inevitable. In addition, CT or MRI scans may be useful for identifying potential ischemic lesions⁴⁶. Clazosentan is an endothelin receptor antagonist that prevents endothelin1 (ET-1) mediated vasoconstriction. In three large randomized controlled trials called 'Clazosentan to Overcome Neurological ischemia and infarction studies' (CONSCIOUS), Clazosentan reduced angiographic vasospasm but failed to decrease mortality, morbidity and occurrence rate of cerebral infarction in SAH patients^{53 54}. On the contrary, the calcium-channel blocker Nimodipine has been shown to relieve arterial narrowing and protect the brain from ischemia in various clinical trials⁵⁵. Voltage-dependent calcium channels were shown to play a role in the formation of vasoconstriction after SAH. Activation of calcium channel leads to a constriction of small cerebral arteries with diameters range from 100 to 200 μm ⁵⁶. Nimodipine blocks calcium mediated vasoconstriction and is beneficial in relieving middle cerebral artery spasms⁵⁷, therefore restoring cerebral blood flow⁵⁸. Additionally, Nimodipine was reported to have neuroprotective effects after SAH in both animal models and in human patients^{55 59}. A meta-analysis based on 16 trials suggests that oral administration of 60 mg

Nimodipine every four hours is helpful for SAH patients⁵⁵, thus application of Nimodipine received the highest possible level of evidence (A) in the American Stroke Association in SAH guidelines⁴⁶. Maintenance of euvolemia with induction of hypertension was considered to be beneficial for maintaining cerebral perfusion pressure in patients with DCI⁴². A recent randomized clinical trial showed that induced hypertension in DCI patients may have serious adverse events⁶⁰. Patients with symptomatic cerebral vasospasm should therefore be treated with cerebral angioplasty and/or intra-arterial application of vasodilators⁴⁶.

Since the disability rate among SAH patients is high, long term rehabilitation is important to regain daily living ability and labor capacity. Physical, occupational as well as psychological therapy should be initiated after being discharged from hospital.

Over the past several decades, treatment for subarachnoid hemorrhage has been improved significantly mainly based on the early obliteration of aneurysms, improved intensive care management and the use of Nimodipine. Although there are several small non-randomized studies showed promising beneficial effects of Cilostazol, heparin, erythropoietin, eicosapentaenoic acid and methylprednisolone, there are no newly emerging therapeutic measures⁶¹ and the clinical outcome of SAH patients is still disappointing.

The failure of the CONSCIOUS trials suggests that the sole focus on treating delayed vasospasm might not be the right target. Actually, the intrinsic correlation between large arterial vasospasm and ischemic injury during DCI is somehow uncertain. Among all surviving SAH patients, only about 20-30% develop delayed ischemia accompanied with delayed vasospasm, while 21% of them suffer from delayed ischemia without the presence of delayed vasospasm⁶². On the contrary, early brain injury (EBI) is the leading cause of mortality after SAH^{63 64}. Moreover, for those who survived from EBI, pathological mechanisms triggered by the initial damage continue affecting the course and outcome of SAH⁶⁵⁻⁶⁷. Therefore within the past decade the focus of SAH research shifted towards EBI. However research regarding EBI after SAH

is still limited. Thus, more research on EBI after SAH is needed to understand the pathophysiology and to identify new therapeutic targets⁶⁸.

1.2 Animal models

There are various animal models being used in SAH research. In the intracisternal vein transection model, venous blood is released by cutting a vein at the skull base (cisterna pontis) that spills into the subarachnoid space⁶⁹. In the extracranial intracranial arterial blood shunting model, the common carotid artery, abdominal aorta or femoral artery are shunted to the prechiasmatic cistern through a connecting catheter⁷⁰. In the extravascular vessel and cerebral vessel puncture model, arterial blood spills into subarachnoid space by direct penetration with a needle through a burr hole⁷⁰.

Currently, the three mainly used animal models in SAH research are the direct intracisternal blood injection, endovascular puncture and clot placement. In the intracisternal blood injection model, single or double injection of autologous blood is performed⁷¹. Autologous arterial or venous blood is injected through a needle which is inserted into the prechiasmatic cistern, prepontine cistern, interpeduncular cistern, or most commonly cisterna magna. The injection volume ranges from 0.3 to 1.5 ml/kg or 1.0 to 5.0 ml for rabbits, 0.1 to 0.5 ml for rats⁷² and 40 to 90 μ l for mice⁷³. For the double blood injection model, the interval time between the first and the second injection is 24 or 48 hours⁷⁴. It mimics bleeding into subarachnoid space with a controllable blood volume and is fast, reproducible and easy to operate. Thus it was widely used for investigation of DCI and vasospasm in rats, rabbits and dogs⁷⁵. However, it does not reproduce the pathophysiology of the process of artery rupture which happens in the clinical situation.

Therefore an alternative approach for induction of SAH was developed in mice and rats: the endovascular puncture.⁷⁰ This model was first described by Bederson et al⁶⁴ and Veelken et al⁷⁶. A filament is inserted into external carotid artery and advanced up to the Circle of Willis in order to penetrate the arterial wall at the bifurcation site

of the middle cerebral artery. This imitation of the rupture of an aneurysm presents some of the most prominent clinical features that are also observed in SAH patients. The model exhibits rebleedings, a common complication after aneurysmal SAH³⁵, and microarterial constrictions which occur in the stage of EBI^{77 78}. Additionally, the adaptation to the mouse offers researchers the opportunity to use transgenic mice. Though microsurgery is relatively complicated to perform, using a standardized protocol set by Buhler et al.⁷⁹ including ICP and CBF monitoring this model can be performed in a highly reproducible manner. Therefore the endovascular perforation model became very popular for the investigation of EBI after SAH.

The craniotomy and clot placement SAH model is most commonly used in dogs and monkeys⁷⁰. Since researchers speculate that a large bleeding volume might increase the risk of delayed cerebral vasospasm, maximum-sized artery blood clots were placed on exposed arteries after frontotemporal craniectomy. Thereby delayed cerebral vasospasms as well as neurological deficits were observed 7 days after clot placement⁸⁰.

Since the failure of the clinical Clazosentan trials, the focus of SAH pathophysiological studies shifted from DCI to EBI. Thus, the rodent model of endovascular puncture became the most common experimental SAH model.

Though the endovascular puncture SAH model successfully replicates the natural course of SAH, by now there is no applicable animal model which could be used to study the pathogenesis of single factors after SAH. One aim of this thesis is therefore to develop a new animal model that allows researchers to study the effect of single or multiple pathogenic factors which influence the pathophysiological process after SAH.

1.3 Pathophysiology

1.3.1 Early brain injury

The notion that early brain injury (EBI) after SAH is the leading cause of mortality in SAH patients was first suggested by Adams et al. in 1981⁸¹. Later, Kusaka et al. defined EBI as an immediate injury to the entire brain after SAH⁸². However for

several decades, studies of delayed brain injury and delayed cerebral vasospasm attracted most of the attention in SAH research. Only when Clazosentan, an endothelin A (ET_A)-receptor antagonist which was shown to effectively decrease delayed vasospasm, did not improve clinical outcome after SAH, many researchers started to realize that the mechanism causing cerebral ischemia after SAH is multifactorial. It could well be that significant pathophysiological events independent of delayed vasospasm of large cerebral vessels occur soon after the bleeding and lead to secondary brain injury which result in poor clinical outcome⁸³.

1.3.1.1 Intracranial pressure

Within one minute after the rupture of an intracranial aneurysm, extravasated blood bursts into the subarachnoid space, thereby causing a sudden increase of intracranial pressure (ICP). It usually reaches a peak as high as the mean systemic blood pressure. In most cases, ICP falls to a lower but still elevated plateau within several minutes⁸⁴. In other cases e.g. when large hematomas form, severe brain edema or hydrocephalus develops and ICP remains high until these factors have been resolved⁸⁵. Rapid rise of ICP may also induce immediate herniation and direct damage to brain tissue. In clinical data, an elevated ICP (> 20 mmHg) is associated with re-bleedings and ischemic lesions within 72 hours and 7 days after SAH. An ICP value over 20 mmHg, however, shows a strong relationship with high mortality in patients⁸⁶.

1.3.1.2 Acute cerebral ischemia

An acute and sudden increase of ICP results in significant decrease of cerebral perfusion pressure (CPP)⁸⁷ and, hence, cerebral blood flow (CBF)⁶⁴, which may lead to global cerebral ischemia. In experimental SAH, a global decrease of CBF was shown in rats 15 and 90 minutes after SAH⁸⁸. In some cases CBF dropped to almost zero⁸⁹. However, ICP increase is not the only cause for decreased cerebral perfusion after SAH. There is experimental evidence showing that cerebral perfusion shows a secondary reduction after CPP normalized⁶⁴. These findings were later corroborated in SAH patients by Schubert et al.: twelve hours after the ictus, global cerebral ischemia still exist in SAH patients who are accompanied by only slight changes in ICP

and CPP. This prolonged hypoperfusion independent of ICP and CPP is speculated to be associated with microvasculatory vasospasm⁹⁰. Meanwhile, this initial impairment of cerebral perfusion correlates with the occurrence of DCI and clinical outcome in patients^{90 91}, and is believed to be the leading cause of morbidity in SAH patients⁹².

The initial CBF impairment activates a cascade of further pathophysiological events⁹³. Apoptosis caused by ischemia was found in endothelial cells, neurons and astrocytes after SAH^{83 93 94}. Blood oxygen content decreases to about 60% immediately after SAH⁸⁸. Hypoxia disturbs metabolic and ionic hemostasis, initiates inflammatory pathways and cerebral edema⁹⁵. Microvasospasm in small superficial arteries and arterioles and decreased capillary density were found in patients three days after SAH⁷⁷. Animal research also showed significant correlation of microvasospasm with decreased cerebral perfusion⁷⁸. However, the mechanism behind formation of microvasospasm is not well understood.

As one of the initial key factors occurring right after the rupture of an aneurysm is intracranial hypertension. The subsequent reduction in CBF may not only result in acute cerebral ischemia, but has also a far reaching influence on microcirculatory dysfunction afterwards^{96 97}. Meanwhile, subarachnoid blood and its components may also play a crucial role in post-hemorrhagic cerebral ischemia. Currently, the mechanistic studies of ischemia after SAH were mostly performed with the blood injection model or perforation model with inconsistent experimental protocols. Despite the question to what extent these models resemble human SAH, the concurrently occurring mixture of different pathogenetic factors, such as increased ICP and blood accumulation, make it difficult to investigate the pathophysiological contribution of single factors in detail. Therefore we hypothesized that it is necessary to establish an animal model with blood accumulation similar to what is observed after MCA perforation but without ICP related hemodynamic changes. With such a model, it should be possible to look into the pathophysiological processes caused by single blood components or its lysates.

1.3.2 Inflammation

Brain tissue damage secondary to global cerebral ischemia immediately activates inflammatory reactions. At the same time also blood coagulation and hemolysis products in the subarachnoid space initiate and exacerbate the inflammatory response. Inflammatory mediators such as intercellular adhesion molecule-1 (ICAM-1), vascular cell adhesion molecule-1, monocyte chemoattractant protein-1 and E-selectin are elevated in the CSF of patients after SAH⁹⁸⁻¹⁰⁰. As inflammatory cascades are being activated right after ictus, early inflammation has been speculated to play an important role in the pathophysiological process after SAH. Clinical studies show a correlation between increased inflammatory markers such as C-reactive protein (CRP) or Interleukin-6 (IL-6) and a poor clinical outcome of SAH patients^{101 102}.

There are several different inflammatory pathways involved in the inflammatory cascades after SAH. The mitogen-activated protein kinase (MAPK) pathway was found to aggravate blood brain barrier (BBB) breakdown and neuronal apoptosis through the downstream effector Matrix metalloproteinase 9 (MMP-9) in EBI after experimental SAH^{103 104}. Also myeloid differentiation factor-dependent pathways were demonstrated to be involved in neuroinflammation during EBI¹⁰⁵. Furthermore, the nuclear factor 'kappa-light-chain-enhancer' of activated B-cells (NF-κB) signaling pathway also plays a crucial role in EBI¹⁰⁶. Animal experiments aiming at suppressing these two pathways showed reliable neuroprotective effects and reduction of inflammation in different studies¹⁰⁷⁻¹⁰⁹. Cell surface receptors were also engaged in the exacerbation of the inflammatory response after SAH. Toll-like receptor 4 (TLR-4) was reported to be an independent predictor for poor neurological outcome in SAH patients¹¹⁰. A small scale phase II randomized controlled clinical trial with 136 patients showed that an Interleukin-1 receptor antagonist, IL-1RA effectively reduced peripheral inflammation after SAH. However further investigation on clinical outcome are needed¹¹¹.

Significant up-regulation of endothelial adhesion molecules after SAH, e.g. ICAM-1, induce cellular interaction between circulating leukocytes and the cerebral

endothelium, a process speculated to be involved in the development of chronic vasospasm^{112 113}. A recent study showed that an increased number of activated NK cells in CSF of SAH patients was associated with an increased risk of cerebral vasospasm and DCI¹¹⁴. Additionally an in vivo experiment showed rolling and adhering leukocytes in the cerebral capillaries 60 minutes after SAH. These leukocytes decrease blood flow velocity and even plug vessels, thereby aggravating microcirculatory dysfunction after SAH¹¹⁵.

Among all factors involved in the inflammatory response in the brain, microglia play a pivotal role¹¹⁶⁻¹¹⁸. Microglia are macrophage like cells which act as the first and main cellular immune defense mechanism in the central nervous system¹¹⁹. Usually, microglia rest in the brain and survey their surroundings for damage or potential threat. Once triggered by danger signals, resting microglia transform into an activated state. Activated microglia are classified into two categories: M1 microglia are considered to be the pro-inflammatory and release pro-inflammatory mediators such as interleukin (IL)-1 β , IL-12, Tumor necrosis factor alpha and nitric oxide. M2 microglia are considered to be anti-inflammatory and to be involved in tissue remodeling and repair¹²⁰. In experimental SAH, microglia were shown to be involved in the induction of vasospasm in both the early and late phases¹²¹, causing delayed brain injury¹¹⁸ and contributing to neuronal cell death¹²². Promoting the polarization of microglia towards M2 phenotype by using erythropoietin could reduce neuronal necrosis and brain edema in EBI¹¹⁶. Thus, a modulation of intracranial immune cells could be a new target for relieving cortical inflammation after SAH.

Although inflammatory reactions are considered to be essential for the pathophysiology of SAH, anti-inflammatory treatments with immune-modulating drugs such as nafamostat mesylate or cyclosporin A showed little success in clinical trials^{123 124}. The only exception was a trial on methylprednisolone which improved functional outcome in patients but did not reduce the incidence of symptomatic vasospasm¹²⁵.

Since neuro-inflammation seems to be a complicated process including various players, more experimental as well as clinical studies are needed to shed more light onto this process in order to identify new therapeutic strategies.

1.3.3 Delayed cerebral ischemia

The first report about cerebral arterial constriction in SAH patients was in 1951¹²⁶. By using arteriogram, arterial spasms were found in SAH patients in the later phase after SAH (23 days or earlier). Because of a strong association between delayed vasospasm and cerebral infarction, it was believed for decades that vasospasms, which occur in 40% to 60% of patients between 3 to 14 days after SAH, are the single cause of DCI and poor outcome^{127 128}. Various basic and clinical researchers focused on finding strategies which targeted delayed vasospasm. Endothelin (ET), by far the most powerful vasoconstrictor, was regarded as a key mediator for delayed vasospasm after SAH^{129 130}.

1.3.3.1 Endothelin receptors

Endothelin (ET) is the most potent and persistent vasoconstrictor in the human cardiovascular system. As its name implies, it is primarily produced by endothelial cells. There are three different isoforms of endothelin: ET-1, ET-2, ET-3 with a similar protein structure but distinct biological activities¹³¹. ET-1 is the strongest vasoconstrictor and also the most abundant isoform among them¹³². ET-1 was reported to be secreted by endothelial cells and vascular smooth muscle cells when superfused with oxyhemoglobin and cause arterial narrowing¹³³. Clinical and experimental data suggest that after SAH, myofilaments in vascular smooth muscle cells become more sensitive to ET-1, which then leads to the development of cerebral vasospasm^{134 135}. Other studies show that ET-1 concentration in the CSF was elevated in SAH patients¹³⁶ and that it was released by monocytes isolated from CSF¹³⁷. Nevertheless, there is conflicting data about the up-regulation of ET-1 in plasma or CSF of SAH patients^{137 138}.

ET-1 plays an essential role in the regulation of cardiovascular function through binding two G-protein coupled receptors, ET_A and ET_B. ET_A receptors are

predominantly expressed in vascular smooth muscle cells and are responsible for vascular activity and function, especially vasoconstriction¹³⁹. ET_B receptors internalize ET-1¹⁴⁰ and facilitate the generation of the vasodilator nitric oxide (NO)¹⁴¹. ET_A receptors have a higher affinity to ET-1 and conducts ET-1 mediated vasoconstriction¹⁴². As more and more studies reported an elevated level of ET-1 after SAH, ET_A receptor antagonists emerged as a promising methods for the treatment of cerebral vasospasm after SAH¹⁴³.

Clazosentan is an ET_A receptor antagonist specifically designed for parenteral application in patients with SAH¹⁴⁴. It was shown to alleviate angiographic vasospasm and prevent CBF reduction in animal SAH experiments^{145 146}. However, Clazosentan failed to improve functional outcome and survival rate in clinical trials, despite an alleviation of delayed cerebral vasospasm^{53 54}. In contrast it was associated with worse clinical outcomes because it was causing side effects like pulmonary edema, hypotension and anemia^{147 148}. The failure of the Clazosentan trials revealed that DCI is actually a multifactorial pathophysiological process: beside vasospasm, neuroinflammation, microthrombosis, cortical spreading depolarization and EBI are also involved in the pathogenesis of DCI^{143 149 150}. The failure of the Clazosentan clinical trials also indicated that poor outcome is caused by mechanisms other than large artery spasms. This moved the whole SAH research community into a new era of re-understanding and re-exploring the relevant mechanisms responsible for delayed cerebral ischemia.

1.3.4 Dysfunction of the cerebral microcirculation

Microcirculatory dysfunction after experimental SAH was first reported by Herz et al. in the early 1970ies. After topical application of blood onto pial vessels Herz and coworkers observed vasoconstriction and disturbed blood flow in cerebral pial vessels of guinea pigs¹⁵¹. In various SAH animal experiments, microcirculatory changes including altered vasoreactivity, increased inflammation, BBB disruption, microvasospasm, increased microthrombosis, and pathological inversion of neurovascular coupling were also reported^{78 82 152-155}. The mechanisms underlying

microcirculatory dysfunction are complex and still remain to be explored. One aim of this thesis was to study the mechanisms behind microvasospasm and identify new therapeutic targets to relieve posthemorrhagic ischemia in EBI after SAH.

1.3.5 Microthrombosis

Clinical studies show a correlation between the activation of the coagulation cascade and the development of DCI^{156 157}. Patients who died from DCI have more microthrombi in the infarcted brain regions¹⁵⁸. Thus microthrombosis is regarded as one of the key mechanisms for the development of DCI¹⁴⁹. It also contributes to the microcirculatory failure in EBI⁷⁸.

Cerebral microthrombi usually consist of aggregated platelets and fibrin and are sometimes mixed with leukocytes¹⁵⁸. After SAH, decreased cerebral blood flow velocity can increase blood viscosity and thereby lead to intravascular microthrombosis and capillary obstruction¹⁵⁹. Furthermore, decreased intravascular NO levels can also promote platelet aggregation and cause microthrombi formation¹⁶⁰. Sehba et al. showed a time line determined by histological staining for the formation of micro thrombi in rats after SAH. 10 minutes as well as 24 hours after SAH, platelet aggregates reached a peak, but no immunoreactive aggregates were observed 48 hours after the bleeding¹⁶¹. An in vivo study from our laboratory showed 30% constricted arterioles with microthrombi occlusion and the degree of vasoconstriction correlating with the frequency of microthrombosis⁷⁸. Consistent results were found in SAH patients where platelet aggregation may promote endothelial damage¹⁶². An increased number of microthrombi is associated with delayed cerebral ischemia¹⁵⁸.

The effect of common antiplatelet drugs such as acetylsalicylic acid, dipyridamole or ticlopidine after SAH is unclear. Apart from the increased risk of hemorrhagic complications, they show a trend to improve outcome by reducing secondary ischemia, but the results were not statistically significant thus to date antiplatelet drugs cannot be recommended for the treatment of secondary ischemia or poor outcome after SAH¹⁶³.

1.3.6 Microvasospasm

Bederson et al. found acute vasoconstriction in the internal carotid artery and the anterior cerebral artery after experimental SAH in rats¹⁶⁴. Interestingly, vasoconstriction occurs independent of ICP and CPP but is associated with decreased CBF, larger hemorrhage size, persistently elevated extracellular glutamate levels and poor general outcome. In this study the authors speculated that acute vasoconstriction might contribute to ischemic brain injury after SAH¹⁶⁴. In SAH patients, microvasospasm of pial vessels was first observed by Uhl et al. who reported that 50% of superficial arteries showed vasospasm and reduced capillary density⁷⁷. Increased microvascular contractility is believed to increase the susceptibility to ischemia and to worsen clinical outcome^{77 165}.

In theory, microvasospasm is a general term describing vasoconstriction that happens in small vessels. The importance of microvasospasm is mainly based on the functional fact that small vessels including superficial cerebral arteries, penetrating arterioles and parenchymal arterioles are resistance arteries. By altering vessel diameter, they provide a major component for the regulation of blood flow^{97 166}. It is easy to assume that constriction of resistance arteries will lead to a drastic change of blood flow on the parenchymal level.

This has been shown by previous work in our lab. Microvasospasm in a mouse SAH model seem to be restricted to pial vessels, 20-40% of pial arterioles constriction were found as early as three hours after hemorrhage and lasted for up to 72 hours⁷⁸. A 20% reduction of superficial arterioles diameter is associated with a 60% reduction of flow, which indicates even small spasms result in a parenchymal perfusion deficit.

Since after SAH, superficial microvasospasms are related with changes of the parenchymal perfusion volume, the disintegration of superficial microvasospasm could probably ameliorate ischemia and improve outcome. Therefore one of the aims of this thesis was to explore the pathomechanisms behind microvasospasm after SAH. As described before, endothelin receptor antagonist Clazosentan could relieve large

artery spasm by competitively binding to the ET_A receptor. We speculated that the mechanism behind large artery spasm and microvasospasm could probably be the same. Thus we aimed to conduct experiments investigating whether Clazosentan could relieve microvasospasm through the inhibition of ET_A receptors.

1.3.7 Hemolysis

Hemolysis describes the rupture of erythrocytes and the release of its contents, mainly hemoglobin (Hb). Two hours after SAH, Barrows et al. found that the hemolysis product hemoglobin (Hb) was present in patients' CSF¹⁶⁷. In animal experiments Peterson et al. showed that the development of vasospasm depends on hemolysis after SAH in dogs¹⁶⁸. In isolated arteries, hemolyzed blood induced significant vasoconstriction via an increase of intracellular Ca²⁺ concentration¹⁶⁹. Widespread cortical infarction can be induced by superfusion of the subarachnoid space with Hb combined with either high potassium or low glucose solution⁹⁴. Hemolysis products including Hb, bilirubin oxidation products, free heme or iron are shown to be responsible for large cerebral vasospasms after SAH in different studies¹⁷⁰⁻¹⁷³.

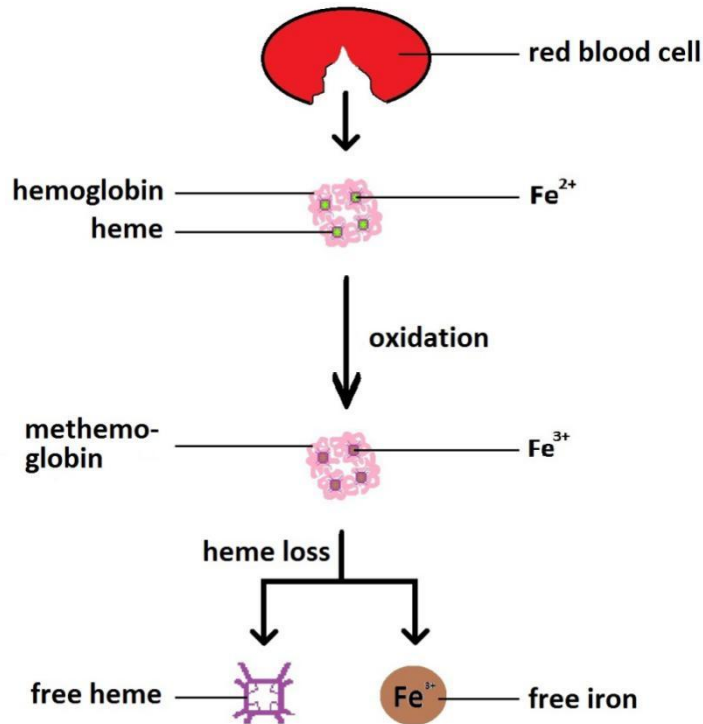


Figure 3

In the systemic circulation the CD163-haptoglobin-hemoglobin (CD163-Hp-Hb) scavenger system is the primary pathway for Hb clearance. The system exists also in the central nerves system (CNS), but its capacity is much lower-than in blood¹⁷⁴. Extracellular Hb in the circulation will be captured by haptoglobin (Hp) and engulfed by macrophages or monocytes through the receptor CD163¹⁷⁵. In the brain, perivascular and meningeal macrophages express CD163 and act as Hb scavengers. By checking Hp and free Hb level in the CSF of patients, it was demonstrated that the CD163-Hp scavenger system is saturated several days after SAH. This indicates an incapability of the subarachnoid space to handle significant hemolysis after SAH¹⁷⁴.

Excessive free Hb due to hemolysis causes damage to cells and tissue mainly through three mechanisms. First, Hb as a small molecule can easily get access to the intercellular space such as subendothelial and perivascular spaces¹⁷⁶. There it can directly generate adverse effects. Second, Hb reacts with reactive oxygen species such as hydrogen peroxide or lipid peroxides and generates superoxides and free

radicals. End products of the oxidization process trigger cellular injury and may be related to delayed vasospasm¹⁷⁷. Scavenging of superoxides and free radicals ameliorates vasospasm after experimental SAH^{178 179}. Oxidation of hemoglobin generates methemoglobin, a product found in the subarachnoid space after SAH in animals¹⁸⁰ and promoting TLR4 mediated neuroinflammation in vitro¹⁸¹.

Third, methemoglobin is an unstable complex so heme is rapidly released and interferes with molecular signaling pathways by binding with certain receptors, transcription factors or enzymes^{182 183}. Free heme will conduct oxidation of membrane lipids and lipoproteins therefore inducing cellular dysfunction and cell death¹⁸⁴. In physiological circumstances, hemopexin binds and transits heme into macrophages where the heme oxygenase-1 (HO-1) breaks down heme into biliverdin, carbon monoxide and iron¹⁸⁵. Unlike biliverdin and carbon monoxide which have anti-inflammatory effects^{186 187}, free heme and iron have a direct cytotoxic effect to cells and are able to activate the innate immune response thereby inducing inflammation¹⁸⁸.

The CD91-hemopexin scavenger system is the second line for Hb clearance; a small amount of hemopexin was found in the cerebral vascular system, expressed in the basement membrane and connective tissues. Though evidence shows that the CD91-HPX system is activated in the brain after SAH, due to low expression of hemopexin, the heme-binding capacity in the brain does not seem to be high enough to process a heme overload after hemolysis as CSF sampling from SAH patients shows that the heme-hemopexin uptake is saturated already early after SAH¹⁸⁹.

Ferritin is an intracellular protein that binds iron and stores it intracellularly in a non-toxic form and is highly expressed in cerebral arteries after SAH in animal models¹⁹⁰ and in CSF samples of patients¹⁹¹. HO-1 concentration in the CSF was shown to be an effective predictor for the clinical outcome of SAH patients¹⁹². The inhibition of HO-1 worsens and prolongs the spasm of the basilar artery in rats after SAH¹⁹³.

Because of its detrimental effects, the binding of free iron with chelators seems to be a promising therapeutic approach in diseases which are associated with hemolysis. In terms of free iron inhibition, various iron chelators were tested in experimental SAH

animal models. 2,2'-dipyridyl was found to reduce delayed vasospasm of the middle cerebral artery and basilar artery in monkeys and rabbits after SAH^{194 195}. Deferiprone was shown to attenuate basilar artery vasospasm in rabbits¹⁹⁶.

Another potent iron chelator is deferoxamine (DFO). DFO is clinical commonly used and was shown to prevent post-hemorrhagic injury by neutralizing iron toxicity and inhibiting oxidative stress, phagocytosis, apoptosis and inflammation after intracerebral hemorrhage^{197 198}. As shown by a meta-analysis, DFO is neuroprotective and improves neurobehavioral outcomes after intracerebral hemorrhage¹⁹⁹. Interestingly, attenuation of large artery vasospasm after DFO application was found in the double injection rat SAH model²⁰⁰ but not in prechiasmatic cistern injection mouse SAH model²⁰¹. A vasospasm independent neuroprotective effect was seen in different studies^{173 200-203}. The possible modes of action include inhibition of cathepsin B/D release, increase of HO-1 and hypoxia-inducible factor-1 expression, reduction of BBB impairment and neuronal cell death and thereby improvement of neurological function^{173 200-203}.

Taken together, hemolysis products in the subarachnoid space might play a substantial role in the pathophysiological processes after SAH. Most previous studies investigating the role of hemolysis products after SAH focused on DCI and only recently the importance of iron chelation in EBI attracted more attention. One aim of this thesis was therefore to investigate the role of hemolysis products in the context of microcirculatory dysfunction after SAH. We aimed to test whether DFO applied directly to the subarachnoid space prevents the formation of microvasospasm by neutralizing iron as soon as it is released by hemolysis.

To sum up, we first aimed at investigating whether ET_A receptor antagonist Clazosentan has an effect on early microvasospasms after SAH, thus checking if the ET_A receptor is involved in the development of acute microcirculatory dysfunction after SAH. The second aim of the study was to describe the distribution pattern of extravasated blood in the MCA perforation model in order to identify its causative relationship with microcirculatory dysfunction. Our hypothesis was that the blood

distribution in the subarachnoid space will have an impact on the cerebral circulation by releasing detrimental hemolysis products. The third aim of the study was to explore the potential effect of free iron in the formation of microvasospasms by using the iron chelator DFO. In order to further study the role of hemolysis products in microcirculatory dysfunction after SAH, we also aimed at establishing a novel in vivo animal model with a similar blood distribution pattern as in SAH but which is unaffected by initial cerebral perfusion deficits.

2. Methods and Materials

2.1 Materials

2.1.1 Equipment

Axio Imager M2 Microscope	Co. Zeiss (Germany)
Cryostat NX70	Co. Thermo Scientific (USA)
DC Temperature Control System	Co. FHC (USA)
Dental Drill	Co. Rewatronik (Germany)
Dental Drill Tip (GD041R, 6mm/ISO, 2.35X70mm)	Co. B-Braun (Germany)
Dumont Forceps (11253-20)	Co. Fine Scientific Tools (Switzerland)
Dumont Laminectomy Forceps (11223-20)	Co. Fine Scientific Tools (Switzerland)
Extra Fine Bonn Scissor (14084-08)	Co. Fine Scientific Tools (Switzerland)
Fume Hood	Co. Wesemann (Germany)
Hartman Hemostat (13003-10)	Co. Fine Scientific Tools (Switzerland)
Incubator	Co. Memmert (Germany)
Intracranial Pressure Express	Co. Codman, J&J (UK)
Intubation tube	Custom made from a 20G venous catheter
LED light source (KL2500)	Co. Leica (Germany)
Leica M80 Stereomicroscope	Co. Leica (Germany)
Li:Ti Laser, Chameleon	Co. Coherent (Scotland)
MediHEAT Heater	Co. Peco Services (UK)
Microcapnograph 340	Co. Hugo Sachs (Germany)
MicroSyringe Pump Controller	Co. World Precision Instruments (USA)
Micro Serrefine (18055-04)	Co. Fine Science Tools (Switzerland)
Micro-Serrefine Clamp Applying Forcep (18057-14)	Co. Fine Science Tools (Switzerland)
Minivent 845	Co. Hugo Sachs (Germany)

Nose Clamp	Co. David Kopf Instrument (USA)
Oslon-Hegar Needle Holder (12002-12)	Co. Fine Science Tools (Switzerland)
Oxygen Sensor, Oxydig	Co. Draegerwerk (Germany)
Perfusion Machine	Co. Leica Biosystems Richmond (Germany)
PeriFlux system 5000	Co. Perimed AB (Sweden)
PhysioSuite PS-03	Co. Kent Scientific (USA)
Powerlab 8/35	Co. AD Instruments (Australia)
RAPIDLab 348 Blood Gas Analyzer	Co. Siemens (Germany)
Stereotactic Injection Platform	Co. Föhr Medical Instruments (Germany)
Synergy Water Purification System	Co. Sigma-Aldrich (USA)
Syringe Pump (SP101IZ)	Co. World Precision Instruments (USA)
Two Photon Microscope LSM 7 MP	Co. Carl Zeiss (Germany)
Vannas Spring Scissors (15000-08)	Co. Fine Science Tools (Switzerland)
Venous Catheter (20G)	Co. BD Biosciences (USA)
Vibratome (Leica VT 1200s)	Co. Leica (Germany)
X-cite 120 Fluorescence Illuminator	Co. Lumen Dynamics (USA)

2.1.2 Software

ImageJ 2	National Institute of Health (USA)
Imaris	Co. Bitplane AG (Switzerland)
LabChart 8 Reader	Co. ADInstruments (Australia)
SigmaPlot 13.0	Co. Systat (USA)
ZEN 2010	Co. Carl Zeiss (Germany)

2.1.3 Consumables

Accelerator Insta-set	Co. Drechseln & Mehr (Germany)
Carboxylatzement Fluid	Co. Dr. Speier (Germany)
Carboxylatzement Powder	Co. Dr. Speier (Germany)

Cotton Swab	Co. Nobamed Paul Danz (Germany)
Coverslips	Co. Warner Instruments (USA)
Cyano Veneer	Co. Hager & Werken (Germany)
Cyano Veneer Powder	Co. Hager & Werken (Germany)
Cyanoacrylate Maxi-Cure	Co. Drechseln & Mehr (Germany)
Dental needle (30G)	Co. Septodont (Germany)
Eukitt Quick-hardening Mounting Medium	Co. O.Kindler (Germany)
Eye and nose ointment	Co. Bayer Vital (Germany)
Fine bore polythene tubing: 0.38mm (ID), 1.09mm (OD)	Co. Smiths Medical ASD (UK)
Gauze (7.5 x 7.5 cm)	Co. Lohmann & Rauscher(Germany)
Injekt-F Syringe (1ml)	Co. BD Biosciences (USA)
Laser Doppler Probe Microtip	Co. Perimed AB (Sweden)
M-1 Embedding Matrix	Co. Thermo Scientific (USA)
Mounting Medium for Fluorescence	Co. Vector Laboratories (USA)
Nail polish (transparent)	Co. Dm Drogerie Markt (Germany)
Needle (30G/0.3mm)	Co. B-Braun (Germany)
Polytetrafluorethylen hose: 0.2mm (ID), 0.4mm (OD)	Co. Bohlender (Germany)
Prolene Suture (5-0)	Co. Ethicon (Germany)
Scalpel (No.11)	Co. Feather (Japan)
SERAFIT Suture (6-0)	Co. Serag Wiessner (Germany)
Silk Braided Suture (7-0)	Co. Pearsalls Limited (UK)
Sugi Sponge Points	Co. Kettenbach (Germany)
Superfrost Plus Microscope Slides	Co. Thermo Scientific (USA)
Surflo Winged Infusion Set	Co. Terumo Medical Corporation (Belgium)
Vasco Nitril Blue Glove (S)	Co. B-Braun (Germany)

2.1.4 Chemicals

ABC kit (Vectastain)	Co. Vector Laboratories (USA)
Acetone	Co. Applichem (Germany)
Agarose	Co. VWR (Germany)
Antipamezol (Alzane 5mg/ml)	Co. Zoetis (USA)
Aqua ad injectabilia	Co. Fresenius Kabi (Germany)
Artificial Cerebrospinal Fluid	Co. Ecocyte bioscience (USA)
Avidin/Biotin Blocking Kit	Co. Vector laboratories (USA)
Bovine Serum Albumin	Co. Sigma-Aldrich (USA)
Buprenorphine (Buprenovet 0.3mg/ml)	Co. Bayer (Germany)
Carprofen (Rimadyl 50mg/ml)	Co. Zoetis (USA)
Clazosentan	Co. Actelion (Switzerland)
3,3'-Diaminobenzidine (DAB) kit	Co. Vector laboratories (USA)
Deferoxamine (Desferal 100mg/ml)	Co. Novartis (Germany)
Dextran Tetramethylrhodamine(TMRM),	Co. Sigma-Aldrich (USA)
Lysine fixable (average 70,000 MW)	
Ethanol (EMSURE, ≥99.8%)	Co. Sigma-Aldrich (USA)
Ethylene glycol	Co. Sigma-Aldrich (USA)
Fentanyl (Fentadon 50mg/ml)	Co. Albrecht (Germany)
FITC (Tomato) Lectin	Co. Vector Laboratories (USA)
Flumazenil	Co. Hexal (Germany)
Fluorescein isothiocyanate-dextran (average 70,000 MW)	Co. Sigma-Aldrich (USA)
Glycerol	Co. Sigma-Aldrich (USA)
Hematoxylin	Co. Sigma-Aldrich (USA)
Heparin-Natrium (25,000 I.E./5ml)	Co. B-Braun (Germany)
Hydrogen Chloride	Co. Sigma-Aldrich (USA)
Hydrogen Peroxide (30%)	Co. Sigma-Aldrich (USA)
Isoflurane Isp-Vet	Co. Chanelle (Ireland)

Isopentane	Co. Sigma-Aldrich (USA)
Lidocaine (2%HCl)	Co. B.Braun (Germany)
Medetomidine	Co. Zoetis (USA)
Midazolam	Co. B-Braun (Germany)
NaCl isotonic solution 0.9%	Co. Fresenius Kabi (Germany)
Naloxone	Co. Inresa Arzneimittel (Germany)
Paraformaldehyde (4% PFA)	Co. Morphisto (Germany)
Pepsin	Co. Dako (Germany)
Phosphate buffer saline (PBS, 10x)	Co. Klinikum Apotheke (Germany)
Sucrose	Co. Sigma-Aldrich (USA)
Tween 20	Co. Carl Roth (Germany)

2.1.5 Antibodies

Anti-Ly76 antibody TER119 (ab91113)	Co. Abcam (UK)
Anti-collagen type IV (Rabbit) antibody (600-401-106.0)	Co. Rockland (USA)
Biotinylated goat anti-rabbit IgG antibody (BA-1000)	Co. Vector Laboratories (USA)
Biotin-SP Affinipure F (ab') ₂ Fragment mouse anti-rat IgG (H+L) (212-066-168)	Co. Jackson ImmunoResearch (USA)
Purified rat anti mouse CD45 (550539)	Co. BD biosciences (USA)

2.1.6 Buffers and solutions

4% Agarose:

8g	Agarose
200ml	PBS (1x)

0.25% PBS-Tween:

2.5ml	Tween20
1L	PBS (1x)

1% Hydrogen peroxide (H₂O₂):

1ml	30% H ₂ O ₂
100ml	PBS (1x)

PBS, 1x:

100ml	PBS (10x)
900ml	Millipore water

Pepsin solution:

2mg	Pepsin
2ml	HCl (0.2N)

Blocking solution for brain tissue sections:

0.2g	Bovine serum albumin
10 ml	PBS (1x)

15% Sucrose solution for cryoprotection:

37.5g	Sucrose
250ml	PBS (1x)

30% Sucrose solution for cryoprotection:

75g	Sucrose
250ml	PBS (1x)

Cryoprotection solution:

250ml	Glycerin
250ml	Ethylenglycol
500ml	PBS (1x)

2.2 Methods

2.2.1 Randomization and blinding

For each set of experiment, animals were randomly assigned to surgical groups. Drugs and blood or artificial cerebral spinal fluid (aCSF) were prepared by an assistant researcher in advance and randomly marked to blind the researcher towards the respective treatment.

Data collection and analysis were performed by the researcher blinded with respect to the treatment group.

2.2.2 Animals

All procedures on animal were approved by the Government of Upper Bavaria (protocol number 136-11 and 209-16) and are reported in accordance with the ARRIVE (Animal Research: Reporting of in Vivo Experiments) guidelines. All efforts were made to minimize animal suffering and to reduce the number of animals.

All experiments were conducted on male C57BL/6N mice obtained from Charles River (Sulzfeld, Germany). Mice were group housed in individually ventilated cages under a twelve hour light cycle with access to food pellets and water.

2.2.3 Filament perforation SAH model

2.2.3.1 Anesthesia

Mice were put into a darkened induction chamber with increasing isoflurane concentration until they lost consciousness then intraperitoneally injected with 0.05

mg/kg Fentanyl, 0.5 mg/kg Medetomidine and 5 mg/kg Midazolam via a 27-gauge BD syringe. Surgical anesthesia was confirmed by the loss of hind paw reflex. For sustained anesthesia, one third of the initial dose was injected regularly.

Anesthetized mice were intubated with a custom tube made from a 20G venous catheter and put on a heating pad for maintenance of the body temperature. Controlled mechanical ventilation with oxygen supplemented room air was performed with a mechanical ventilator (Minivent). Ventilation volume as well as respiratory frequency was adjusted according to end tidal partial pressure of carbon dioxide ($p\text{CO}_2$), which was measured with a microcapnograph (Microcapnograph 340). A pulse oximeter (PhysioSuite PS-03) was clipped at the right hind paw to monitor heart rate and peripheral oxygen saturation during anesthesia.

All physiological parameters were recorded by Powerlab and displayed, stored and analyzed using LabChart software.

2.2.3.2 SAH model

SAH induction was performed as previously described²⁰⁴ by endovascular perforation of the Circle of Willis. As illustrated in Figure 4, an intracranial pressure (ICP) probe was first implanted through a burr hole between skull and dura mater. A laser Doppler probe for continuous measurement of cerebral blood flow (CBF) was fixed with glue (Cyanoacrylate Maxi-Cure) on the ipsilateral temporal bone above the territory of the middle cerebral artery. Afterwards, the mouse was placed in a supine position.

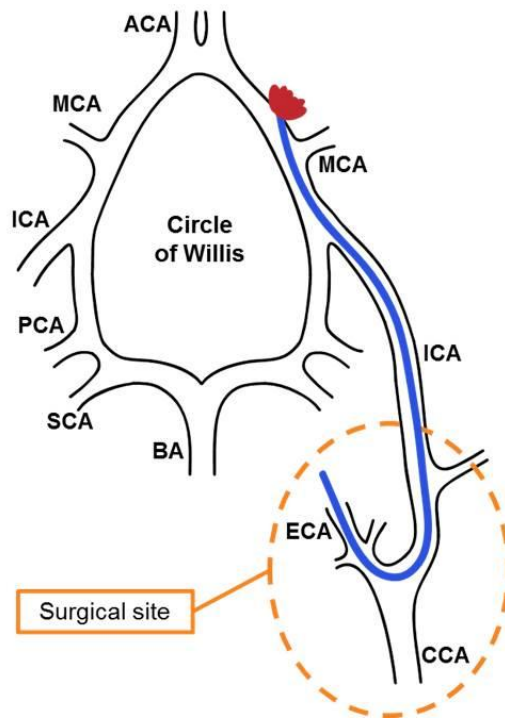


Figure 4: Schematic of intravascular perforation SAH model. The surgical site is located at the left side of the neck. Common carotid artery (CCA) and external carotid artery (ECA) are exposed. A blunt-ended filament (5-0 prolene, 12mm) is inserted through the ECA, advanced up to internal carotid artery (ICA) and penetrating the vessel wall at the Circle of Willis close to the middle cerebral artery (MCA). ACA = anterior cerebral artery, BA = basilar artery, PCA = posterior cerebral artery, SCA = superior cerebellar artery. (adapted from Schuller et al²⁰⁴.)

Common carotid arteries were exposed at the neck by a midline skin incision. A filament with a blunt end was inserted into the external carotid artery and advanced up to the bifurcation of the middle cerebral artery at the Circle of Willis. A sharp increase of ICP indicated the rupture of the arterial wall. The filament was quickly withdrawn in order to allow blood to freely flow into the subarachnoid space. The filament was removed and the external carotid artery as well as the skin wound was sutured. 0.1 mg/kg Buprenorphine was injected for postoperative analgesia. The physiologic parameters were continuously monitored for another 20 minutes. For termination of anesthesia 2.5 mg/kg Atipamezol, 0.5 mg/kg Flumazenil and 1.2 mg/kg Naloxone were injected subcutaneously.

2.2.4 Cisterna magna injection (CMI) model

2.2.4.1 Anesthesia

Mice were first put into a darkened chamber with increasing isoflurane concentration until loss of consciousness and then anesthetic agents (0.05 mg/kg Fentanyl, 0.5 mg/kg Medetomidine and 5 mg/kg Midazolam) were injected intraperitoneally. Hind paw withdrawal reflex was checked regularly. Anesthesia during surgery was maintained by intraperitoneal injections of one third of the initial dose of anesthetics. Carprofen (4 mg/kg) was injected subcutaneously for analgesia. Buprenorphine 0.1 mg/kg was injected 30 minutes before wake up of the mice for acute postoperative analgesia.

Mice were put on a heating pad to maintain normal body temperature and ventilated with oxygenized (30%) room air. A pulse oximeter was clipped on the right hind paw to monitor heart rate and peripheral oxygen saturation during anesthesia. A syringe flushed with 0.1 % heparin in saline was used to withdraw 0.1 ml autologous blood from the left femoral vein. An intraperitoneal injection of 0.15ml saline reconstituted the volume loss. Blood was stored on ice for no longer than 15 minutes. The wound was sutured, mice were turned over and a laser Doppler probe was fixed on the right temporal bone.

2.2.4.2 Cisterna magna injection (CMI)

CMI was redesigned and performed based on a previously described blood injection SAH mouse model²⁰⁵.

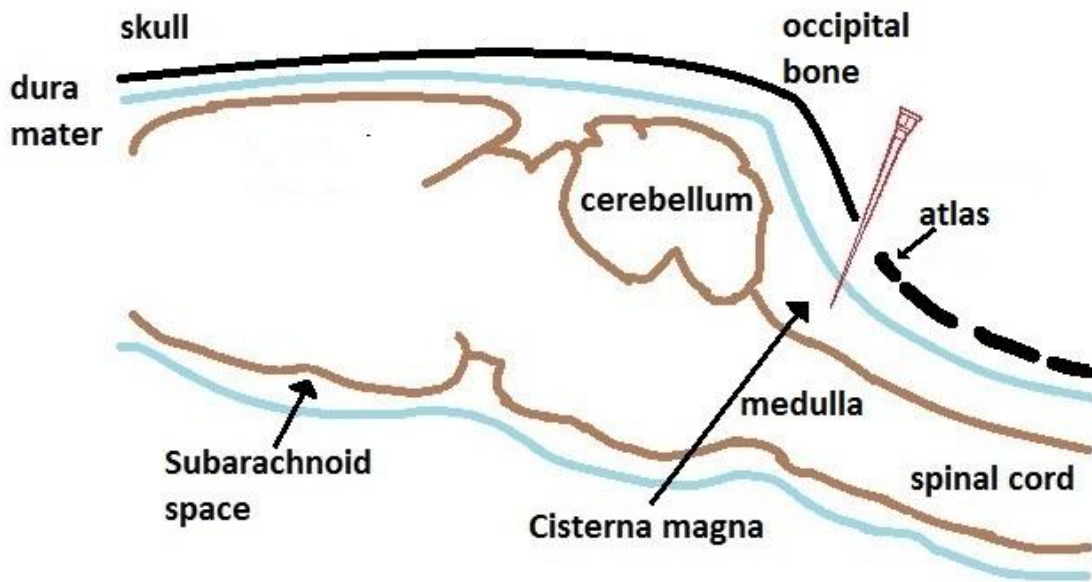


Figure 5 : Simplified sketch of cisterna magna injection edited from Light et al²⁰⁶. The cisterna magna is one of the subarachnoid cisterns. It located between the cerebellum and the dorsal surface of the medulla and covered by the dura mater and atlanto-occipital membrane. By widening the space between the end of occipital bone and atlas, it can be exposed for injection.

A sketch of the injection point is shown in Figure 5. Briefly, mice were placed in a prone position and the head was fixed with ear bars. A midline incision was made and the occipital muscles were dissected bluntly to expose the posterior atlanto-occipital membrane. The head was then bent down rostral. A 30G dental needle fixed on a stereotactic micromanipulator was used to puncture the atlanto-occipital membrane. 0.1 ml autologous blood was warmed by hand and mixed with 10 μ l FITC dextran, or 0.1 ml previously prepared aCSF (pH 7.4) was mixed with 10 μ l FITC dextran. 22 μ l of blood or aCSF was injected using a micro-syringe pump controller with an injection speed of 6.7 μ l/min. After injection, the mouse was continuously monitored for five minutes. Then the wound was sutured and anesthesia was antagonized as described above.

2.2.5 Two-photon microscopy

Anesthetized mice were fixed in a nose clamp and placed under the 2PM. FITC dextran (0.5% in saline) was injected through the femoral catheter to stain blood plasma. The excitation wavelength for FITC dextran and TMRM dextran was 830nm. 500-550 nm and 565-610 nm band pass filter was used to detect the fluorescence of FITC dextran and TMRM dextran.

Intravital microscopy is illustrated in Figure 6 B and C. Four or two regions of interest (ROI) as well as thinned skull area with at least one artery with several branches or a vein were focused under the 2PM. By recording a pile of images at different focal planes with one μm step distance, Z-stacks of each ROI were obtained. Detailed information will be described in each experiment protocol.

Blood flow velocity was recorded by performing line scans along pial arterioles, veins and capillaries²⁰⁷. Each vessel was scanned repetitively for 1000 times with maximum speed over a length of 20-50 μm to detect travelling erythrocyte.

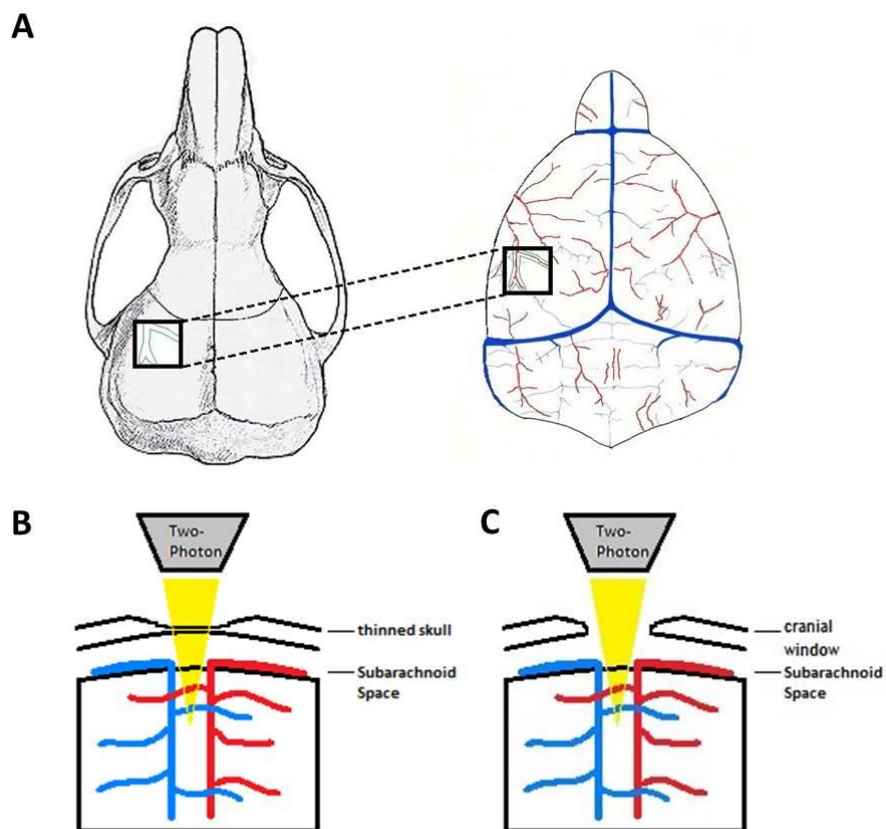


Figure 6: (A) Sketch of an open cranial window (black frame) and a thinned skull window (green outline) on the left parietal cortex (Edited from discoverlife.org). (B) Four or two randomly chosen ROI within the cranial window were investigated by 2PM.

2.2.5.1 Cranial window preparation

2.2.5.1.1 Thinned skull window

A thinned-skull window preparation was conducted as previously described²⁰⁸. Mice were anesthetized and fixed in a nose clamp. After topic application of lidocaine (2% HCl), the skull bone was thinned by using a dental drill (Dental Drill Tip GD041R). Topic saline was constantly applied to absorb the heat generated from the drilling process and thereby protecting the brain surface from overheating. The location of the thinned skull window is depicted in Figure 6 A.

2.2.5.1.2 Open cranial window

An open cranial window preparation was conducted as previously described²⁰⁹. Mice were anesthetized and fixed in a nose clamp. After topic application of lidocaine, a 3 x 3 mm sized window was drilled over the right hemisphere under constant cooling with topical saline. The dura mater was kept intact during drilling. After careful removal of the bone flap, the exposed dura mater was kept wet. The location of the open cranial window is depicted in Figure 6 A.

2.2.6 Tissue harvesting

At the end of imaging, an arterial blood sample from the femoral artery catheter was collected with a glass capillary for blood gas analysis.

Transcardial perfusion was performed under a fume hood in deep anesthesia. The cardiovascular system was first perfused with saline for five minutes and then with 4% PFA for ten minutes. Perfusion pressure was kept at 150 mmHg throughout the process.

Subsequently, brains were collected and post-fixed in 4% PFA overnight at 4°C. Brains were washed in PBS, embedded in 4% agarose and cut into 50 µm thick sections

using a vibratome (Leica VT 1200s). Sections were collected in a cryoprotectant solution and then analyzed or stored at -20°C for long-term preservation.

In the DFO experiment, brains were collected and post-fixed in 4% PFA overnight at 4°C. After washing in PBS, brains were cryoprotected by saturation in 30% sucrose solution. Then brains were rapidly frozen in -80°C isopentane and cut into 20µm thick sections at a cryostat. Sections were stored at -20°C until further processing.

2.2.7 Experimental protocols

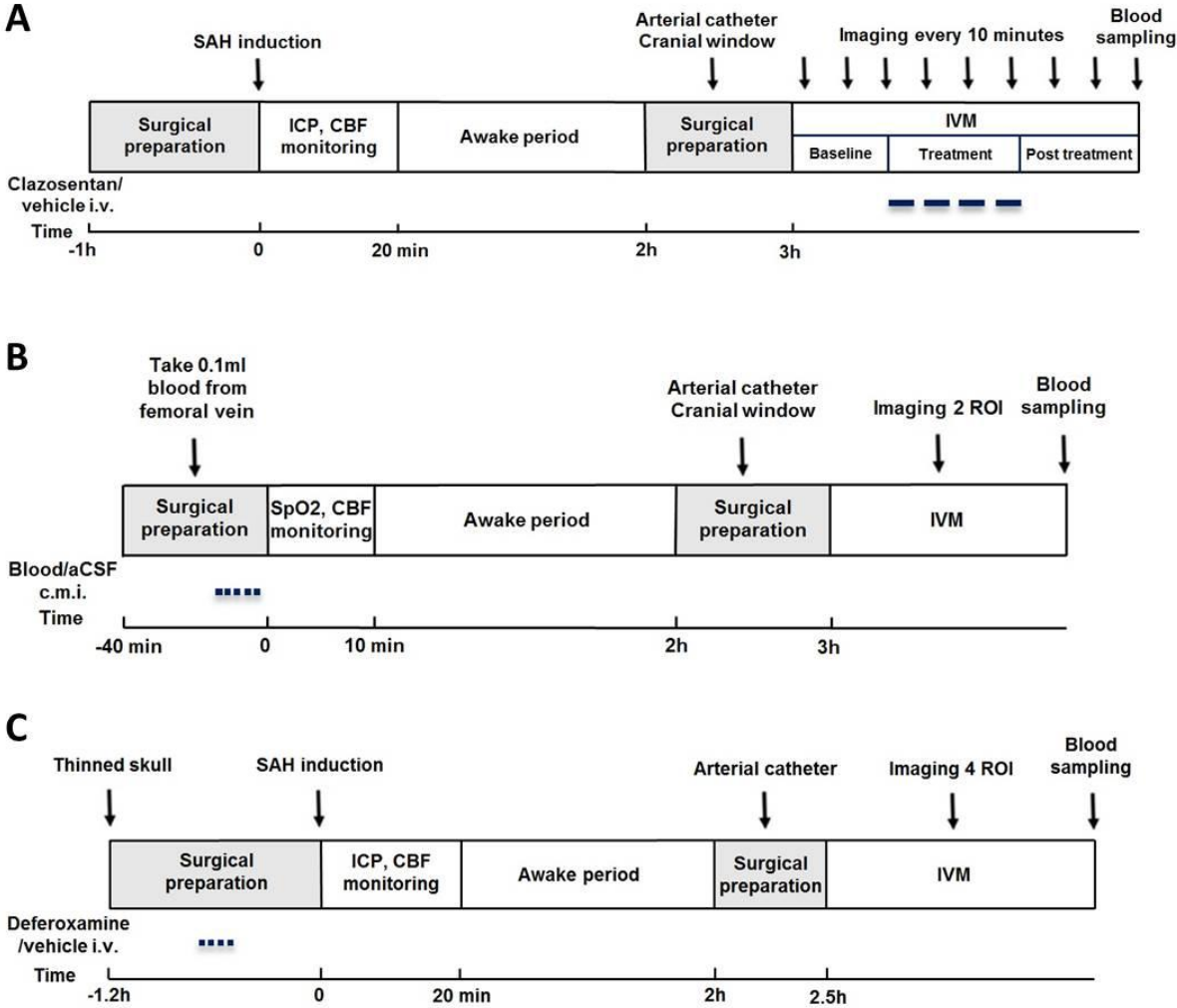


Figure 7: The intravital microscopy experimental groups and protocols used in this thesis. The dark blue dotted lines indicate infusion of drug/blood or vehicle/aCSF. (A) Clazosentan experiment. (B) CMI experiment. (C) DFO experiment.

2.2.7.1 Clazosentan

The experimental protocol for the Clazosentan experiments is illustrated in Figure 7 A. Briefly, MCA perforation SAH was induced at time point zero. After monitoring of physiologic parameters for 20 minutes, mice were allowed to wake up for two hours and then re-anesthetized. An arterial catheter was inserted into the femoral artery to monitor blood pressure. A venous catheter at the same site was prepared for drug application. One bolus of Clazosentan (10 mg/kg) or vehicle was given three hours and 20 minutes after the induction of SAH. Afterwards a continuous administration via a femoral vein catheter was maintained by a syringe pump with a speed of 0.2 ml/h for 30 minutes. A cranial window was prepared and cerebral vessels were imaged under the 2PM. Either Clazosentan or saline was continuously infused for 30 minutes. During one hour of treatment and post treatment, two ROIs, each 1x2 tile scan with 0.7 x zoom were scanned. Therefore the size of each ROI was 607 x 1215 μm . Imaging was performed at a depth of 150 to 500 μm every ten minutes. At the end of imaging a blood sample was drawn from the femoral artery catheter for blood gas analysis and mice were sacrificed by perfusion fixation.

2.2.7.2 Blood and aCSF injection

The experimental protocol for the injection of blood and aCSF into the cisterna magna is illustrated in Figure 7 B. Briefly, cisterna magna injection of blood or aCSF was done at time point 0. After monitoring the cerebral perfusion for five minutes, mice were allowed to wake up for two hours. Before re-anesthetizing the animal the neuroscore (Table 1) was assessed. A catheter was inserted into the femoral artery to monitor blood pressure. A cranial window was drilled and mice were put under the 2PM for in vivo microscopy (IVM). Two ROIs with a size of 425 x 425 μm were imaged at a depth of 150 to 500 μm . At the end of imaging a blood sample was drawn and mice were perfused for histological examination.

2.2.7.3 Deferoxamine

The surgical protocol of DFO experiments is illustrated in Figure 7 C. Briefly, a thinned skull window was drilled followed by a randomized intravenous infusion of DFO (200

mg/kg) or vehicle (aqua ad injectabilia). DFO (200 mg/kg) was injected approximately 30 minutes before SAH via the femoral vein by using a vein injection syringe, which was composed of a sharp-tipped polytetrafluorethylen hose. At the same time TMRM dextran (0.5% in saline) was injected to label extravasated blood plasma. MCA perforation SAH was induced at time point zero. After 20 minutes monitoring of physiologic parameters, mice were woken up for about two and a half hours. Then they were anesthetized and a catheter was inserted into the femoral artery to continuously monitor blood pressure. Mice were put under the 2PM for IVM. During imaging, four ROI with a size of 607 x 607 μm were obtained with a 0.7 x zoom. The depth of the scan was 150 to 400 μm . At the end of imaging, a blood sample was drawn from the femoral catheter for blood gas analysis and mice were transcardially perfused with 4% PFA.

Table 1: Neuroscore sheet

1. General behavior		
Attention	Normal searching behavior	= 0 point
	Awake, but passive	= 1 point
	No spontaneous movement	= 2 points
2. Cranial nerves status		
Movement of whiskers	Present	= 0 point
	Not present	= 1 point
Hearing	Present	= 0 point
	Ear movements	= 1 point
	Not present	= 2 points
3. Motor activity		
Forelegs movement: left	Normal	= 0 point
	Stiffened	= 1 point
	Paralyzed	= 2 points
Forelegs movement: right	Normal	= 0 point
	Stiffened	= 1 point

	Paralyzed	= 2 points
Hind legs movement: left	Normal	= 0 point
	Stiffened	= 1 point
	Paralyzed	= 2 points
Hind legs movement: right	Normal	= 0 point
	Stiffened	= 1 point
	Paralyzed	= 2 points
4. Coordination		
Beam walk 3 cm		= 0-4 points
Beam walk 1.5 cm		= 0-4 points
Beam walk 1 cm		= 0-4 points
<p>Criteria: 0 points: normal movement/no failure</p> <p>1 points: wrong placement of the foot/unstable movements</p> <p>2 points: stay seated/ stays on the beam</p> <p>3 points: falls after a few steps from the beam</p> <p>4 points: falls directly from the beam without further movement</p>		
Floor cross test: Both	Present	= 0 point
forepaws touch the ground when the mouse is lifted by the tail	Not present	= 1 point
5. Neuroscore (Bederson)		
	No deterioration	= 0 point
	Bent forepaws	= 1 point
	Reduced resistance of the left side	= 2 points
	Circling behavior when pulling the tail	= 3 points
	Spontaneous circling	= 4 points
	No spontaneous movements	= 5 points
Total score		
		0-31 points

Immunohistochemistry

2.2.7.4 Antigen retrieval

Pepsin digestion was used to retrieve the collagen IV antigen as described in the literature²¹⁰. Slices were first submerged in 37°C distilled water for five minutes and incubated in pepsin solution for ten minutes at 37°C, then washed in PBS.

2.2.7.5 DAB staining

Slices were fixed in acetone for ten minutes. After washing in PBS, slices were incubated in 1% H₂O₂ solution for ten minutes to block endogenous peroxidase activity and pretreated in 0.25% PBS-Tween for ten minutes. 3 drops of avidin and biotin were applied to block avidin and biotin binding proteins for 15 minutes respectively.

Next, slices were incubated with the following primary antibodies in blocking solution for three hours:

- 1:200 Anti-Ly76 antibody (TER119)
- 1:200 Anti-collagen type IV antibody
- 1: 200 Anti-mouse CD45 antibody

After being rinsed with 0.25% PBS-Tween for ten minutes, slices were then incubated in the following secondary antibodies in blocking solution for 30 minutes:

- 1:200 Biotinylated goat anti-rabbit IgG antibody
- 1:300 Biotin-SP Affinipure F (ab')₂ Fragment mouse anti-rat IgG (H+L)

After being rinsed with 0.25% PBS-Tween for another ten minutes, slices were incubated in ABC solutions (Vectastain, Vector Laboratories, USA) for another 30 minutes; afterwards DAB solution (3,3'-Diaminobenzidine kit, Vector Laboratories, USA) was added. Slices were incubated until the brownish biocytin staining becomes visible (three to five minutes) and immediately transferred to water in order to stop the reaction.

Slices were counterstained for nuclei with hematoxylin and dehydrated with an increasing concentration of ethanol solution (70%, 96%, 100%).

In the end, slices were air-dried for three minutes, embedded with quick-hardening mounting medium (Eukitt, O.Kindler, Germany) and covered with coverslips.

2.2.7.6 Microscopic analysis

An Axio Imager M2 microscope was used for observation and image recording. For immunofluorescence, an X-cite 120 fluorescence illuminator was used to excite FITC-lectin and TMRM dextran. 525-550 nm and 605-670 nm filter sets were used to capture each section with a 40x objective. DAB staining were observed and recorded by light microscopy. A mosaic scanning tool was used to record the whole section with a 20x objective.

2.2.7.7 Cell and vessel measuring

For quantification, 8 ROI were selected across both hemispheres on three representative sections, as shown in Figure 8. For FITC dextran and TMRM dextran analysis, images were collected, transformed to 8-bit and quantified for pixel numbers for each ROI. CD45 positive cells were counted per ROI. Pixel numbers of TER119 and collagen IV positive cells were quantified using Image J. The ratio of non-perfused vessels per ROI was calculated by comparing the pixels of TER119 positive cells to collagen IV positive cells in each brain.

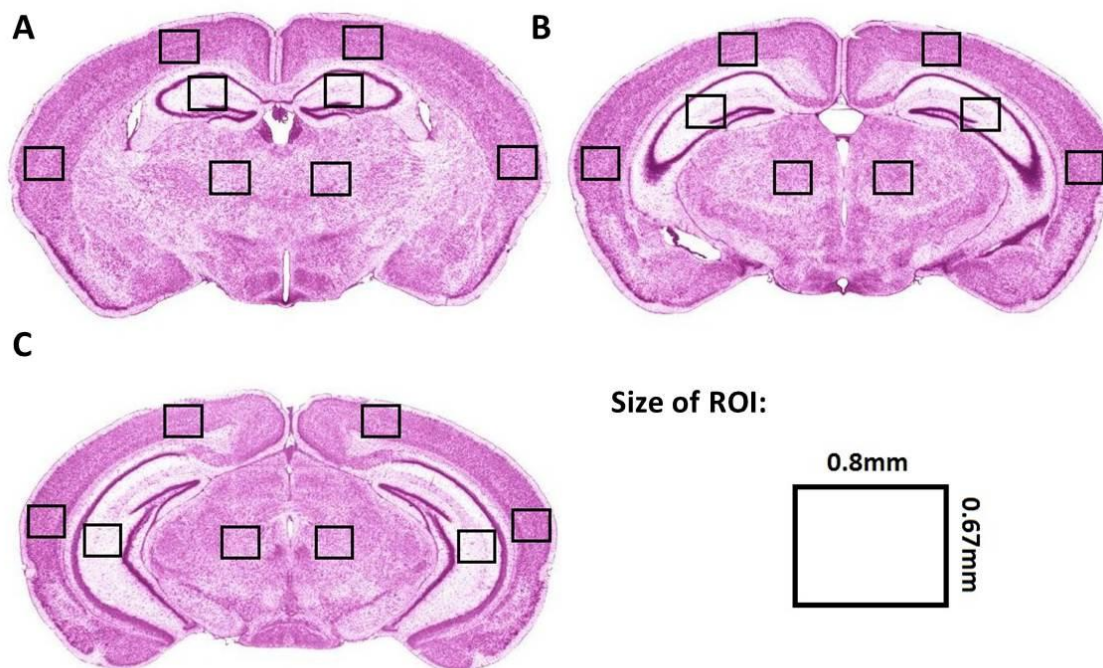


Figure 8: 8 ROIs was selected from three representative sections²¹¹: (A) Bregma -1.7mm, (B) Bregma -2.54mm and (C) Bregma -2.8mm. The original size of each ROI is 1000 x 1200 pixels and 0.8 x 0.67mm.

2.2.8 Quantification of two photon microscopy images

2.2.8.1 Vessel measurement

Vessel diameter was manually measured in randomly chosen Z-stacks. In each selected vessel segments, the maximal vessel diameter was measured along a distance of 60 to 80µm at more than five positions. Measurement started 15 µm away from vessel bifurcations.

The measurement of vasospasm was carried out by measuring the narrowest diameter and the diameters of the two flanking non-spastic vessel segments.

Several parameters were calculated to quantify the change in vessel diameter. Within a measured vessel segment the range percentage of mean describes the variation of the vessel diameter.

$$\text{range\% of mean} = \frac{\text{max} - \text{min}}{\text{mean}} \times 100$$

The method of measuring microvasospasms and the formula used for calculations are depicted in Figure 9 B. The degree of vasospasm represents the severity of vessel constriction. We defined a spastic segment with a vessel constriction more than 15% as a vasospasm. Anything less than a variation of 85% was considered as a normal variation of vessel diameter.

The spasticity index is a comparison of the degree of vasospasm at different time points. It depicts the changes of the degree of vasospasm over time.

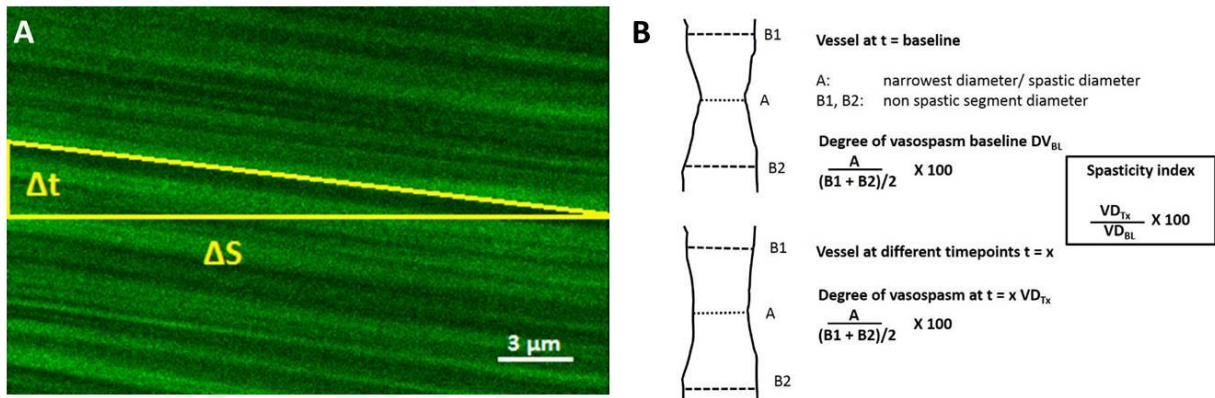


Figure 9: (A) Example of a repetitive line scan for blood flow velocity measurement. (B) Measurement of microvasospasms and calculation of degree of vasospasm and spasticity index.

2.2.8.2 Perfusion volume

Imaris software was used to reconstruct the vessels in a 3D stack ($607 \times 607 \times 140 \mu\text{m}$). The total volume of FITC-containing pixels, namely the perfused vessel volume after SAH was calculated. Then co-localizing TMRM dextran and FITC dextran containing pixels were excluded and the total volume of remaining TMRM dextran-containing pixels was calculated to quantify the extravasated blood volume.

Each ROI was divided into a superior layer ($0-70 \mu\text{m}$) with pial vessels and an inferior layer ($70-140 \mu\text{m}$) with parenchymal vessels.

2.2.8.3 Blood flow velocity

Line scan data are represented as space-time images, in which time increases from top to bottom over the length of the scanned vessel. As is shown in Figure 9 A, dark stripes represent the trajectory of a single erythrocyte. By dividing the scanned vessel length (μm) by the respective scanning time (msec), blood flow velocity was calculated for arteries, veins and capillaries.

2.2.8.4 Statistical analysis

Statistical analyses were performed with SigmaPlot 13.0 software. Normally distributed data were compared with the Student t-test, while not normally distributed data was compared with the Mann Whitney U test. Differences with p values less than 0.05 were considered to be statistically significant.

3. Results

3.1 Clazosentan experiment

3.1.1 Physiological monitoring

After SAH induction, ICP rapidly increased because a hematoma formed within the rigid skull. ICP went up to values close to systemic blood pressure (Figure 10 A); Consequently cerebral perfusion pressure (CPP), which is calculated by subtracting ICP from mean arterial pressure (MAP), decreased and immediately caused a dramatic drop of regional cerebral blood flow (rCBF) (Figure 10 B). Therefore, the brain suffered from global cerebral ischemia for several minutes. Within five minutes, ICP values stabilized around 20 mmHg (Figure 10 A) and stayed stable until the end of the monitoring period. Regional CBF normalized within ten minutes after hemorrhage. There was no significant difference between the Clazosentan and vehicle group.

Mice were randomly assigned to the Clazosentan or vehicle treatment group and intravital microscopy was performed by an investigator blinded to the treatment of the animals. Imaging consisted of three different periods: baseline imaging started at 2.7 hours after SAH, imaging after treatment started at three hours after SAH and lasted for 30 minutes, and post-treatment imaging started after cessation of intravenous infusion and lasted for 20 minutes.

During intravital imaging MAP remained within physiological range and was not significantly different between groups (Figure 10 C).

During SAH induction and IVM, body temperature, heart rate, blood pressure and peripheral oxygen saturation (SpO_2) were within the physiological range and showed no significant difference between groups (Table 2). Since increased arterial pCO_2 has a vasodilatory effect, end-expiratory pCO_2 was maintained within the physiologic range throughout the whole experiment by adjusting the ventilation frequency. Blood gases including pH, pCO_2 and partial pressure of oxygen (pO_2) were measured at the end of imaging and did not show any difference between the groups (Table 2).

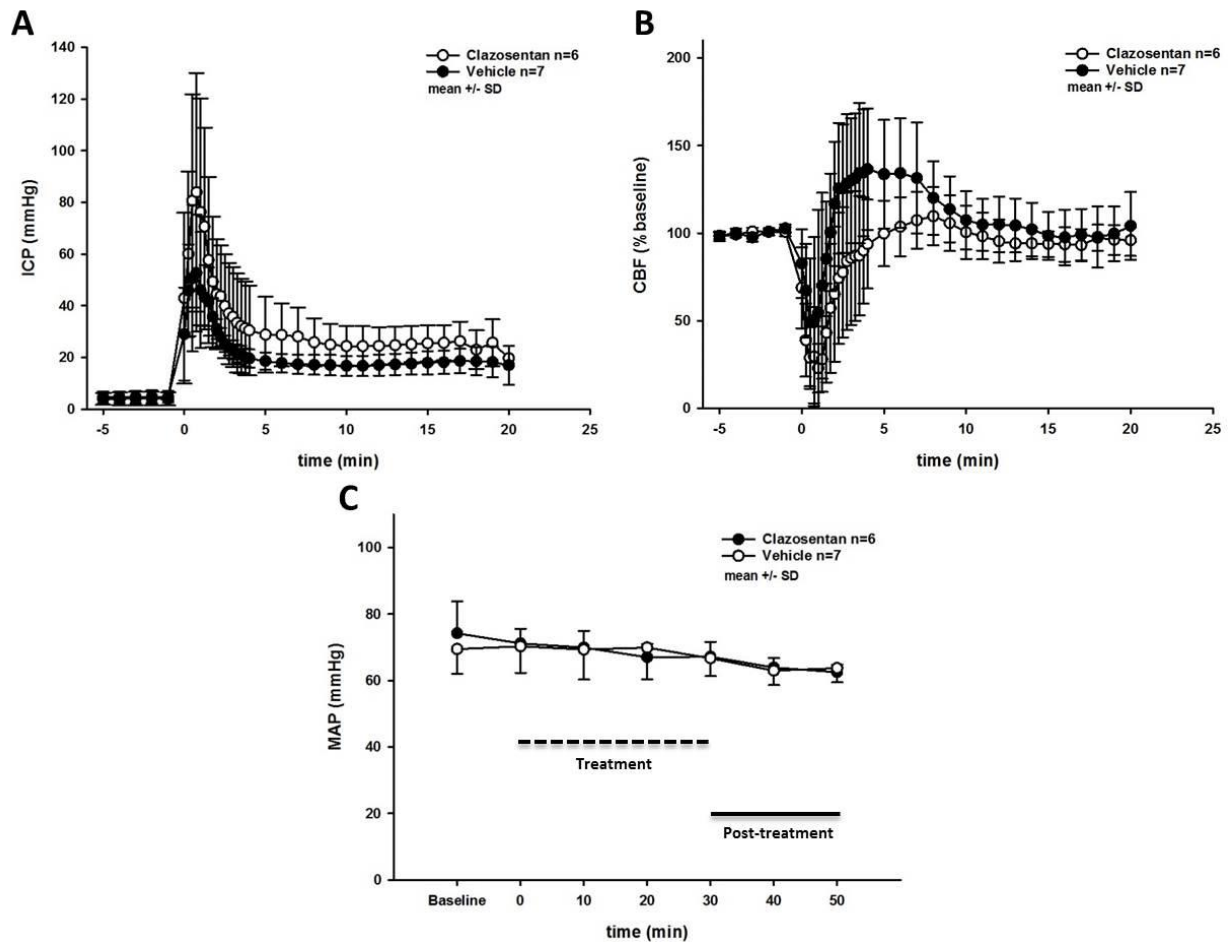


Figure 10: (A) Intracranial pressure (ICP) rapidly increased over 60mmHg and (B) regional cerebral blood flow (CBF) decrease as the middle cerebral artery was perforated. C. Continuously measured mean arterial blood pressure (MAP) was not affected by the Clazosentan infusion.

Table 2: Physiological data from Clazosentan experiment. I: MCA perforation surgery, II: Imaging period, * $p < 0.05$, ** $p < 0.01$.

	Vehicle (n=7) Mean \pm SD	Clazosentan (n=6) Mean \pm SD	P-value
<i>Body temperature (°C) I</i>	37.3 \pm 0.09	37.2 \pm 0.10	0.162
<i>Body temperature (°C) II</i>	37.3 \pm 0.14	37.2 \pm 0.09	0.636
<i>End tidal pCO₂ (mmHg) I</i>	22.6 \pm 1.96	23.0 \pm 1.07	0.776
<i>End tidal pCO₂ (mmHg) II</i>	20.9 \pm 1.04	20.9 \pm 0.73	0.792
<i>SpO₂ I</i>	97% \pm 1%	96% \pm 1%	0.154

<i>SpO₂ II</i>	97% ± 1%	97% ± 1%	0.223
<i>Respiratory Rate (times/min) I</i>	158 ± 6	160 ± 5	0.426
<i>Respiratory Rate (times/min) II</i>	161 ± 13	166 ± 9	0.537
<i>Heart Rate (beats/min) I</i>	280 ± 28	251 ± 35	0.663
<i>Blood Pressure (mmHg)II</i>	76 ± 5	75 ± 5	0.432
<i>pH</i>	7,31 ± 0,03	7,27 ± 0,03	0.248
<i>pCO₂ (mmHg)</i>	36,2 ± 3,19	34,7 ± 1,67	0.305
<i>pO₂ (mmHg)</i>	106,2 ± 10,79	108,4 ± 7,99	0.456

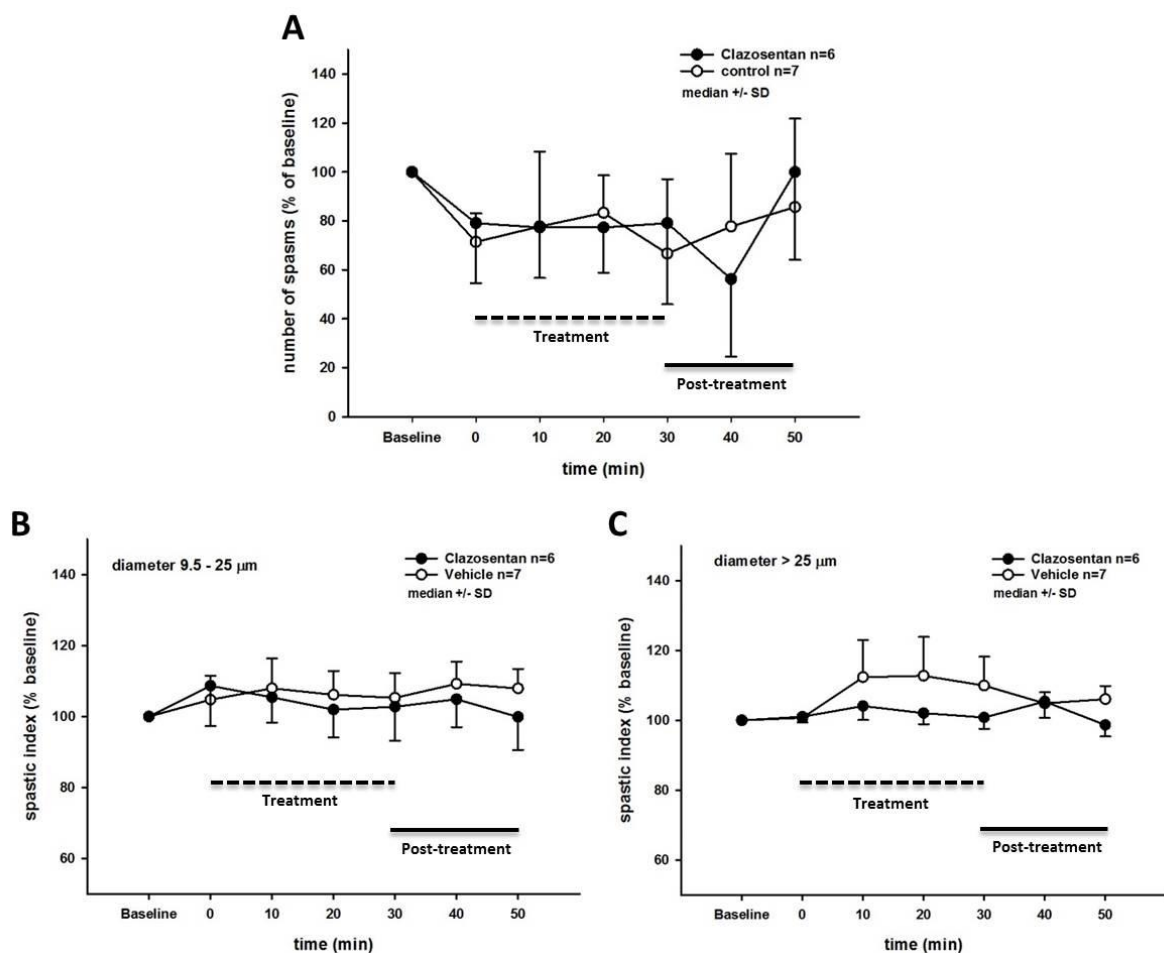


Figure 11: (A) Clazosentan does not relieve microvasospasm after SAH. The number of vasospasms as well as the spasticity index in both small-caliber (diameter 9.5-25 μ m) (B) and large-caliber vessels (diameter >25 μ m) (C) relative to baseline are not affected during treatment with Clazosentan or vehicle.

3.1.2 Microvasospasms of the pial arterioles during imaging

Three hours after MCA perforation, narrowing of cerebral arterioles, namely microvasospasms were observed under the 2PM (Figure 16 C). The amount and degree of constriction is consistent with previous studies^{77 78}. As illustrated in Figure 11 A, as soon as treatment with Clazosentan or vehicle started, the number of microvasospasms decreased by 20% compared to baseline in both groups. This effect could be due to the relatively rapid increase in total blood volume by the bolus injection. Thereafter the number of microvasospasms stayed in the same range throughout the treatment and post-treatment period and was not affected by Clazosentan treatment. Similarly, also the spastic index of small and large microvessels was not affected by infusion of Clazosentan (Figure 11 B and 11 C, respectively). Additionally, Clazosentan did not show any significant effect on the diameter of small nor large non-spastic vessels (Figure 12 A and B, respectively). This indicates that the selective blocking of the ET_A receptor does not relieve acute constriction of microvessels, suggesting the mechanism behind microvasospasm is different from that of macrovasospasm.

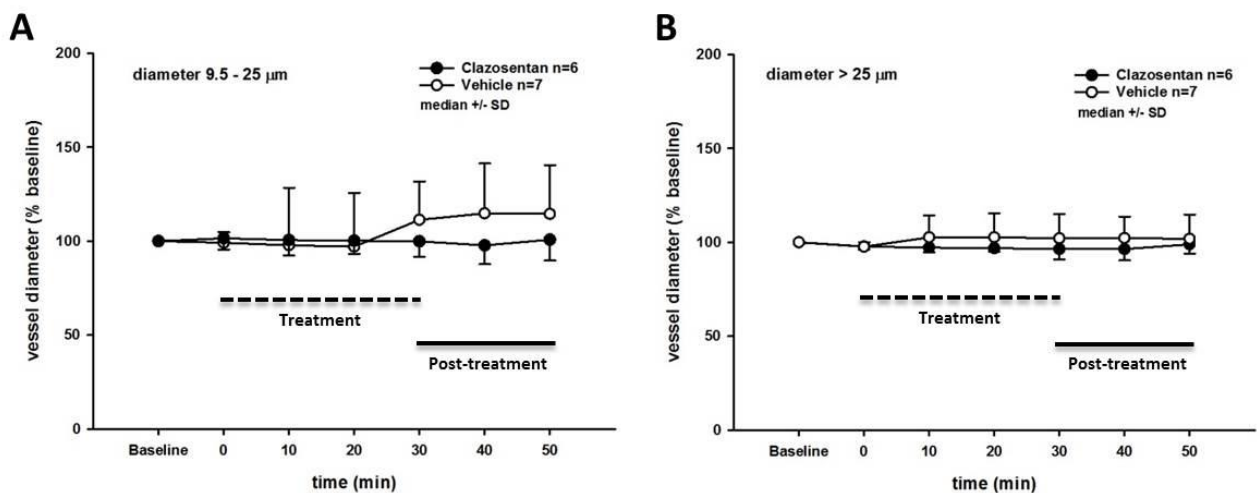


Figure 12: (A) Clazosentan does not affect the diameter (relative to baseline) of both small-caliber (B) and larger-caliber non-spastic vessel segments in mice treated with Clazosentan or vehicle.

3.2 Cisterna magna injection

3.2.1 Establishment of CMI model

A CMI model with a perivascular blood distribution pattern and without interference of the cerebral hemodynamics was established.

Table 3: Physiological data from CMI experiment. I: Surgical period of cisterna magna injection, II: Imaging period, * $p < 0.05$, ** $p < 0.01$

	aCSF (n=5) Mean \pm SD	Blood (n=8) Mean \pm SD	p-value
<i>Body temperature (°C) I</i>	37.2 \pm 0,03	37.3 \pm 0.13	0.236
<i>Body temperature (°C) II</i>	37.3 \pm 0,13	37.3 \pm 0.26	0.949
<i>End tidal pCO₂ (mmHg) II</i>	21.0 \pm 2.15	22.1 \pm 1.78	0.868
<i>SpO₂ I</i>	87% \pm 7%	86% \pm 4%	0.730
<i>SpO₂ II</i>	96% \pm 1%	97% \pm 1%	*
<i>Respiratory Rate (times/min) II</i>	197 \pm 9	174 \pm 23	0.192
<i>Heart Rate (beats/min) I</i>	369 \pm 14	340 \pm 39	0.168
<i>Blood Pressure (mmHg)II</i>	72 \pm 3	79 \pm 11	0.810
<i>pH</i>	7.27 \pm 0.02	7.32 \pm 0.06	0.140
<i>pCO₂ (mmHg)</i>	44.6 \pm 1.44	40.3 \pm 7.93	0.931
<i>pO₂ (mmHg)</i>	95.16 \pm 7.10	106.9 \pm 11.18	*
<i>pH of aCSF</i>	7.39 \pm 0.03	-	-

3.2.1.1 Physiological monitoring

Freshly prepared aCSF (pH=7.4) and heparinized blood were injected into the CSF via the cisterna magna. Physiologic parameters including body temperature, heart rate, blood pressure and SpO₂ were recorded during the CMI and the IVM imaging. All parameters were within the physiological range and there were no significant differences between groups expect for SpO₂ and pO₂ (Table 3). SpO₂ is slightly lower than the normal range during the surgical period of cisterna magna injection. This may be explained by the positioning of the mouse during the injection. The head needed to be bended by 120 ° in order to stretch the atlanto-occipital membrane and

expose the cisterna magna ^{205 212}. Bending of the head may affect the normal breathing pattern thereby resulting in reduced oxygen saturation. The difference, however, was so small that the effect may not be biologically relevant. There was also a significant difference between both groups in the blood oxygenation status at the end of the experiment. We cannot exclude the possibility that this is caused by the direct stimulation of the respiratory center around the pons and medulla during injection. Since both SpO₂ and pO₂ are within the physiological range, the difference between both groups should not have a big influence on our readout.

3.2.1.2 Blood distribution pattern and hemodynamic changes

After injection of 20 µl blood into the cisterna magna, animals were transcardially perfused with saline and 4% PFA. The brain was removed and observed under a light microscope. In theory, injected blood spreads across the whole ventricular system. On the brain surface, we found blood deposits in the cisterna magna, the gyrus of the cerebellum, and along the superior sagittal sinus (Figure 13 A and B) as well as along the pial arteries of both hemispheres (Figure 16 B). With 2PM, the blood distribution of the injected blood could be observed with higher resolution: the FITC signal was detected along pial vessels as well as inside cell-like structures which were located within the subarachnoid space (Figure 13 C). In the brain parenchyma, the FITC signal was detected in the perivascular space around penetrating arterioles and capillaries (Figure 13 D).

We measured CBF and blood flow velocity as indicators for changes of cerebral hemodynamics. A slight increase of regional CBF after the injection was observed (Figure 14 A) in both groups. This could be a result of a transient and slight increase in ICP. Blood flow velocity was measured by line-scan during two-photon imaging and did not differ between groups in all investigated vessel categories (Figure 14B).

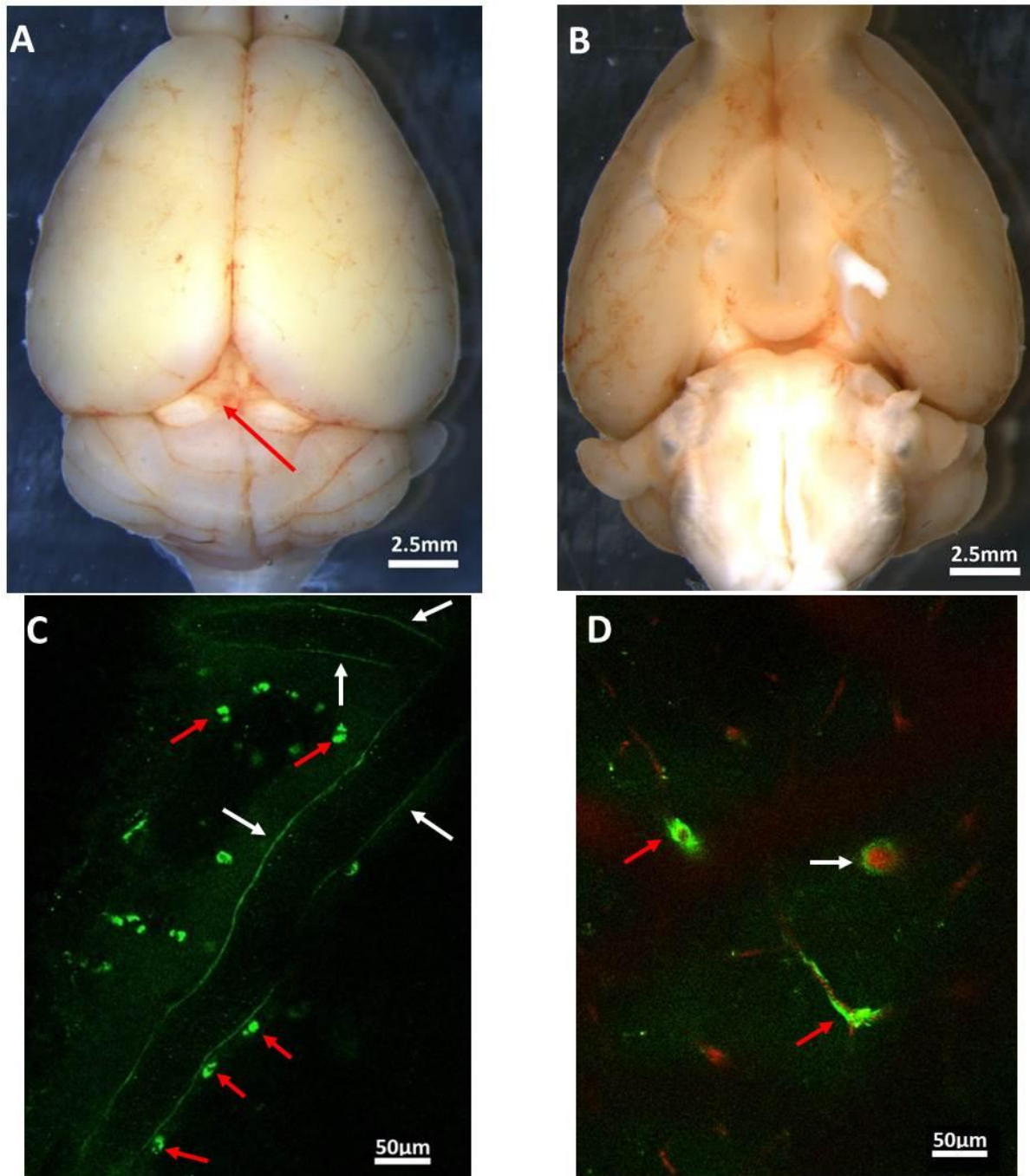


Figure 13: (A) Gross anatomy picture shows blood distribution on cortices of a brain after cisterna magna injection of blood, red arrow indicates the location of CMI. (B) Blood distribution on the ventral side of the brain after injection of blood. (C) Exemplary two-photon image of a superficial cerebral artery. Injected FITC can be detected along both sides of the vessels (white arrows) and also accumulated in cell-like structures (red arrows). (D) Exemplary two-photon image at the level of the brain parenchyma. White arrow indicated perivascular FITC dextran distribution around a penetrating artery. Red arrows indicate FITC dextran accumulating around capillaries.

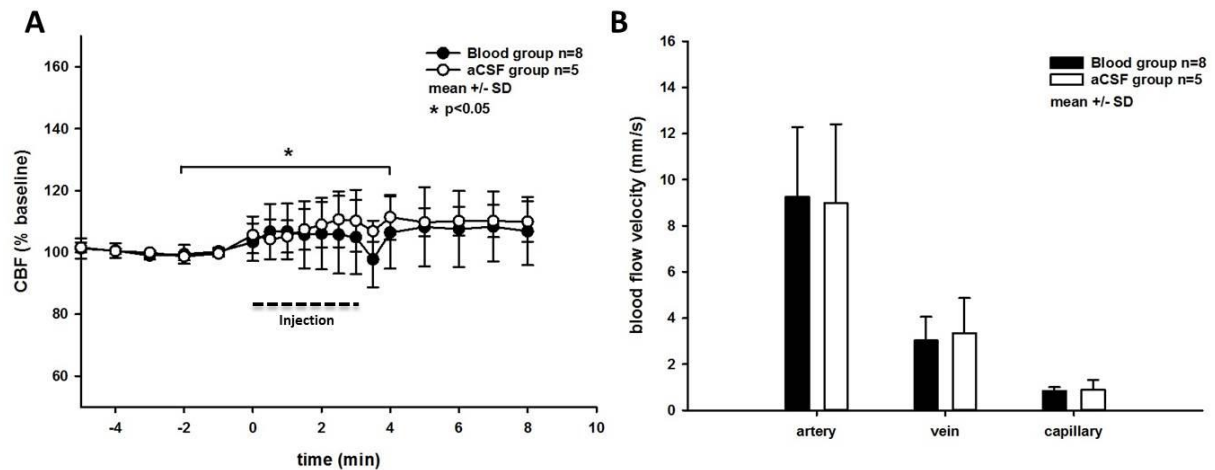


Figure 14: (A) Increase of regional CBF after cisterna magna injection of blood and aCSF. (B) Blood flow velocity in arteries, veins and capillaries: no significant difference was detected between both groups.

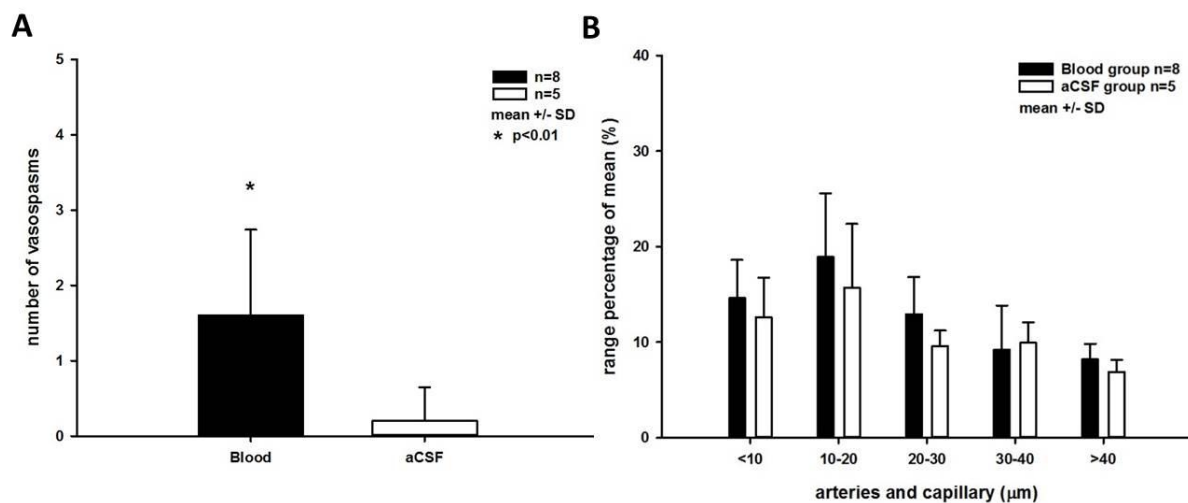


Figure 15: (A) The number of microvasospasms was increased in the blood injection group. (B) There is no significant difference in vessel diameter variability between both groups in different vessel categories.

3.2.1.3 Microvasospasms of pial arterioles

Two ROIs were recorded during IVM imaging. Three hours after cisterna magna injection, pearl-string like vasoconstrictions were observed in the blood injection group (Figure 16 D). As shown in Figure 15 A, the blood injection group had significantly more microvasospasms compared to the aCSF injection group. When looking at the variance of the vessel diameter, there is a trend that the aCSF group

has less variance, however, there is no significant difference between both groups. We think that incorporation of non-spastic vessel segments might dilute the significant difference found in the number of spastic vessel segments.

3.2.2 Comparison between CMI and perforation model

The induction of SAH by endovascular perforation is a well-established SAH mouse model which mimics the natural course after aneurysm rupture. Severe microvasospasms can be observed by intravital microscopy (Figure 16 C). As described previously massive perivascular blood distribution on the surface of perfused brains especially along the branches of the MCA were observed (Figure 16 A)²¹³. Moreover, by observing SAH brain slices that were stained with FITC lectin and TMRM dextran for extravasated blood, we found that also penetrating arterioles were surrounded by perivascular blood (Figure 17 A and C). A similar distribution pattern as well as microvasospasms was present in the cisterna magna blood injection model (Figure 16 D). Blood injected into the cisterna magna spread onto the surface of the cortex and distributed along the branches of the MCA on both hemispheres (Figure 16 B and Figure 17 B and D).

In terms of hemodynamic changes, unlike in the perforation model, injection of blood into the cisterna magna did not induce a decrease in CBF (Figure 18 A). In addition, three hours after injection of blood or aCSF, blood flow velocity did not differ between both groups (Figure 18 B and C).

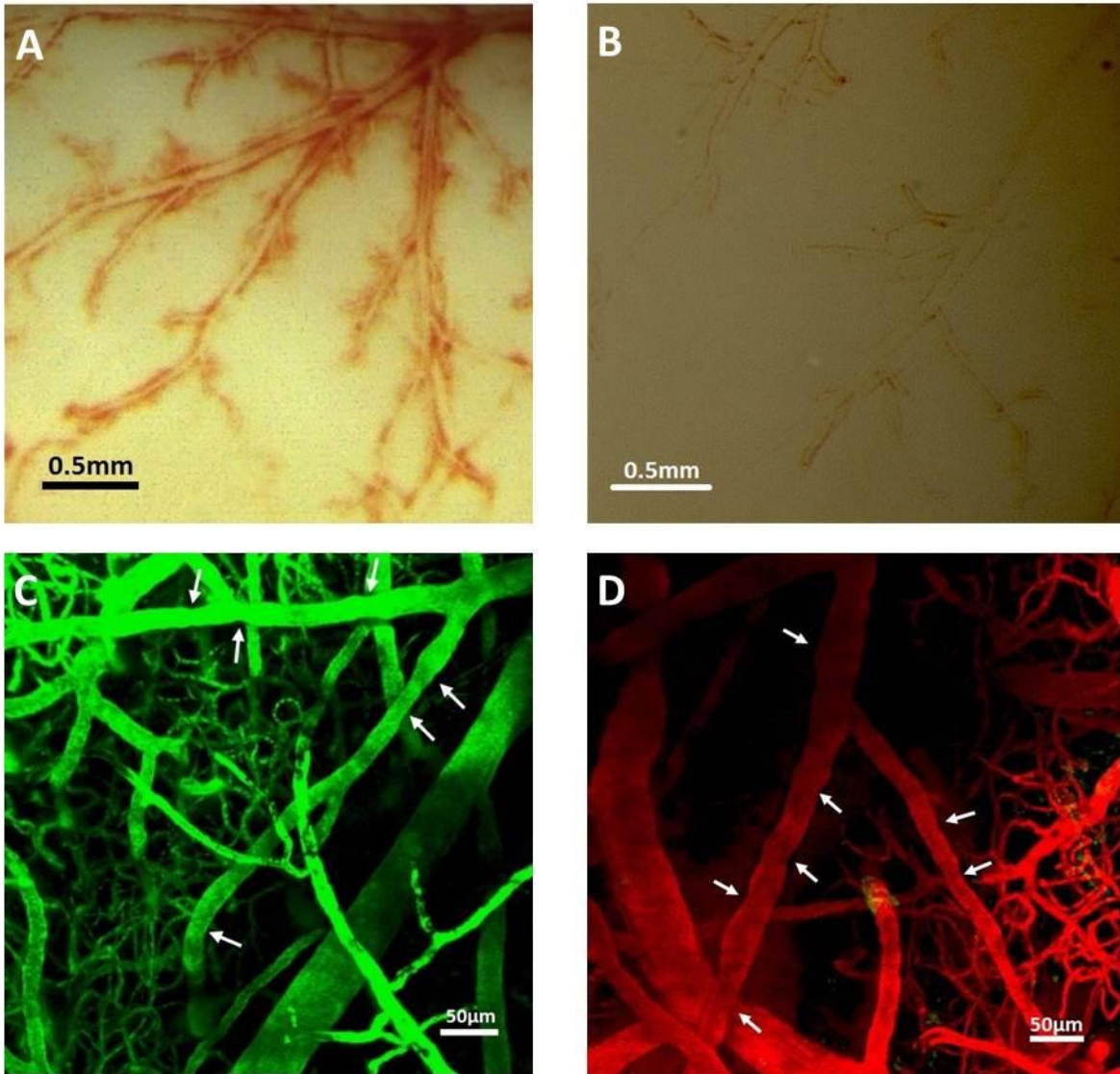


Figure 16: (A) and (B) Gross anatomy of middle cerebral arteries branches of perfused brains. Extravasated blood distributed around pial vessels in the perforation model (A). Less perivascular blood were seen in the cisterna magna blood injection model (B). (C) and (D) Microvasospasms (white arrows) were observed in both the perforation SAH model (C) and the cisterna magna blood injection model (D).

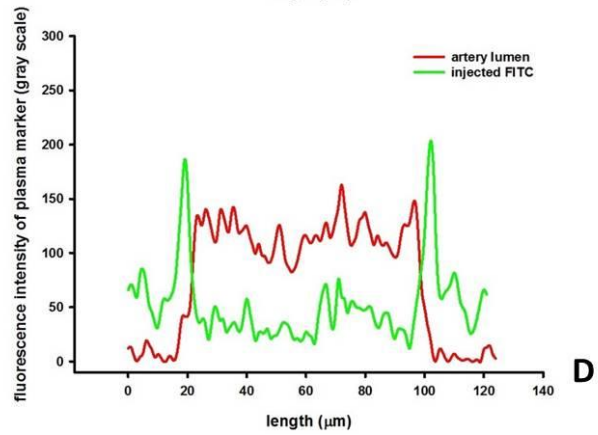
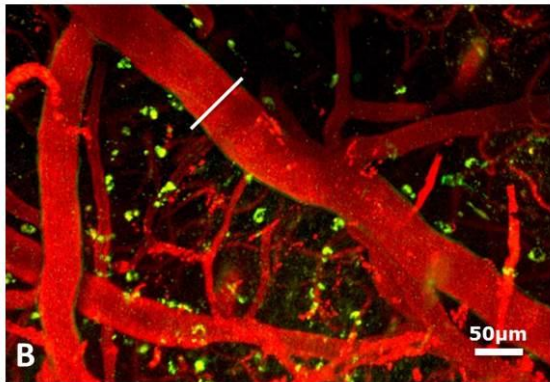
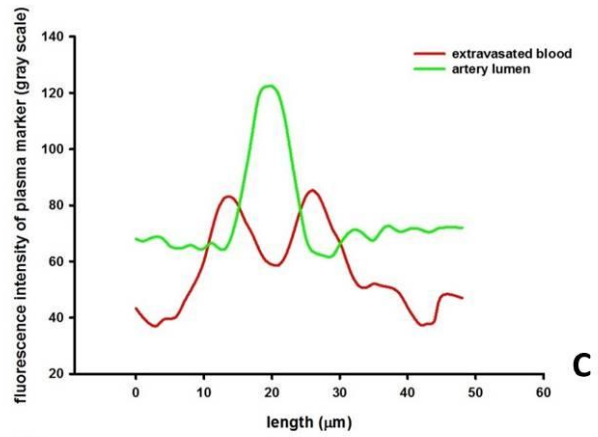
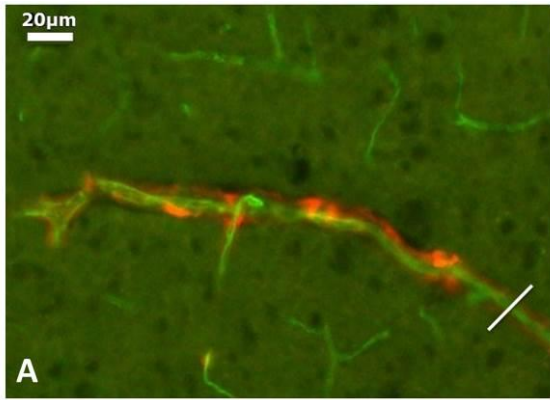


Figure 17: (A) An exemplary immunofluorescence picture of a penetrating arteriole from a mouse subjected to perforation SAH. FITC lectin (green) stains the vessel wall and TMRM (red) marks extravasated blood. (B) An exemplary two-photon image showing a superficial arteriole from a mouse subjected to cistern magna blood injection. TMRM dextran marks the vessel lumen and FITC dextran labels injected blood. (C) and (D) Fluorescence intensity was measured along the white lines depicted in (A) and (B). In (C), the FITC signal peak represents the arterial lumen and TMRM signal accumulates in two smaller peaks on both sides of the arterial lumen, representing perivascular blood distribution. The pattern is comparable in (D), TMRM signal shows the vessel lumen, and FITC is located on both sides of the arterial lumen, representing perivascular distribution of injected blood.

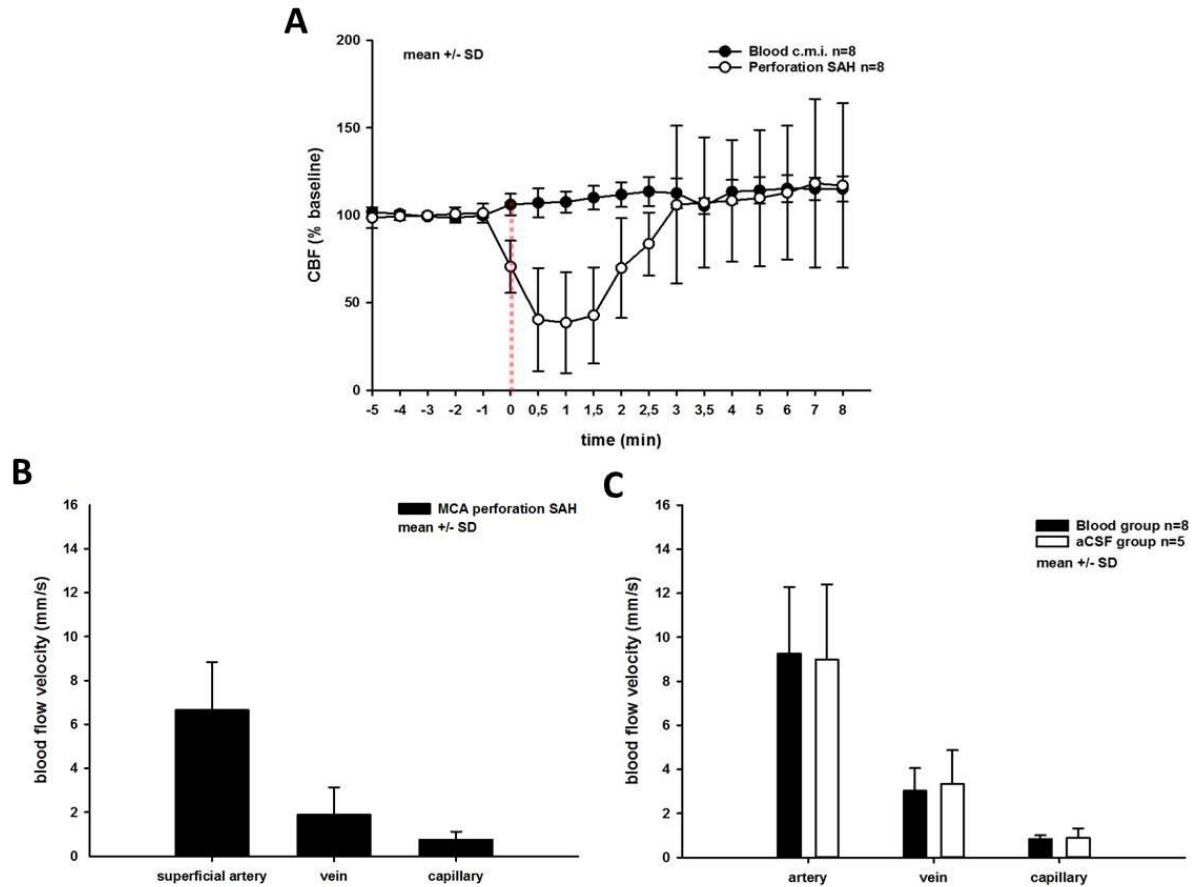


Figure 18: Quantification of hemodynamic changes in the perforation model and cisterna magna injection model. (A) In the perforation model, CBF dramatically decreased after arterial perforation (red dashed line) compared to baseline and recovered to pre-perforation levels in about three to four minutes. In the blood CMI model, CBF increased a little after injection (red dashed line) at the 30 seconds and 1 minute time points, then stays around pre-injection levels until the end of the observation period. Blood flow velocity after perforation SAH was significantly lower than after cisterna magna injection (B) and (C) and did not differ between blood and aCSF injection groups.

3.3 Deferoxamine experiment

3.3.1 Physiological monitoring

Intravenous infusion of DFO or vehicle was done in a randomized fashion before SAH. After penetration of the MCA, ICP rapidly increased (Figure 19 A) and regional CBF (rCBF) significantly decreased (Figure 19 B). Within 5 minutes, ICP dropped but still remained on a higher plateau until the end of the monitoring period. Regional CBF normalized within ten minutes after the perforation. There was no significant

difference between the DFO and vehicle group regarding ICP or rCBF (Figure 19 A and B).

Physiologic parameters including body temperature, heart rate, blood pressure and SpO₂ were recorded during SAH induction and IVM imaging. All monitored parameters and blood gases measured at the end of the imaging were in the physiologic range and did not show a difference between groups except for heart rate (Table 4). During SAH induction, heart rate is higher in the DFO group compared to the vehicle group (Table 4). We postulate that this could be a systemic side effect of DFO. Intravenous infusion of DFO was associated with mild hypotension²¹⁴, thus for compensation heart rate may increase. Because of the interference with the cardiovascular system, the filament needed to be inserted several times in the DFO group (Figure 19 C) in order to release the same amount of blood into the subarachnoid space and causes a comparable increase in ICP (Figure 19 D).

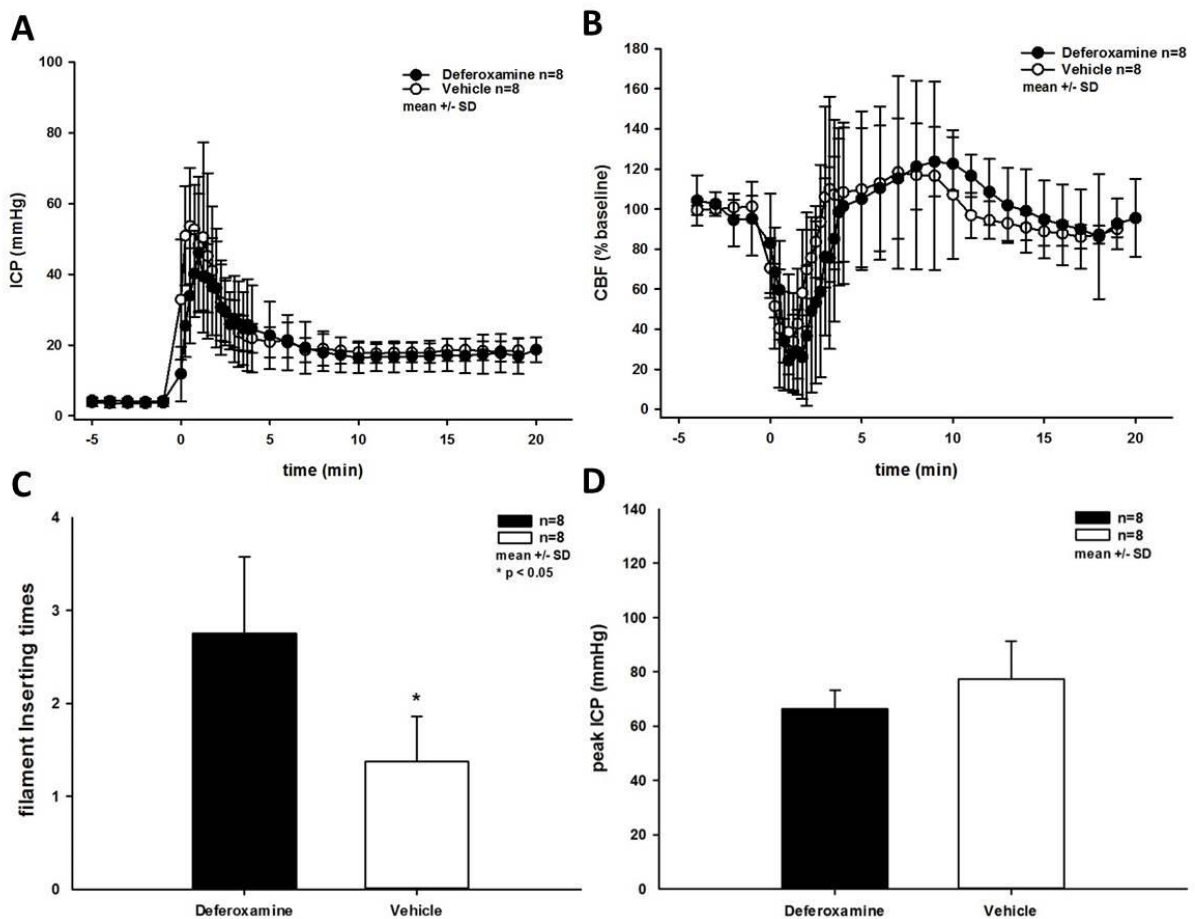


Figure 19: (A) Intracranial pressure (ICP) rapidly increased to around 60 mmHg and regional cerebral blood flow (rCBF) decreased after perforation of the MCA (B). In order to reach more or less the same level of peak ICP (D), the filament needed to be reinserted several times in the DFO group (C).

Table 4: Physiological data from DFO experiment. I: Surgical preparation of SAH, II: Imaging, * $p < 0.05$, ** $p < 0.01$.

	Vehicle (n=8) Mean \pm SD	DFO (n=8) Mean \pm SD	p-value
<i>Body temperature (°C) I</i>	37.1 \pm 0.10	37.1 \pm 0.07	0.398
<i>Body temperature (°C) II</i>	37.1 \pm 0.07	37.1 \pm 0.08	0.798
<i>End tidal pCO₂ (mmHg) I</i>	21.1 \pm 0.54	21.1 \pm 0.95	0.382
<i>End tidal pCO₂ (mmHg) II</i>	20.2 \pm 0.70	19.9 \pm 0.71	0.234
<i>SpO₂ I</i>	94% \pm 2%	93% \pm 2%	0.721
<i>SpO₂ II</i>	96% \pm 1%	96% \pm 3%	0.442
<i>Respiratory Rate (times/min) I</i>	145 \pm 7	144 \pm 3	0.803
<i>Respiratory Rate (times/min) II</i>	142 \pm 7	141 \pm 8	0.793
<i>Heart Rate (beats/min) I</i>	260 \pm 23	353 \pm 13	**
<i>Blood Pressure (mmHg)II</i>	73 \pm 6	67 \pm 7	0.078
<i>pH</i>	7.27 \pm 0.03	7.26 \pm 0.03	0.267
<i>pCO₂ (mmHg)</i>	44.2 \pm 3.83	42.3 \pm 6.78	0.499
<i>pO₂ (mmHg)</i>	95.7 \pm 13.83	101.4 \pm 18.90	0.500

3.3.2 Vessel quantification and hemodynamic changes

Three hours after MCA perforation, microvasospasms were observed with the 2PM. As illustrated in Figure 20 A, the total number of microvasospasms was significantly decreased in DFO treated animals, especially no microvasospasms were found in arterioles with a diameter larger than 30 μ m. The degree of vasospasm in the remaining vessels did not differ between groups (Figure 20 C). Since we hypothesized that DFO may relieve vasoconstriction by chelating iron, we quantified the number of vasospasms found in vessels with or without blood distributed around them. We

found that DFO resolved microvasospasms mainly in larger vessel (Figure 20 C) which were covered with blood (Figure 20 B), suggesting that DFO relieves microvasospasms only at sites where blood is present. In smaller-sized vessel segments, there is no significant difference between both groups, though there is a trend that the DFO group shows less variance in vessel diameter (Figure 20 D).

Considering that vasoconstriction may cause insufficient perfusion after SAH which could be compensated by an increase of blood flow velocity, we compared blood flow velocity and the perfusion volume of parenchymal vessels after SAH in both groups. Neither of them showed a distinguishable difference between groups in all observed vessel categories (Figure 21). We postulate that even though the iron chelating effects of DFO reduced the occurrence of vasospasm, the systemic cardiovascular side effect of DFO may have masked the expected improvement in cerebral blood flow.

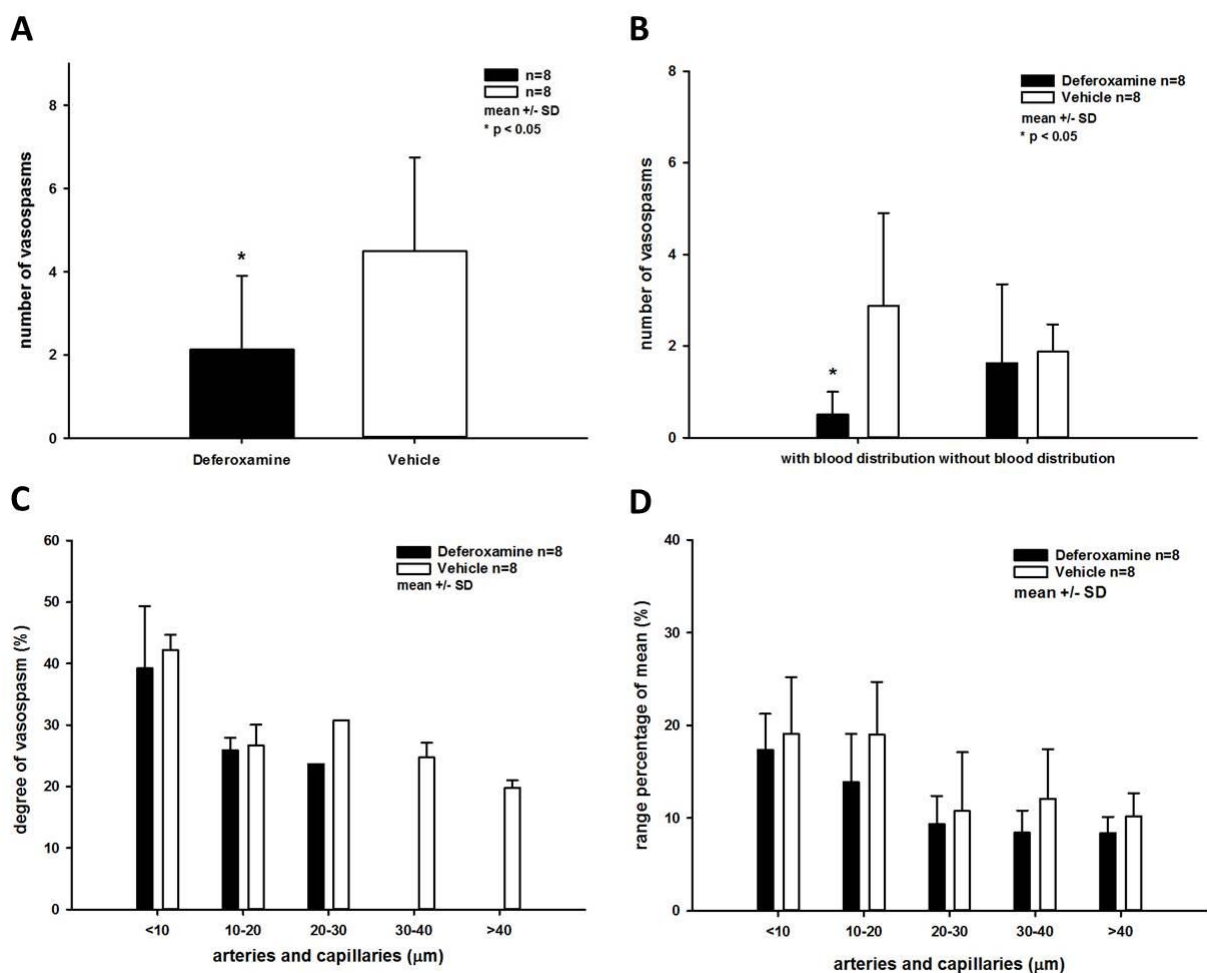


Figure 19: DFO relieved microvasospasm after SAH. (A) The number of vasospasms was reduced in the DFO treated group primarily in vessel segments that were covered with blood (B). Though the degree of vessel diameter variability does not differ between both groups, no vasospasms were found in arteries larger than 30 μ m (C). Among all measured vessels, there is no significant difference in range percentage of mean between both groups.

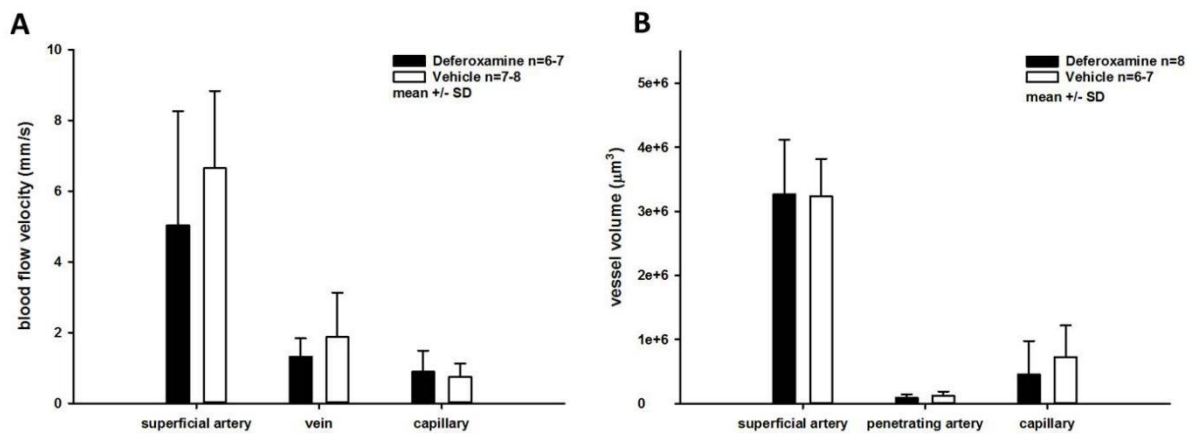


Figure 21: There is no significant difference in blood flow velocity (A) and perfusion volume (B) between the DFO and vehicle treated group.

3.3.3 Characteristic of blood distribution and investigation of erythrocytes and leukocytes after SAH

In order to investigate the blood distribution pattern in the perforation model, two-photon microscopy images were 3D reconstructed and divided in a superior layer (0-70 μ m) containing pial vessels and an inferior layer (70-140 μ m) containing parenchymal vessels. In most images we observed three patterns of blood/TMRM dextran distribution: around superficial vessels, along penetrating vessels (Figure 22 A and C) and a dotted accumulation under the dura mater (Figure 22 B). Quantification of extravasated blood in both layers showed that the majority of blood accumulated within the subarachnoid space, whereas only a small amount of the plasma marker TMRM dextran penetrated into the parenchyma (Figure 22 D)

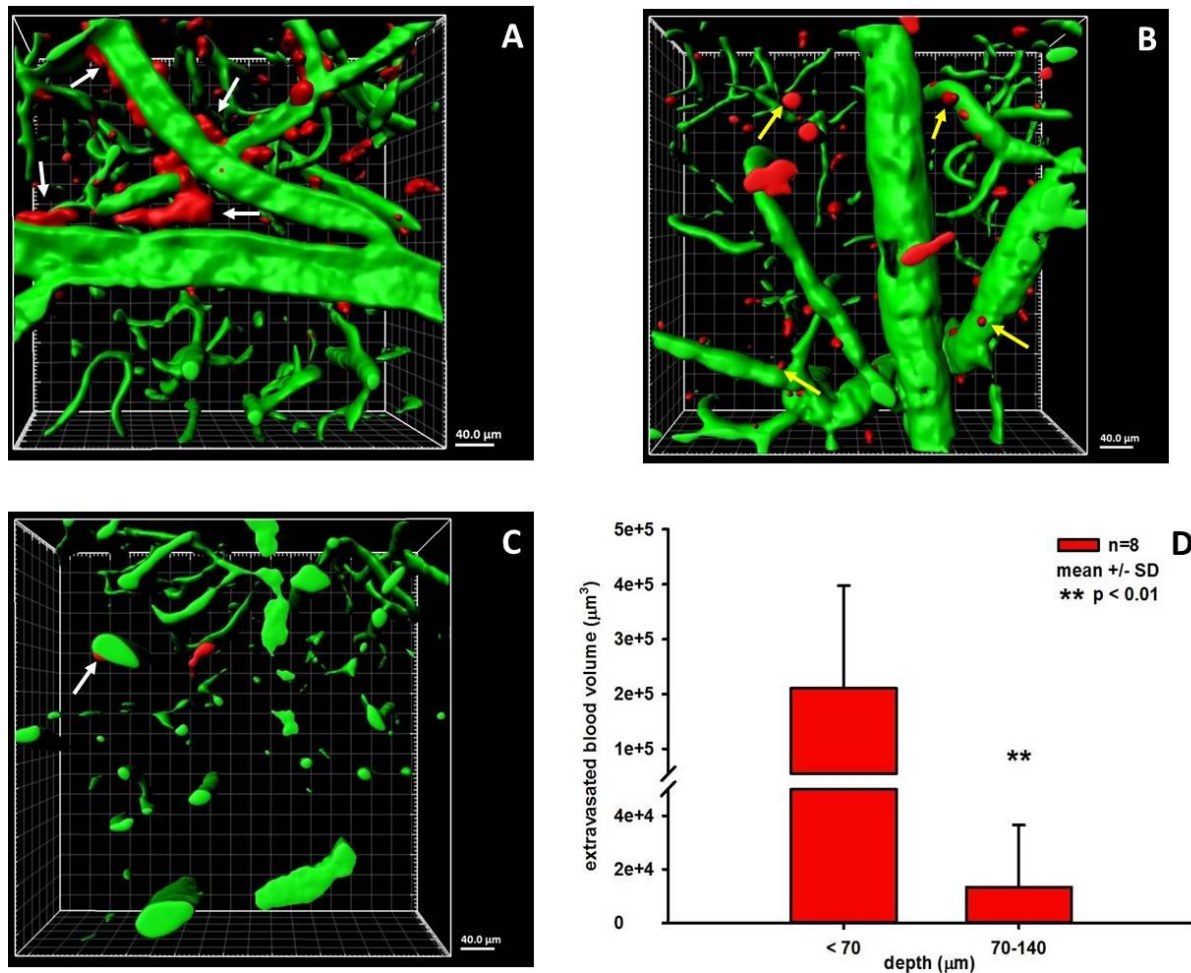


Figure 20: Exemplary 3D reconstructed two-photon images from two ROI (A, B and C) showing blood distribution patterns and the quantification of extravasated blood in superior (B) and inferior (C) layer. Extravasated blood distributed along vessels (white arrows in A and C) or accumulated in a dotted pattern (yellow arrows in B). It mainly distributes in the superior layer, only a small amount of blood penetrates deep into the parenchyma (D).

In order to further investigate this issue we applied TMRM dextran before SAH. It stains extravasated blood and labels non-perfused vessels after SAH. FITC lectin injected before sacrifice stains still perfused vessels after SAH. Non- or incompletely perfused vessels accounted for 4% of all observed vessels. There was no significant difference between hemispheres suggesting that microvascular perfusion deficits are a global phenomenon. (Figure 23)

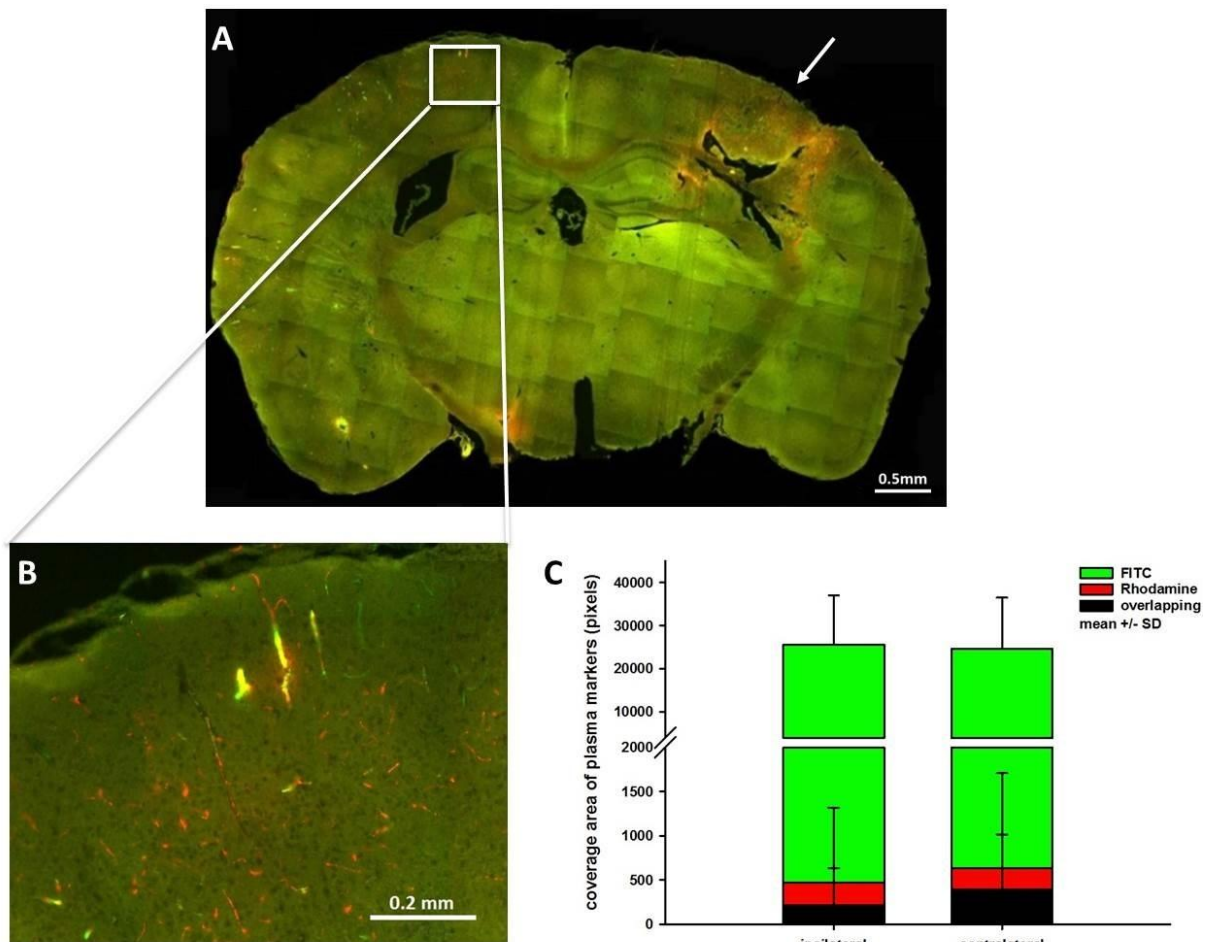


Figure 21: (A) An exemplary fluorescent section shows the damaged right hemisphere (white arrow) caused by removal of the ICP probe. TMRM dextran (red) stains extravasated blood and non-perfused vessels after SAH (A & B). FITC lectin (green) stains walls of perfused vessels (A & B). (B) A magnification of the cortical vessels (white frame in A). Large amount of non-perfused and incompletely perfused vessels (FITC and TMRM signal overlap) were found. (C) Quantification of total coverage of FITC lectin and TMRM dextran signal and their overlapping areas. No significant difference was found between both hemispheres (n=7).

TER119 stains erythrocytes therefore vessels positive for TER119 after perfusion fixation suggest a lack of perfusion at that specific time point. Collagen IV stains the vascular extracellular matrix and may therefore be used to stain the whole cerebral vasculature, i.e. perfused and non-perfused vessel segments (Figure 24). Consistent with our findings using plasma markers (Figure 23 C), the quantification using TER119 showed about 4% of non-perfused vessels after SAH. TER119 positive vessels did not differ between both hemispheres (Figure 24 C).

Since leukocyte may get stuck in capillaries and may therefor contribute to the “no - reflow” phenomenon²¹⁵, we investigated the number of capillary leukocytes after SAH by CD45 staining. In a previous in vivo study from our group, sticking and plugging leukocytes were observed in the microcirculation three hours after SAH²¹³. In the current study we tried to find the presence of leukocytes in perfused brain sections. With DAB staining, only a very small amount of CD45 positive cells were found three hours after SAH (Figure 25 A). There was no significant difference between hemispheres (Figure 25 B).

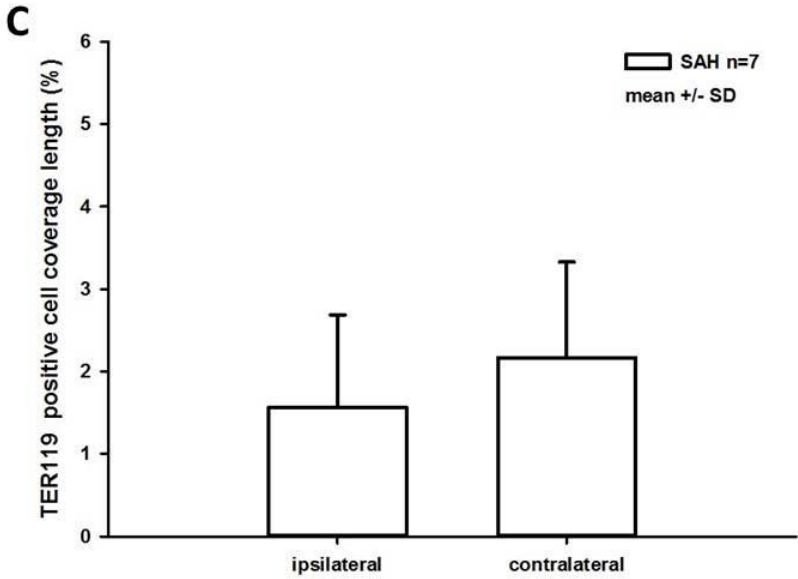
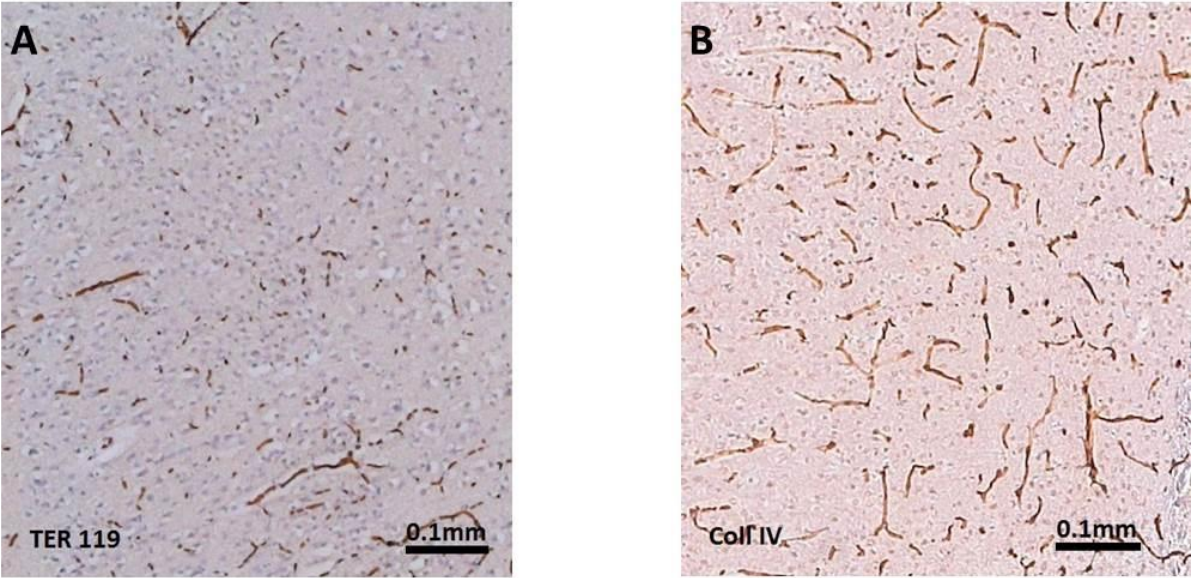


Figure 22: Exemplary DAB staining shows dotted or linear TER119 positive cells (A) and Collagen IV positive vasculature (B) TER119 positive cell coverage length does not differ between both hemispheres (C).

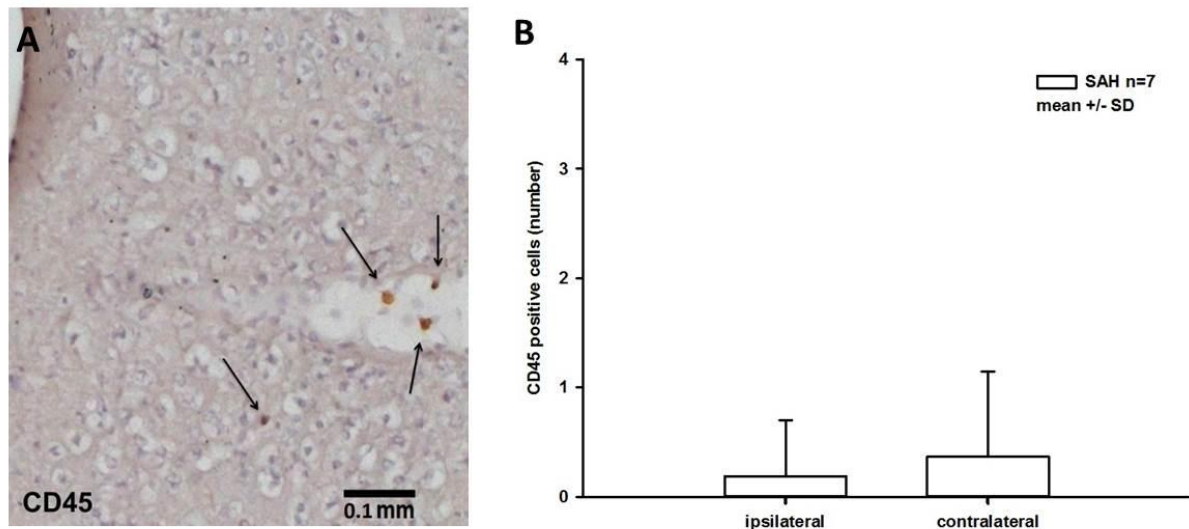


Figure 23: (A) Exemplary DAB stained section shows CD45 positive cells. (B) The number of CD45 positive cells per mice does not differ between both hemispheres.

4. Discussion

4.1 Comprehensive summary of the results

SAH is a subtype of hemorrhage with a very high mortality and disability rate which mainly affects people at working age. So far, there is no effective treatment to decrease in hospital mortality and improve patients' functional outcome.

Cerebral ischemia is the key factor in the pathophysiology of SAH. However the mechanisms causing cerebral ischemia after SAH are still unclear. Clinical and experimental studies have focused on the mechanisms of delayed cerebral ischemia (DCI) for several decades, however, we and other demonstrated that microcirculatory dysfunction occurs already within minutes after SAH and that this process may be the root for cerebral ischemia as well as other pathophysiological processes resulting in brain injury after SAH²¹⁶. In particular, our group aimed to understand the mechanisms of acute pial artery constriction, namely microvasospasm, which was

shown to be responsible for early cerebral ischemia after SAH⁷⁸. The pathophysiological process of microvasospasms and related microcirculatory dysfunction in EBI has not been investigated to date. By making use of two-photon in vivo microscopy (2PM), we are the first ones to conduct in vivo pathomechanistic research in early microcirculatory dysfunction after SAH.

In this thesis I investigated the pathomechanism underlying acute microvasospasms after SAH. Since endothelin (ET) A receptors play an important role for the formation of large artery spasms and DCI, we investigated whether these receptors are also responsible for acute microvasospasm formation by using the ET_A receptor antagonist Clazosentan. We found that inhibition of ET_A receptors does not change the number or degree of microvasospasm, therefore ET_A receptors do not seem to be involved in the development of microcirculatory dysfunction after SAH.

The outcome after SAH is determined by the acute global ischemia occurring immediately after the bleeding and the impact of extravasated blood on cerebral vessels, i.e. acute microvasospasms. In order to identify the mechanism of acute microvascular constriction after SAH without the confounding effects of global cerebral ischemia, we established a cisterna magna injection mouse model which mimics the blood distribution pattern of the MCA perforation model without causing global cerebral ischemia. With this newly developed model we were able to investigate the consequences of blood in the subarachnoid space without the initial increase in ICP which causes global cerebral ischemia and cannot be avoided in the vessel perforation model.

Therefore we were able to isolate the effect of different blood components in the subarachnoid space from the impact of rapidly increasing ICP and reduced blood flow directly after the bleeding. By using the cisterna magna blood injection model we found that injection of autologous blood but not artificial CSF into the subarachnoid space induces microvasospasm. However the vessel constrictions were not as severe

as in the filament perforation model and did not induce a drop of cerebral parenchymal perfusion.

In order to tease out which blood components induce acute vessel constriction we further tested the effect of the iron chelator Deferoxamine on microvasospasms three hours after experimental SAH. Our data show that application of Deferoxamine before SAH decreases the number of microvasospasms and relieves vasoconstriction in those pial arterioles that are covered with blood and have a diameter of 30 μm or more. This suggests that iron released from burst erythrocytes plays an important role in the formation of microvasospasms.

Taken together, we demonstrated that the ET_A receptor antagonist Clazosentan neither affects the number nor the severity of microvasospasms, suggesting that ET_A receptor are not involved in the formation of microvasospasm. Further, we described the characteristic of blood distribution after MCA perforation and cisterna magna injection in mice. Perivascular blood distribution is commonly observed and most of the blood stays on the surface of the brain instead of draining down into the parenchyma along the paravascular space (PVS). We believe that blood and its lysates, especially free iron, are potential culprits for acute vasoconstriction which interfere with the microcirculation and lead to early cerebral ischemia after SAH. Moreover, we show that the iron chelator Deferoxamine relieves microvasospasm after MCA perforation in mice, indicating that free iron plays an important role in the formation of microvasospasms. Future investigations are required to unravel the role of different hemolysis products in the pathomechanisms during EBI after SAH.

4.2 Clazosentan does not relieve microvasospasm in EBI after SAH

Delayed vasospasm has long been considered to be the key factor in DCI. Therefore reversion of arterial spasm was thought to be a promising therapeutic target for improving patients' neurological outcome after SAH. Several experimental studies identified the ET_A receptor antagonist Clazosentan as an effective vasodilator^{217 218}. In a large phase two clinical trial⁵³ known as CONSCIOUS-1 (Clazosentan to Overcome

Neurological Ischemia and Infarction Occurring after Subarachnoid Hemorrhage), Clazosentan significantly relieved SAH induced angiographic vasospasms in patients. Based on these results, we hypothesized that ET_A receptors may also be involved in the pathogenesis of early microcirculatory dysfunction. This hypothesis was supported by investigations showing that endothelin was not only elevated during delayed angiographic vasospasm^{129 130}, but already elevated early after experimental SAH^{219 220}.

Our results show that pharmacological inhibition of ET_A receptors by Clazosentan does not affect the number and severity of microvasospasms, as well as the degree of global microvascular constriction after SAH. Moreover, data from the same series of experiment three days after SAH shows no significant difference in neurological outcome between vehicle and drug treated animals²²¹. Therefore we conclude that microvasospasms do not depend on ET_A receptors. These data show that the mechanisms inducing large vessel spasm are different from those causing microvasospasm formations. Our findings are consistent with other studies showing that Clazosentan has no effect on microthrombosis, endothelial NO synthase expression, and neuronal cell death after SAH^{146 222 223}. Although pharmacologic and pharmacokinetic characteristic of Clazosentan has been studied in detail in rodents^{144 217 218}, we cannot exclude the possibility that some unrevealed side effects of Clazosentan may neutralize the beneficial effect of ET_A receptor inhibition. However it is most likely not the case because tight monitoring of a whole range of physiologic variable did not reveal any systemic side effects of Clazosentan in our experimental series.

Our experiments also confirmed the presence of microarterial constrictions starting three hours after SAH⁷⁸ and the fact that microvasospasms are associated with a severe reduction of parenchymal perfusion and impaired functional outcome after SAH^{213 224}. Our findings corroborate clinical data showing that Clazosentan did not improve outcome after SAH. These findings further highlight the importance of restoring normal microcirculatory function after SAH and explain the failure of the

CONscious trials: inhibition of ET_A receptors did not affect cerebral microcirculatory perfusion, thus ischemia and neurological outcome were not ameliorated.

4.3 Distribution and characteristic of extravasated blood and non-perfused vessels in perforation SAH model

A previous study from our group showed that a 20% reduction of pial arteriolar diameter caused by microvasospasms results in a 60% reduction of parenchymal perfusion after SAH in mice²¹³. Based on these findings, we hypothesize that relieving microvasospasm will represent a promising therapeutic target for the prevention of brain injury after SAH. In order to develop such an effective therapeutic approach, we decided to explore the mechanism underlying the formation of microvasospasm after SAH.

Since it is essential to clarify the blood distribution pattern after SAH in order to understand the structural etiology behind microvasospasm, we investigated the distribution character of extravasated blood after perforation SAH in detail. Three hours after the arterial perforation, a larger amount of subarachnoid blood distributed along pial vessels, whereas a smaller amount invaded into the parenchyma along penetrating arteries through the perivascular space (PVS), a continuous space surrounding cerebral vessels connecting arteries, capillaries and veins^{225 226}. The PVS is the anatomic correlate of the glymphatic system, a drainage system using the CSF to clear interstitial solutes from the brain^{227 228}. Our finding is consistent with a previous histological report showing the presence of blood draining within the brain parenchyma after SAH in mice²²⁹. In addition to these previous findings we used a tracer based method to indeed prove that subarachnoid blood enters the brain parenchyma after SAH and quantified and compared the volume of intraparenchymal blood. Our data demonstrate that there is an order-of-magnitude difference between the amount of blood found on the surface of the brain as compared to the amount found within the brain parenchyma. This observation may be explained by the limited capacity of the PVS to transport blood together with an impaired CSF circulation after SAH. Only molecules with a size of less than 100 kDa

may enter the PVS. The permeability of the PVS has also been shown to be changed after SAH^{228 229}. This is in agreement with experiments showing that the glymphatic flow is severely impaired already two hours after SAH in the macaca fascicularis and is associated with perivascular blood clots²³⁰.

Our group previously found that 30% of spastic pial arterioles were occluded by microthrombosis three hours after SAH. In the current study investigating microthrombosis within the brain parenchyma by examining TMRM dextran marked vessels and the ratio of TER119 positive cells to Collagen IV stained vasculature at the same time point we found only 4% not perfused vessels. Based on the fact that the expression of collagen IV in basal lamina starts to decrease three hours after SAH²³¹, the actual percentage of non-perfused vessel could even be lower. These numbers are in contrast with a study using the blood injection model, where 15% of parenchymal vessels were reported to be not perfused under 2PM²³². This discrepancy between the in vivo tracer study and the histological studies may be explained by the fact that most of the not perfused vessels observed in vivo are not completely blocked and may therefore be flushed open by transcardial perfusion.

In addition to microthrombosis also leukocytes may be important factors for microcirculatory dysfunction after SAH. They were found in the CSF of SAH patients and in the subarachnoid space of SAH animals from day one to three after the bleeding^{233 234}. Recently more studies started to look into leukocyte migration into the brain parenchyma shortly after SAH. A prominent amount of neutrophil is accumulating in the cerebral microcirculation already ten minutes after SAH and is believed to play a role in early vascular injury¹⁵⁵. Leukocytes were shown to roll and stick inside pial venules and interact with platelets two hours after SAH¹¹². Del Zoppo et al. reported that leukocytes which are sticking inside capillaries can block perfusion and are involved in formation of microthrombi²¹⁵. A previous study from our group presents a small amount of leukocyte plugging in parenchymal capillaries²¹³. Our immunohistological results demonstrate a consistent finding that not many CD45 positive cells migrate into the parenchyma in the early phase after the bleeding. Our

data of perivascular blood distribution, non-perfused vessels and CD45 positive cells suggest that cerebral vasculature is undergoing pathological changes which are caused by nearby extravasated blood.

4.4 Cisterna magna injection model

The endovascular perforation SAH model is the best available animal model to mimic the rupture of an intracranial aneurysm, though it has the inherent shortcoming that the bleeding volume cannot be controlled. Another commonly used SAH model, the cisterna magna blood injection model, does not mimic aneurysm rupture, but has the advantage that ICP and blood volume can be tightly controlled.

In the perforation SAH mouse model, immediately after perforation of the circle of Willis ICP rises close to arterial blood pressure. Concomitantly, CPP drops and CBF is reduced by over 80%⁷⁹. In the cisterna magna blood injection mouse model, a 50 μ l injection of blood over 15 seconds induces an immediate ICP increase up to 100 mmHg which also goes along with a severe decrease of CBF²³⁵. Both animal models are widely used and both exhibit initial perfusion deficits during the bleeding.

In the current study we aimed to establish a model that mimics the blood distribution pattern of SAH but does not cause early perfusion deficits in order to investigate the role of blood on the cerebral microcirculation without the confounder of a previous global ischemic insult.

We injected 20 μ l of blood into the cisterna magna over three minutes. This procedure induced only a slight change of ICP while sufficient perivascular blood was present in the brain after perfusion fixation. When we added the plasma marker FITC dextran to the injected blood we were able to investigate the distribution of the injected blood by intravital fluorescence microscopy. This allowed us to investigate for the first time the distribution of blood in the subarachnoid space. Surprisingly, the blood did not distribute homogeneously within the subarachnoid space, but it spread preferentially along subarachnoid arteries. This finding shows that the subarachnoid space is not an open space which allows free diffusion of liquids, but that it is

compartmentalized and allows liquids to spread preferentially along vessels, more specifically, along arteries. More importantly for the context of the current study, we were able to show that distribution of blood within the subarachnoid perivascular space leads to the formation of microvasospasm. In shape and distribution these microvasospasms were identical to microvasospasms observed in the filament perforation SAH model and in humans. Since cisternal blood does not induce a drop in CBF we can conclude that post-hemorrhagic microvasospasms are induced by perivascular blood and not by the global ischemia which occurs immediately after SAH. This conclusion is further supported by the fact that number and severity of microvasospasms found after SAH seem to depend on the amount of perivascular blood, since we found significant more arteriolar vasospasms in the vessel perforation model of SAH, which displays more perivascular blood, than in the blood injection model where only 20 μ l were injected. Less perivascular blood may represent a lower burden for the local Hb scavenging systems and may interfere less with the clearance capacity of the glymphatic system. Accordingly, the reduction of perivascular blood may represent a valid therapeutic target for the treatment of SAH.

One shortcoming of the current experiments was that we flushed the catheters used to inject the blood into the cisterna magna with heparin. It is known that already a low dose of heparin is able to bind Hb and inflammatory molecules and may therefore mitigate vasospasm after SAH²³⁶⁻²³⁸. Future studies using different anticoagulants may help to further improve this model.

In summary, the CMI model is easy to perform and highly reproducible. It does not lead to a decrease in CBF, but has a similar blood distribution pattern as the perforation SAH model. Therefore it is very well suited to investigate the pathomechanisms of microvasospasms after SAH.

4.5 Deferoxamine relieves microvasospasm in EBI after SAH

Topical application of erythrocyte lysates causes immediate severe basilar arterial spasms and vasoconstriction of pial arteries^{96 168} After SAH free blood is effectively

eliminated by microglia¹¹⁷. The degradation works through the CD163-Hp-Hb system and the intracellular enzyme HO-1, which degrade Hb into bilirubin, carbon monoxide and free iron. Iron is also found to be immediately released from hemoglobin during the lysis of erythrocytes²³⁹. Beside its direct cytotoxicity, free iron has been shown to activate oxidation reaction and generate reactive oxygen species which contribute to the formation of cerebral arteriolar vasoconstriction^{195 240}.

After SAH in patients, free iron is detected in the CSF one day after the bleeding and keeps increasing for at least 5 days.^{241 242} Iron chelators have successfully been shown to reduce oxidative stress, neurodegeneration and delayed arterial vasospasm after SAH^{194-198 214 243 244}. We now aimed to investigate the effect of iron chelation on the formation of microvasospasms during EBI after SAH. Our data demonstrate that Deferoxamine (DFO), a water soluble iron chelator, reduced vasospasm only in larger arterioles which were surrounded by extravasated blood following SAH. This suggests that hemolysis induced iron overload plays an important role in the formation of microvasospasm. Since this effect was only observed in vessels larger than 30 μm these findings also indicate that the mechanisms underlying vasospasm in larger arterioles and capillaries are different.

The only difference between the vehicle and DFO treated animals was a significant increase of heart rate in the DFO group during the surgery. We believe that the increase in heart rate is a compensatory response to the known mild blood-pressure-lowering effects induced by intravenous application of DFO²¹⁴. We measured blood pressure in both groups and found no significant effect at the time of imaging, however, in order to reach the target peak ICP the filament needed to be reinserted several times in the DFO group. Since the peak ICP after MCA perforation depends on systemic blood pressure we assume that the MAP was lower in the DFO group during the time of SAH induction. This side effect of DFO could explain why there were no differences in both blood flow velocity and perfused vessel volume between the DFO and vehicle group even though DFO reduced the number of vasospasm. Additionally, DFO has a direct cellular toxicity and can cause severe toxicity in normal-dose-

patients with a low iron burden²⁴⁵. Moreover different studies showed that hemin could bind to DFO and together promote protein oxidation and generate cytotoxic radicals²⁵⁰⁻²⁵². Even though in the current study DFO was used as a tool for mechanistic research, these possible side effects of DFO need to be considered.

Our data using DFO suggest that blood which extravasates after SAH into the subarachnoid space distributes within the perivascular space of pial vessels and then penetrates into the brain parenchyma. In vitro experiments showed that pretreatment with DFO could prevent erythrocyte membrane damage and hemolysis by reducing lipid peroxidation²⁴⁶. In our current study, we injected DFO systemically before SAH to ensure that the drug evenly distributes in the subarachnoid space together with the extravasated blood. As soon as hemolysis starts, released free ferric iron is scavenged by DFO and iron mediated molecular reactions are most likely completely prevented. DFO mainly binds ferric iron, while ferrous iron catalyzes reactive oxygen species formation and is considered to be more toxic than the ferric form. Contrary to this Fox et al. showed that topic application of ferric iron causes mild cerebral arterial vasoconstriction whereas ferrous iron solution causes no changes²⁴⁷. Almost all studies investigating the vasospasm relieving effect of both ferrous and ferric iron chelators were performed in large arterial vasospasm models. According to our results, the ferric iron chelator DFO showed the ability to relieve microvasospasms during EBI after SAH and that this is most probably due to its iron chelating effect. In combination with the CMI model we established, further studies aiming at identifying the therapeutic effect of DFO will reveal important findings on the pathomechanisms behind microvasospasms.

4.6 Conclusion

In summary, our data show that after SAH, the majority of extravasated blood distributed along pial vessels, only a small amount penetrated into the brain parenchyma via the perivascular space. Relieving microvasospasm is the key to maintain the normal function of the cerebral microcirculation and improve outcome after SAH. Our current data show that the development of microvasospasm after SAH

does not depend on ET_A receptors but is related to the hemolysis product ferric iron. Meanwhile, without ICP induced initial cerebral ischemia, a small amount of perivascular blood components alone can cause microvasospasm within hours. In the future this CMI model can be used for in vivo studies of vasospasm and the pathomechanisms that cause microvascular dysfunction after SAH.

5. References

1. Tsvigoulis G, Patousi A, Pikilidou M, et al. Stroke Incidence and Outcomes in Northeastern Greece: The Evros Stroke Registry. *Stroke* 2018;49(2):288-95. doi: 10.1161/STROKEAHA.117.019524
2. Farhoudi M, Mehrvar K, Sadeghi-Bazargani H, et al. Stroke subtypes, risk factors and mortality rate in northwest of Iran. *Iran J Neurol* 2017;16(3):112-17.
3. Krishnamurthi RV, Barker-Collo S, Parag V, et al. Stroke Incidence by Major Pathological Type and Ischemic Subtypes in the Auckland Regional Community Stroke Studies: Changes Between 2002 and 2011. *Stroke* 2018;49(1):3-10. doi: 10.1161/STROKEAHA.117.019358
4. Lantigua H, Ortega-Gutierrez S, Schmidt JM, et al. Subarachnoid hemorrhage: who dies, and why? *Crit Care* 2015;19:309. doi: 10.1186/s13054-015-1036-0
5. Stienen MN, Germans M, Burkhardt JK, et al. Predictors of In-Hospital Death After Aneurysmal Subarachnoid Hemorrhage: Analysis of a Nationwide Database (Swiss SOS [Swiss Study on Aneurysmal Subarachnoid Hemorrhage]). *Stroke* 2018;49(2):333-40. doi: 10.1161/STROKEAHA.117.019328
6. Vergouwen MD, Jong-Tjien-Fa AV, Algra A, et al. Time trends in causes of death after aneurysmal subarachnoid hemorrhage: A hospital-based study. *Neurology* 2016;86(1):59-63. doi: 10.1212/WNL.0000000000002239
7. Ridwan S, Urbach H, Greschus S, et al. Health Care Costs of Spontaneous Aneurysmal Subarachnoid Hemorrhage for Rehabilitation, Home Care, and In-Hospital Treatment for the First Year. *World neurosurgery* 2017;97:495-500. doi: 10.1016/j.wneu.2016.09.123
8. Al-Khindi T, Macdonald RL, Schweizer TA. Cognitive and functional outcome after aneurysmal subarachnoid hemorrhage. *Stroke* 2010;41(8):e519-36. doi: 10.1161/STROKEAHA.110.581975
9. Nieuwkamp DJ, Setz LE, Algra A, et al. Changes in case fatality of aneurysmal subarachnoid haemorrhage over time, according to age, sex, and region: a meta-analysis. *Lancet Neurol* 2009;8(7):635-42. doi: 10.1016/S1474-4422(09)70126-7
10. Wiebers DO, Torner JC, Meissner I. Impact of unruptured intracranial aneurysms on public health in the United States. *Stroke* 1992;23(10):1416-9.
11. Bikmaz K, Erdem E, Krisht A. Arteriovenous fistula originating from proximal part of the anterior cerebral artery. *Clin Neurol Neurosurg* 2007;109(7):589-91. doi: 10.1016/j.clineuro.2007.04.002
12. Rogers LR. Cerebrovascular complications in patients with cancer. *Semin Neurol* 2010;30(3):311-9. doi: 10.1055/s-0030-1255224
13. Jung JY, Kim YB, Lee JW, et al. Spontaneous subarachnoid haemorrhage with negative initial angiography: a review of 143 cases. *J Clin Neurosci* 2006;13(10):1011-7. doi: 10.1016/j.jocn.2005.09.007
14. Sergides IG, Minhas PS, Anotun N, et al. Pituitary apoplexy can mimic subarachnoid haemorrhage clinically and radiologically. *Emerg Med J* 2007;24(4):308. doi: 10.1136/emj.2006.036616
15. Karabatsou K, Lecky BR, Rainov NG, et al. Cerebral amyloid angiopathy with symptomatic or occult subarachnoid haemorrhage. *Eur Neurol* 2007;57(2):103-5. doi: 10.1159/000098060

16. Macdonald RL, Schweizer TA. Spontaneous subarachnoid haemorrhage. *Lancet* 2017;389(10069):655-66. doi: 10.1016/S0140-6736(16)30668-7
17. Vlak MH, Algra A, Brandenburg R, et al. Prevalence of unruptured intracranial aneurysms, with emphasis on sex, age, comorbidity, country, and time period: a systematic review and meta-analysis. *Lancet Neurol* 2011;10(7):626-36. doi: 10.1016/S1474-4422(11)70109-0
18. Alfano JM, Kolega J, Natarajan SK, et al. Intracranial aneurysms occur more frequently at bifurcation sites that typically experience higher hemodynamic stresses. *Neurosurgery* 2013;73(3):497-505. doi: 10.1227/NEU.0000000000000016
19. Chatziprodromou I, Poulikakos D, Ventikos Y. On the influence of variation in haemodynamic conditions on the generation and growth of cerebral aneurysms and atherogenesis: a computational model. *J Biomech* 2007;40(16):3626-40. doi: 10.1016/j.jbiomech.2007.06.013
20. Watton PN, Ventikos Y, Holzapfel GA. Modelling the growth and stabilization of cerebral aneurysms. *Math Med Biol* 2009;26(2):133-64. doi: 10.1093/imammb/dqp001
21. Kissela BM, Sauerbeck L, Woo D, et al. Subarachnoid hemorrhage: a preventable disease with a heritable component. *Stroke* 2002;33(5):1321-6.
22. Broderick JP, Viscoli CM, Brott T, et al. Major risk factors for aneurysmal subarachnoid hemorrhage in the young are modifiable. *Stroke* 2003;34(6):1375-81. doi: 10.1161/01.STR.0000074572.91827.F4
23. Linn FH, Wijdicks EF, van der Graaf Y, et al. Prospective study of sentinel headache in aneurysmal subarachnoid haemorrhage. *Lancet* 1994;344(8922):590-3.
24. Polmear A. Sentinel headaches in aneurysmal subarachnoid haemorrhage: what is the true incidence? A systematic review. *Cephalalgia* 2003;23(10):935-41. doi: 10.1046/j.1468-2982.2003.00596.x
25. Linn FH, Rinkel GJ, Algra A, et al. Headache characteristics in subarachnoid haemorrhage and benign thunderclap headache. *J Neurol Neurosurg Psychiatry* 1998;65(5):791-3.
26. Ostergaard JR. Headache as a warning symptom of impending aneurysmal subarachnoid haemorrhage. *Cephalalgia* 1991;11(1):53-5. doi: 10.1046/j.1468-2982.1991.1101053.x
27. van Gijn J, Kerr RS, Rinkel GJ. Subarachnoid haemorrhage. *Lancet* 2007;369(9558):306-18. doi: 10.1016/S0140-6736(07)60153-6
28. Landtblom AM, Fridriksson S, Boivie J, et al. Sudden onset headache: a prospective study of features, incidence and causes. *Cephalalgia* 2002;22(5):354-60. doi: 10.1046/j.1468-2982.2002.00368.x
29. Pinto AN, Canhao P, Ferro JM. Seizures at the onset of subarachnoid haemorrhage. *J Neurol* 1996;243(2):161-4.
30. Butzkueven H, Evans AH, Pitman A, et al. Onset seizures independently predict poor outcome after subarachnoid hemorrhage. *Neurology* 2000;55(9):1315-20.
31. McCarron MO, Alberts MJ, McCarron P. A systematic review of Terson's syndrome: frequency and prognosis after subarachnoid haemorrhage. *J Neurol Neurosurg Psychiatry* 2004;75(3):491-3.
32. Medele RJ, Stummer W, Mueller AJ, et al. Terson's syndrome in subarachnoid hemorrhage and severe brain injury accompanied by acutely raised intracranial pressure. *J Neurosurg* 1998;88(5):851-4. doi: 10.3171/jns.1998.88.5.0851
33. Khechinashvili G, Asplund K. Electrocardiographic changes in patients with acute stroke: a systematic review. *Cerebrovasc Dis* 2002;14(2):67-76.
34. Toussaint LG, 3rd, Friedman JA, Wijdicks EF, et al. Survival of cardiac arrest after aneurysmal subarachnoid hemorrhage. *Neurosurgery* 2005;57(1):25-31; discussion 25-31.
35. Larsen CC, Astrup J. Rebleeding after aneurysmal subarachnoid hemorrhage: a literature review. *World neurosurgery* 2013;79(2):307-12. doi: 10.1016/j.wneu.2012.06.023
36. van Gijn J, Hijdra A, Wijdicks EF, et al. Acute hydrocephalus after aneurysmal subarachnoid hemorrhage. *J Neurosurg* 1985;63(3):355-62. doi: 10.3171/jns.1985.63.3.0355

37. Pegoli M, Mandrekar J, Rabinstein AA, et al. Predictors of excellent functional outcome in aneurysmal subarachnoid hemorrhage. *J Neurosurg* 2015;122(2):414-8. doi: 10.3171/2014.10.JNS14290
38. Hop JW, Rinkel GJ, Algra A, et al. Initial loss of consciousness and risk of delayed cerebral ischemia after aneurysmal subarachnoid hemorrhage. *Stroke* 1999;30(11):2268-71.
39. Brouwers PJ, Wijdicks EF, Van Gijn J. Infarction after aneurysm rupture does not depend on distribution or clearance rate of blood. *Stroke* 1992;23(3):374-9.
40. Vergouwen MD, Vermeulen M, van Gijn J, et al. Definition of delayed cerebral ischemia after aneurysmal subarachnoid hemorrhage as an outcome event in clinical trials and observational studies: proposal of a multidisciplinary research group. *Stroke* 2010;41(10):2391-5. doi: 10.1161/STROKEAHA.110.589275
41. Vermeulen M, van Gijn J. The diagnosis of subarachnoid haemorrhage. *J Neurol Neurosurg Psychiatry* 1990;53(5):365-72.
42. Long B, Koyfman A, Runyon MS. Subarachnoid Hemorrhage: Updates in Diagnosis and Management. *Emergency medicine clinics of North America* 2017;35(4):803-24. doi: 10.1016/j.emc.2017.07.001 [published Online First: 2017/10/11]
43. Backes D, Rinkel GJ, Kemperman H, et al. Time-dependent test characteristics of head computed tomography in patients suspected of nontraumatic subarachnoid hemorrhage. *Stroke* 2012;43(8):2115-9. doi: 10.1161/STROKEAHA.112.658880
44. Mitchell P, Wilkinson ID, Hoggard N, et al. Detection of subarachnoid haemorrhage with magnetic resonance imaging. *J Neurol Neurosurg Psychiatry* 2001;70(2):205-11.
45. Westerlaan HE, van Dijk JM, Jansen-van der Weide MC, et al. Intracranial aneurysms in patients with subarachnoid hemorrhage: CT angiography as a primary examination tool for diagnosis--systematic review and meta-analysis. *Radiology* 2011;258(1):134-45. doi: 10.1148/radiol.10092373
46. Connolly ES, Jr., Rabinstein AA, Carhuapoma JR, et al. Guidelines for the management of aneurysmal subarachnoid hemorrhage: a guideline for healthcare professionals from the American Heart Association/American Stroke Association. *Stroke* 2012;43(6):1711-37. doi: 10.1161/STR.0b013e3182587839
47. Kowalski RG, Claassen J, Kreiter KT, et al. Initial misdiagnosis and outcome after subarachnoid hemorrhage. *JAMA* 2004;291(7):866-9. doi: 10.1001/jama.291.7.866
48. Smith ER, Carter BS, Ogilvy CS. Proposed use of prophylactic decompressive craniectomy in poor-grade aneurysmal subarachnoid hemorrhage patients presenting with associated large sylvian hematomas. *Neurosurgery* 2002;51(1):117-24; discussion 24.
49. Sasaki T, Sato M, Oinuma M, et al. Management of poor-grade patients with aneurysmal subarachnoid hemorrhage in the acute stage: Importance of close monitoring for neurological grade changes. *Surg Neurol* 2004;62(6):531-5; discussion 35-7. doi: 10.1016/j.surneu.2004.01.015
50. Hillman J, Fridriksson S, Nilsson O, et al. Immediate administration of tranexamic acid and reduced incidence of early rebleeding after aneurysmal subarachnoid hemorrhage: a prospective randomized study. *J Neurosurg* 2002;97(4):771-8. doi: 10.3171/jns.2002.97.4.0771
51. Hasan D, Vermeulen M, Wijdicks EF, et al. Management problems in acute hydrocephalus after subarachnoid hemorrhage. *Stroke* 1989;20(6):747-53.
52. Green DM, Burns JD, DeFusco CM. ICU management of aneurysmal subarachnoid hemorrhage. *J Intensive Care Med* 2013;28(6):341-54. doi: 10.1177/0885066611434100
53. Macdonald RL, Kassell NF, Mayer S, et al. Clazosentan to overcome neurological ischemia and infarction occurring after subarachnoid hemorrhage (CONSCIOUS-1): randomized, double-blind, placebo-controlled phase 2 dose-finding trial. *Stroke* 2008;39(11):3015-21. doi: 10.1161/STROKEAHA.108.519942
54. Macdonald RL, Higashida RT, Keller E, et al. Clazosentan, an endothelin receptor antagonist, in patients with aneurysmal subarachnoid haemorrhage undergoing surgical clipping: a

- randomised, double-blind, placebo-controlled phase 3 trial (CONSCIOUS-2). *Lancet Neurol* 2011;10(7):618-25. doi: 10.1016/S1474-4422(11)70108-9
55. Dorhout Mees SM, Rinkel GJ, Feigin VL, et al. Calcium antagonists for aneurysmal subarachnoid haemorrhage. *Cochrane Database Syst Rev* 2007(3):CD000277. doi: 10.1002/14651858.CD000277.pub3
 56. Ishiguro M, Wellman GC. Cellular basis of vasospasm: role of small diameter arteries and voltage-dependent Ca²⁺ channels. *Acta Neurochir Suppl* 2008;104:95-8.
 57. Cho WS, Kang HS, Kim JE, et al. Intra-arterial nimodipine infusion for cerebral vasospasm in patients with aneurysmal subarachnoid hemorrhage. *Interv Neuroradiol* 2011;17(2):169-78. doi: 10.1177/159101991101700205
 58. Hockel K, Diedler J, Steiner J, et al. Long-Term, Continuous Intra-Arterial Nimodipine Treatment of Severe Vasospasm After Aneurysmal Subarachnoid Hemorrhage. *World neurosurgery* 2016;88:104-12. doi: 10.1016/j.wneu.2015.11.081
 59. Thomas S, Herrmann B, Samii M, et al. Experimental subarachnoid hemorrhage in the rat: influences of nimodipine. *Acta Neurochir Suppl* 2008;102:377-9.
 60. Gathier CS, van den Bergh WM, van der Jagt M, et al. Induced Hypertension for Delayed Cerebral Ischemia After Aneurysmal Subarachnoid Hemorrhage: A Randomized Clinical Trial. *Stroke* 2018;49(1):76-83. doi: 10.1161/STROKEAHA.117.017956
 61. Veldeman M, Hollig A, Clusmann H, et al. Delayed cerebral ischaemia prevention and treatment after aneurysmal subarachnoid haemorrhage: a systematic review. *Br J Anaesth* 2016;117(1):17-40. doi: 10.1093/bja/aew095
 62. Alaraj A, Charbel FT, Amin-Hanjani S. Peri-operative measures for treatment and prevention of cerebral vasospasm following subarachnoid hemorrhage. *Neurol Res* 2009;31(6):651-9. doi: 10.1179/174313209X382395
 63. Broderick JP, Brott TG, Duldner JE, et al. Initial and recurrent bleeding are the major causes of death following subarachnoid hemorrhage. *Stroke* 1994;25(7):1342-7.
 64. Bederson JB, Germano IM, Guarino L. Cortical blood flow and cerebral perfusion pressure in a new noncraniotomy model of subarachnoid hemorrhage in the rat. *Stroke* 1995;26(6):1086-91; discussion 91-2.
 65. Friedrich V, Flores R, Muller A, et al. Escape of intraluminal platelets into brain parenchyma after subarachnoid hemorrhage. *Neuroscience* 2010;165(3):968-75. doi: 10.1016/j.neuroscience.2009.10.038
 66. Stein SC, Browne KD, Chen XH, et al. Thromboembolism and delayed cerebral ischemia after subarachnoid hemorrhage: an autopsy study. *Neurosurgery* 2006;59(4):781-7; discussion 87-8. doi: 10.1227/01.NEU.0000227519.27569.45
 67. Nau R, Haase S, Bunkowski S, et al. Neuronal apoptosis in the dentate gyrus in humans with subarachnoid hemorrhage and cerebral hypoxia. *Brain Pathol* 2002;12(3):329-36.
 68. Macdonald RL, Pluta RM, Zhang JH. Cerebral vasospasm after subarachnoid hemorrhage: the emerging revolution. *Nat Clin Pract Neurol* 2007;3(5):256-63. doi: 10.1038/ncpneuro0490
 69. Altay T, Smithason S, Volokh N, et al. A novel method for subarachnoid hemorrhage to induce vasospasm in mice. *J Neurosci Methods* 2009;183(2):136-40. doi: 10.1016/j.jneumeth.2009.06.027
 70. Marbacher S, Fandino J, Kitchen ND. Standard intracranial in vivo animal models of delayed cerebral vasospasm. *Br J Neurosurg* 2010;24(4):415-34. doi: 10.3109/02688691003746274
 71. Sabri M, Jeon H, Ai J, et al. Anterior circulation mouse model of subarachnoid hemorrhage. *Brain Res* 2009;1295:179-85. doi: 10.1016/j.brainres.2009.08.021
 72. Guresir E, Schuss P, Borger V, et al. Experimental subarachnoid hemorrhage: double cisterna magna injection rat model--assessment of delayed pathological effects of cerebral vasospasm. *Translational stroke research* 2015;6(3):242-51. doi: 10.1007/s12975-015-0392-z
 73. Lin CL, Calisaneller T, Ukita N, et al. A murine model of subarachnoid hemorrhage-induced cerebral vasospasm. *J Neurosci Methods* 2003;123(1):89-97.

74. Kikkawa Y, Kurogi R, Sasaki T. The single and double blood injection rabbit subarachnoid hemorrhage model. *Translational stroke research* 2015;6(1):88-97. doi: 10.1007/s12975-014-0375-5
75. Jackowski A, Crockard A, Burnstock G, et al. The time course of intracranial pathophysiological changes following experimental subarachnoid haemorrhage in the rat. *J Cereb Blood Flow Metab* 1990;10(6):835-49. doi: 10.1038/jcbfm.1990.140
76. Veelken JA, Laing RJ, Jakubowski J. The Sheffield model of subarachnoid hemorrhage in rats. *Stroke* 1995;26(7):1279-83; discussion 84.
77. Uhl E, Lehmborg J, Steiger HJ, et al. Intraoperative detection of early microvasospasm in patients with subarachnoid hemorrhage by using orthogonal polarization spectral imaging. *Neurosurgery* 2003;52(6):1307-15; discussion 15-7.
78. Friedrich B, Muller F, Feiler S, et al. Experimental subarachnoid hemorrhage causes early and long-lasting microarterial constriction and microthrombosis: an in-vivo microscopy study. *J Cereb Blood Flow Metab* 2012;32(3):447-55. doi: 10.1038/jcbfm.2011.154
79. Buhler D, Schuller K, Plesnila N. Protocol for the induction of subarachnoid hemorrhage in mice by perforation of the Circle of Willis with an endovascular filament. *Translational stroke research* 2014;5(6):653-9. doi: 10.1007/s12975-014-0366-6
80. Espinosa F, Weir B, Overton T, et al. A randomized placebo-controlled double-blind trial of nimodipine after SAH in monkeys. Part 1: Clinical and radiological findings. *J Neurosurg* 1984;60(6):1167-75. doi: 10.3171/jns.1984.60.6.1167
81. Adams HP, Jr., Kassell NF, Torner JC, et al. Early management of aneurysmal subarachnoid hemorrhage. A report of the Cooperative Aneurysm Study. *J Neurosurg* 1981;54(2):141-5. doi: 10.3171/jns.1981.54.2.0141
82. Kusaka G, Ishikawa M, Nanda A, et al. Signaling pathways for early brain injury after subarachnoid hemorrhage. *J Cereb Blood Flow Metab* 2004;24(8):916-25. doi: 10.1097/01.WCB.0000125886.48838.7E
83. Cahill J, Calvert JW, Zhang JH. Mechanisms of early brain injury after subarachnoid hemorrhage. *J Cereb Blood Flow Metab* 2006;26(11):1341-53. doi: 10.1038/sj.jcbfm.9600283
84. Grote E, Hassler W. The critical first minutes after subarachnoid hemorrhage. *Neurosurgery* 1988;22(4):654-61.
85. Nornes H, Magnaes B. Intracranial pressure in patients with ruptured saccular aneurysm. *J Neurosurg* 1972;36(5):537-47. doi: 10.3171/jns.1972.36.5.0537
86. Zoerle T, Lombardo A, Colombo A, et al. Intracranial pressure after subarachnoid hemorrhage. *Crit Care Med* 2015;43(1):168-76. doi: 10.1097/CCM.0000000000000670
87. Fisher CM. Clinical syndromes in cerebral thrombosis, hypertensive hemorrhage, and ruptured saccular aneurysm. *Clin Neurosurg* 1975;22:117-47.
88. Prunell GF, Mathiesen T, Svendgaard NA. Experimental subarachnoid hemorrhage: cerebral blood flow and brain metabolism during the acute phase in three different models in the rat. *Neurosurgery* 2004;54(2):426-36; discussion 36-7.
89. Ostrowski RP, Colohan AR, Zhang JH. Mechanisms of hyperbaric oxygen-induced neuroprotection in a rat model of subarachnoid hemorrhage. *J Cereb Blood Flow Metab* 2005;25(5):554-71. doi: 10.1038/sj.jcbfm.9600048
90. Schubert GA, Seiz M, Hegewald AA, et al. Acute hypoperfusion immediately after subarachnoid hemorrhage: a xenon contrast-enhanced CT study. *J Neurotrauma* 2009;26(12):2225-31. doi: 10.1089/neu.2009.0924
91. van der Schaaf I, Wermer MJ, van der Graaf Y, et al. CT after subarachnoid hemorrhage: relation of cerebral perfusion to delayed cerebral ischemia. *Neurology* 2006;66(10):1533-8. doi: 10.1212/01.wnl.0000216272.67895.d3
92. Frykholm P, Andersson JL, Langstrom B, et al. Haemodynamic and metabolic disturbances in the acute stage of subarachnoid haemorrhage demonstrated by PET. *Acta Neurol Scand* 2004;109(1):25-32.

93. Friedrich V, Flores R, Sehba FA. Cell death starts early after subarachnoid hemorrhage. *Neurosci Lett* 2012;512(1):6-11. doi: 10.1016/j.neulet.2012.01.036
94. Dreier JP, Ebert N, Priller J, et al. Products of hemolysis in the subarachnoid space inducing spreading ischemia in the cortex and focal necrosis in rats: a model for delayed ischemic neurological deficits after subarachnoid hemorrhage? *J Neurosurg* 2000;93(4):658-66. doi: 10.3171/jns.2000.93.4.0658
95. Sehba FA, Hou J, Pluta RM, et al. The importance of early brain injury after subarachnoid hemorrhage. *Prog Neurobiol* 2012;97(1):14-37. doi: 10.1016/j.pneurobio.2012.02.003
96. Sun BL, Zheng CB, Yang MF, et al. Dynamic alterations of cerebral pial microcirculation during experimental subarachnoid hemorrhage. *Cell Mol Neurobiol* 2009;29(2):235-41. doi: 10.1007/s10571-008-9316-8
97. Tso MK, Macdonald RL. Subarachnoid hemorrhage: a review of experimental studies on the microcirculation and the neurovascular unit. *Translational stroke research* 2014;5(2):174-89. doi: 10.1007/s12975-014-0323-4 [published Online First: 2014/02/11]
98. Kaynar MY, Tanriverdi T, Kafadar AM, et al. Detection of soluble intercellular adhesion molecule-1 and vascular cell adhesion molecule-1 in both cerebrospinal fluid and serum of patients after aneurysmal subarachnoid hemorrhage. *J Neurosurg* 2004;101(6):1030-6. doi: 10.3171/jns.2004.101.6.1030
99. Gaetani P, Tartara F, Pignatti P, et al. Cisternal CSF levels of cytokines after subarachnoid hemorrhage. *Neurol Res* 1998;20(4):337-42.
100. Tanriverdi T, Sanus GZ, Ulu MO, et al. Serum and cerebrospinal fluid concentrations of E-selectin in patients with aneurysmal subarachnoid hemorrhage. *Braz J Med Biol Res* 2005;38(11):1703-10. doi: /S0100-879X2005001100020
101. Fountas KN, Tasiou A, Kapsalaki EZ, et al. Serum and cerebrospinal fluid C-reactive protein levels as predictors of vasospasm in aneurysmal subarachnoid hemorrhage. Clinical article. *Neurosurg Focus* 2009;26(5):E22. doi: 10.3171/2009.2.FOCUS08311
102. Kao HW, Lee KW, Kuo CL, et al. Interleukin-6 as a Prognostic Biomarker in Ruptured Intracranial Aneurysms. *PLoS One* 2015;10(7):e0132115. doi: 10.1371/journal.pone.0132115
103. Suzuki H, Kawakita F. Tenascin-C in aneurysmal subarachnoid hemorrhage: deleterious or protective? *Neural Regen Res* 2016;11(2):230-1. doi: 10.4103/1673-5374.177721
104. Liu L, Kawakita F, Fujimoto M, et al. Role of Periostin in Early Brain Injury After Subarachnoid Hemorrhage in Mice. *Stroke* 2017;48(4):1108-11. doi: 10.1161/STROKEAHA.117.016629
105. Huang XP, Peng JH, Pang JW, et al. Peli1 Contributions in Microglial Activation, Neuroinflammatory Responses and Neurological Deficits Following Experimental Subarachnoid Hemorrhage. *Front Mol Neurosci* 2017;10:398. doi: 10.3389/fnmol.2017.00398
106. Wang CX, Xie GB, Zhou CH, et al. Baincalein alleviates early brain injury after experimental subarachnoid hemorrhage in rats: possible involvement of TLR4/NF-kappaB-mediated inflammatory pathway. *Brain Res* 2015;1594:245-55. doi: 10.1016/j.brainres.2014.10.014
107. Teng Z, Jiang L, Hu Q, et al. Peroxisome Proliferator-Activated Receptor beta/delta Alleviates Early Brain Injury After Subarachnoid Hemorrhage in Rats. *Stroke* 2016;47(1):196-205. doi: 10.1161/STROKEAHA.115.011701
108. Guo Z, Hu Q, Xu L, et al. Lipoxin A4 Reduces Inflammation Through Formyl Peptide Receptor 2/p38 MAPK Signaling Pathway in Subarachnoid Hemorrhage Rats. *Stroke* 2016;47(2):490-7. doi: 10.1161/STROKEAHA.115.011223
109. Peng Y, Jin J, Fan L, et al. Rolipram Attenuates Early Brain Injury Following Experimental Subarachnoid Hemorrhage in Rats: Possibly via Regulating the SIRT1/NF-kappaB Pathway. *Neurochem Res* 2018 doi: 10.1007/s11064-018-2480-4
110. Ma C, Zhou W, Yan Z, et al. Toll-like receptor 4 (TLR4) is correlated with delayed cerebral ischemia (DCI) and poor prognosis in aneurysmal subarachnoid hemorrhage. *J Neurol Sci* 2015;359(1-2):67-71. doi: 10.1016/j.jns.2015.10.018
111. Galea J, Ogungbenro K, Hulme S, et al. Reduction of inflammation after administration of interleukin-1 receptor antagonist following aneurysmal subarachnoid hemorrhage: results of

- the Subcutaneous Interleukin-1Ra in SAH (SCIL-SAH) study. *J Neurosurg* 2018;128(2):515-23. doi: 10.3171/2016.9.JNS16615
112. Ishikawa M, Kusaka G, Yamaguchi N, et al. Platelet and leukocyte adhesion in the microvasculature at the cerebral surface immediately after subarachnoid hemorrhage. *Neurosurgery* 2009;64(3):546-53; discussion 53-4. doi: 10.1227/01.NEU.0000337579.05110.F4
 113. Chaichana KL, Pradilla G, Huang J, et al. Role of inflammation (leukocyte-endothelial cell interactions) in vasospasm after subarachnoid hemorrhage. *World neurosurgery* 2010;73(1):22-41. doi: 10.1016/j.surneu.2009.05.027
 114. Spitzer D, Spitzer NJ, Deininger M, et al. Activation of Cytotoxic Natural Killer Cells After Aneurysmal Subarachnoid Hemorrhage. *World neurosurgery* 2017;101:666-76 e1. doi: 10.1016/j.wneu.2017.03.026
 115. Ishikawa M, Kajimura M, Morikawa T, et al. Leukocyte plugging and cortical capillary flow after subarachnoid hemorrhage. *Acta Neurochir (Wien)* 2016;158(6):1057-67. doi: 10.1007/s00701-016-2792-6
 116. Wei S, Luo C, Yu S, et al. Erythropoietin ameliorates early brain injury after subarachnoid haemorrhage by modulating microglia polarization via the EPOR/JAK2-STAT3 pathway. *Exp Cell Res* 2017;361(2):342-52. doi: 10.1016/j.yexcr.2017.11.002
 117. Schallner N, Pandit R, LeBlanc R, 3rd, et al. Microglia regulate blood clearance in subarachnoid hemorrhage by heme oxygenase-1. *J Clin Invest* 2015;125(7):2609-25. doi: 10.1172/JCI78443
 118. Schneider UC, Davids AM, Brandenburg S, et al. Microglia inflict delayed brain injury after subarachnoid hemorrhage. *Acta Neuropathol* 2015;130(2):215-31. doi: 10.1007/s00401-015-1440-1
 119. Filiano AJ, Gadani SP, Kipnis J. Interactions of innate and adaptive immunity in brain development and function. *Brain Res* 2015;1617:18-27. doi: 10.1016/j.brainres.2014.07.050
 120. Tang Y, Le W. Differential Roles of M1 and M2 Microglia in Neurodegenerative Diseases. *Mol Neurobiol* 2016;53(2):1181-94. doi: 10.1007/s12035-014-9070-5
 121. Hanafy KA. The role of microglia and the TLR4 pathway in neuronal apoptosis and vasospasm after subarachnoid hemorrhage. *J Neuroinflammation* 2013;10:83. doi: 10.1186/1742-2094-10-83
 122. Atangana E, Schneider UC, Blecharz K, et al. Intravascular Inflammation Triggers Intracerebral Activated Microglia and Contributes to Secondary Brain Injury After Experimental Subarachnoid Hemorrhage (eSAH). *Translational stroke research* 2017;8(2):144-56. doi: 10.1007/s12975-016-0485-3
 123. Manno EM, Gress DR, Ogilvy CS, et al. The safety and efficacy of cyclosporine A in the prevention of vasospasm in patients with Fisher grade 3 subarachnoid hemorrhages: a pilot study. *Neurosurgery* 1997;40(2):289-93.
 124. Yanamoto H, Kikuchi H, Sato M, et al. Therapeutic trial of cerebral vasospasm with the serine protease inhibitor, FUT-175, administered in the acute stage after subarachnoid hemorrhage. *Neurosurgery* 1992;30(3):358-63.
 125. Gomis P, Graftieaux JP, Sercombe R, et al. Randomized, double-blind, placebo-controlled, pilot trial of high-dose methylprednisolone in aneurysmal subarachnoid hemorrhage. *J Neurosurg* 2010;112(3):681-8. doi: 10.3171/2009.4.JNS081377
 126. Ecker A, Riemenschneider PA. Arteriographic demonstration of spasm of the intracranial arteries, with special reference to saccular arterial aneurysms. *J Neurosurg* 1951;8(6):660-7. doi: 10.3171/jns.1951.8.6.0660
 127. Stornelli SA, French JD. Subarachnoid Hemorrhage--Factors in Prognosis and Management. *J Neurosurg* 1964;21:769-80. doi: 10.3171/jns.1964.21.9.0769
 128. Kassell NF, Sasaki T, Colohan AR, et al. Cerebral vasospasm following aneurysmal subarachnoid hemorrhage. *Stroke* 1985;16(4):562-72.

129. Macdonald RL, Higashida RT, Keller E, et al. Preventing vasospasm improves outcome after aneurysmal subarachnoid hemorrhage: rationale and design of CONSCIOUS-2 and CONSCIOUS-3 trials. *Neurocrit Care* 2010;13(3):416-24. doi: 10.1007/s12028-010-9433-3
130. Vatter H, Konzalla J, Seifert V. Endothelin related pathophysiology in cerebral vasospasm: what happens to the cerebral vessels? *Acta Neurochir Suppl* 2011;110(Pt 1):177-80. doi: 10.1007/978-3-7091-0353-1_31
131. Guan Z, VanBeusecum JP, Inscho EW. Endothelin and the renal microcirculation. *Semin Nephrol* 2015;35(2):145-55. doi: 10.1016/j.semnephrol.2015.02.004
132. Motte S, McEntee K, Naeije R. Endothelin receptor antagonists. *Pharmacol Ther* 2006;110(3):386-414. doi: 10.1016/j.pharmthera.2005.08.012
133. Kasuya H, Weir BK, White DM, et al. Mechanism of oxyhemoglobin-induced release of endothelin-1 from cultured vascular endothelial cells and smooth-muscle cells. *J Neurosurg* 1993;79(6):892-8. doi: 10.3171/jns.1993.79.6.0892
134. Kikkawa Y, Matsuo S, Kameda K, et al. Mechanisms underlying potentiation of endothelin-1-induced myofilament Ca(2+) sensitization after subarachnoid hemorrhage. *J Cereb Blood Flow Metab* 2012;32(2):341-52. doi: 10.1038/jcbfm.2011.132
135. Alabadi JA, Salom JB, Torregrosa G, et al. Changes in the cerebrovascular effects of endothelin-1 and nicardipine after experimental subarachnoid hemorrhage. *Neurosurgery* 1993;33(4):707-14; discussion 14-5.
136. Seifert V, Löffler BM, Zimmermann M, et al. Endothelin concentrations in patients with aneurysmal subarachnoid hemorrhage. Correlation with cerebral vasospasm, delayed ischemic neurological deficits, and volume of hematoma. *J Neurosurg* 1995;82(1):55-62. doi: 10.3171/jns.1995.82.1.0055
137. Fassbender K, Hodapp B, Rossol S, et al. Endothelin-1 in subarachnoid hemorrhage: An acute-phase reactant produced by cerebrospinal fluid leukocytes. *Stroke* 2000;31(12):2971-5.
138. Hamann G, Isenberg E, Strittmatter M, et al. Absence of elevation of big endothelin in subarachnoid hemorrhage. *Stroke* 1993;24(3):383-6.
139. Lima VV, Giachini FR, Hardy DM, et al. O-GlcNAcylation: a novel pathway contributing to the effects of endothelin in the vasculature. *Am J Physiol Regul Integr Comp Physiol* 2011;300(2):R236-50. doi: 10.1152/ajpregu.00230.2010
140. Thorin E, Webb DJ. Endothelium-derived endothelin-1. *Pflugers Arch* 2010;459(6):951-8. doi: 10.1007/s00424-009-0763-y
141. Bourque SL, Davidge ST, Adams MA. The interaction between endothelin-1 and nitric oxide in the vasculature: new perspectives. *Am J Physiol Regul Integr Comp Physiol* 2011;300(6):R1288-95. doi: 10.1152/ajpregu.00397.2010
142. Masaki T. The endothelin family: an overview. *J Cardiovasc Pharmacol* 2000;35(4 Suppl 2):S3-5.
143. Chow M, Dumont AS, Kassell NF. Endothelin receptor antagonists and cerebral vasospasm: an update. *Neurosurgery* 2002;51(6):1333-41; discussion 42.
144. Roux S, Breu V, Giller T, et al. Ro 61-1790, a new hydrosoluble endothelin antagonist: general pharmacology and effects on experimental cerebral vasospasm. *J Pharmacol Exp Ther* 1997;283(3):1110-8.
145. Schubert GA, Schilling L, Thome C. Clazosentan, an endothelin receptor antagonist, prevents early hypoperfusion during the acute phase of massive experimental subarachnoid hemorrhage: a laser Doppler flowmetry study in rats. *J Neurosurg* 2008;109(6):1134-40. doi: 10.3171/JNS.2008.109.12.1134
146. Sabri M, Ai J, Macdonald RL. Dissociation of vasospasm and secondary effects of experimental subarachnoid hemorrhage by clazosentan. *Stroke* 2011;42(5):1454-60. doi: 10.1161/STROKEAHA.110.604728
147. Vergouwen MD, Fang J, Casaubon LK, et al. Higher incidence of in-hospital complications in patients with clipped versus coiled ruptured intracranial aneurysms. *Stroke* 2011;42(11):3093-8. doi: 10.1161/STROKEAHA.111.619510

148. Diringer MN, Bleck TP, Claude Hemphill J, 3rd, et al. Critical care management of patients following aneurysmal subarachnoid hemorrhage: recommendations from the Neurocritical Care Society's Multidisciplinary Consensus Conference. *Neurocrit Care* 2011;15(2):211-40. doi: 10.1007/s12028-011-9605-9
149. Vergouwen MD, Vermeulen M, Coert BA, et al. Microthrombosis after aneurysmal subarachnoid hemorrhage: an additional explanation for delayed cerebral ischemia. *J Cereb Blood Flow Metab* 2008;28(11):1761-70. doi: 10.1038/jcbfm.2008.74
150. Dreier JP, Major S, Manning A, et al. Cortical spreading ischaemia is a novel process involved in ischaemic damage in patients with aneurysmal subarachnoid haemorrhage. *Brain* 2009;132(Pt 7):1866-81. doi: 10.1093/brain/awp102
151. Herz DA, Baez S, Shulman K. Pial microcirculation in subarachnoid hemorrhage. *Stroke* 1975;6(4):417-24.
152. Park IS, Meno JR, Witt CE, et al. Impairment of intracerebral arteriole dilation responses after subarachnoid hemorrhage. Laboratory investigation. *J Neurosurg* 2009;111(5):1008-13. doi: 10.3171/2009.3.JNS096
153. Sehba FA, Friedrich V. Early micro vascular changes after subarachnoid hemorrhage. *Acta Neurochir Suppl* 2011;110(Pt 1):49-55. doi: 10.1007/978-3-7091-0353-1_9
154. Balbi M, Koide M, Wellman GC, et al. Inversion of neurovascular coupling after subarachnoid hemorrhage in vivo. *J Cereb Blood Flow Metab* 2017;37(11):3625-34. doi: 10.1177/0271678X16686595
155. Friedrich V, Flores R, Muller A, et al. Reduction of neutrophil activity decreases early microvascular injury after subarachnoid haemorrhage. *J Neuroinflammation* 2011;8:103. doi: 10.1186/1742-2094-8-103
156. Frijns CJ, Fijnheer R, Algra A, et al. Early circulating levels of endothelial cell activation markers in aneurysmal subarachnoid haemorrhage: associations with cerebral ischaemic events and outcome. *J Neurol Neurosurg Psychiatry* 2006;77(1):77-83. doi: 10.1136/jnnp.2005.064956
157. Suzuki M, Kudo A, Otawara Y, et al. Extrinsic pathway of blood coagulation and thrombin in the cerebrospinal fluid after subarachnoid hemorrhage. *Neurosurgery* 1999;44(3):487-93; discussion 93-4.
158. Suzuki S, Kimura M, Souma M, et al. Cerebral microthrombosis in symptomatic cerebral vasospasm--a quantitative histological study in autopsy cases. *Neurol Med Chir (Tokyo)* 1990;30(5):309-16.
159. Ames A, 3rd, Wright RL, Kowada M, et al. Cerebral ischemia. II. The no-reflow phenomenon. *Am J Pathol* 1968;52(2):437-53.
160. Konidala S, Gutterman DD. Coronary vasospasm and the regulation of coronary blood flow. *Prog Cardiovasc Dis* 2004;46(4):349-73.
161. Sehba FA, Mostafa G, Friedrich V, Jr., et al. Acute microvascular platelet aggregation after subarachnoid hemorrhage. *J Neurosurg* 2005;102(6):1094-100. doi: 10.3171/jns.2005.102.6.1094
162. Rosenblum WI. Platelet adhesion and aggregation without endothelial denudation or exposure of basal lamina and/or collagen. *J Vasc Res* 1997;34(6):409-17. doi: 10.1159/000159251
163. Dorhout Mees SM, van den Bergh WM, Algra A, et al. Antiplatelet therapy for aneurysmal subarachnoid haemorrhage. *Cochrane Database Syst Rev* 2007(4):CD006184. doi: 10.1002/14651858.CD006184.pub2
164. Bederson JB, Levy AL, Ding WH, et al. Acute vasoconstriction after subarachnoid hemorrhage. *Neurosurgery* 1998;42(2):352-60; discussion 60-2.
165. Pennings FA, Bouma GJ, Ince C. Direct observation of the human cerebral microcirculation during aneurysm surgery reveals increased arteriolar contractility. *Stroke* 2004;35(6):1284-8. doi: 10.1161/01.STR.0000126039.91400.cb
166. Nishimura N, Schaffer CB, Friedman B, et al. Penetrating arterioles are a bottleneck in the perfusion of neocortex. *Proc Natl Acad Sci U S A* 2007;104(1):365-70. doi: 10.1073/pnas.0609551104

167. Barrows LJ, Hunter FT, Banker BQ. The nature and clinical significance of pigments in the cerebrospinal fluid. *Brain* 1955;78(1):59-80.
168. Peterson JW, Roussos L, Kwun BD, et al. Evidence of the role of hemolysis in experimental cerebral vasospasm. *J Neurosurg* 1990;72(5):775-81. doi: 10.3171/jns.1990.72.5.0775
169. Cseplo P, Vamos Z, Torok O, et al. Hemolyzed Blood Elicits a Calcium Antagonist and High CO₂ Reversible Constriction via Elevation of [Ca²⁺]_i in Isolated Cerebral Arteries. *J Neurotrauma* 2017;34(2):529-34. doi: 10.1089/neu.2015.4365
170. Joerk A, Seidel RA, Walter SG, et al. Impact of heme and heme degradation products on vascular diameter in mouse visual cortex. *J Am Heart Assoc* 2014;3(4) doi: 10.1161/JAHA.114.001220
171. Clark JF, Sharp FR. Bilirubin oxidation products (BOXes) and their role in cerebral vasospasm after subarachnoid hemorrhage. *J Cereb Blood Flow Metab* 2006;26(10):1223-33. doi: 10.1038/sj.jcbfm.9600280
172. Macdonald RL, Weir BK. A review of hemoglobin and the pathogenesis of cerebral vasospasm. *Stroke* 1991;22(8):971-82.
173. Lee JY, Keep RF, He Y, et al. Hemoglobin and iron handling in brain after subarachnoid hemorrhage and the effect of deferoxamine on early brain injury. *J Cereb Blood Flow Metab* 2010;30(11):1793-803. doi: 10.1038/jcbfm.2010.137
174. Galea J, Cruickshank G, Teeling JL, et al. The intrathecal CD163-haptoglobin-hemoglobin scavenging system in subarachnoid hemorrhage. *Journal of neurochemistry* 2012;121(5):785-92. doi: 10.1111/j.1471-4159.2012.07716.x
175. Melamed-Frank M, Lache O, Enav BI, et al. Structure-function analysis of the antioxidant properties of haptoglobin. *Blood* 2001;98(13):3693-8.
176. Nakai K, Sakuma I, Ohta T, et al. Permeability characteristics of hemoglobin derivatives across cultured endothelial cell monolayers. *J Lab Clin Med* 1998;132(4):313-9.
177. Reeder BJ, Sharpe MA, Kay AD, et al. Toxicity of myoglobin and haemoglobin: oxidative stress in patients with rhabdomyolysis and subarachnoid haemorrhage. *Biochem Soc Trans* 2002;30(4):745-8. doi: 10.1042/
178. Kamii H, Kato I, Kinouchi H, et al. Amelioration of vasospasm after subarachnoid hemorrhage in transgenic mice overexpressing CuZn-superoxide dismutase. *Stroke* 1999;30(4):867-71; discussion 72.
179. Aladag MA, Turkoz Y, Parlakpinar H, et al. Melatonin ameliorates cerebral vasospasm after experimental subarachnoidal haemorrhage correcting imbalance of nitric oxide levels in rats. *Neurochem Res* 2009;34(11):1935-44. doi: 10.1007/s11064-009-9979-7
180. Pluta RM, Afshar JK, Boock RJ, et al. Temporal changes in perivascular concentrations of oxyhemoglobin, deoxyhemoglobin, and methemoglobin after subarachnoid hemorrhage. *J Neurosurg* 1998;88(3):557-61. doi: 10.3171/jns.1998.88.3.0557
181. Kwon MS, Woo SK, Kurland DB, et al. Methemoglobin is an endogenous toll-like receptor 4 ligand-relevance to subarachnoid hemorrhage. *Int J Mol Sci* 2015;16(3):5028-46. doi: 10.3390/ijms16035028
182. Schaer DJ, Buehler PW, Alayash AI, et al. Hemolysis and free hemoglobin revisited: exploring hemoglobin and heme scavengers as a novel class of therapeutic proteins. *Blood* 2013;121(8):1276-84. doi: 10.1182/blood-2012-11-451229
183. Hvidberg V, Maniecki MB, Jacobsen C, et al. Identification of the receptor scavenging hemopexin-heme complexes. *Blood* 2005;106(7):2572-9. doi: 10.1182/blood-2005-03-1185
184. Chiabrando D, Vinchi F, Fiorito V, et al. Heme in pathophysiology: a matter of scavenging, metabolism and trafficking across cell membranes. *Front Pharmacol* 2014;5:61. doi: 10.3389/fphar.2014.00061
185. Gladwin MT, Kanas T, Kim-Shapiro DB. Hemolysis and cell-free hemoglobin drive an intrinsic mechanism for human disease. *J Clin Invest* 2012;122(4):1205-8. doi: 10.1172/JCI62972
186. Baranano DE, Rao M, Ferris CD, et al. Biliverdin reductase: a major physiologic cytoprotectant. *Proc Natl Acad Sci U S A* 2002;99(25):16093-8. doi: 10.1073/pnas.252626999

187. Otterbein LE, Bach FH, Alam J, et al. Carbon monoxide has anti-inflammatory effects involving the mitogen-activated protein kinase pathway. *Nat Med* 2000;6(4):422-8. doi: 10.1038/74680
188. Gozzelino R, Andrade BB, Larsen R, et al. Metabolic adaptation to tissue iron overload confers tolerance to malaria. *Cell Host Microbe* 2012;12(5):693-704. doi: 10.1016/j.chom.2012.10.011
189. Garland P, Durnford AJ, Okemefuna AI, et al. Heme-Hemopexin Scavenging Is Active in the Brain and Associates With Outcome After Subarachnoid Hemorrhage. *Stroke* 2016;47(3):872-6. doi: 10.1161/STROKEAHA.115.011956
190. Ono S, Zhang ZD, Marton LS, et al. Heme oxygenase-1 and ferritin are increased in cerebral arteries after subarachnoid hemorrhage in monkeys. *J Cereb Blood Flow Metab* 2000;20(7):1066-76. doi: 10.1097/00004647-200007000-00006
191. Petzold A, Worthington V, Appleby I, et al. Cerebrospinal fluid ferritin level, a sensitive diagnostic test in late-presenting subarachnoid hemorrhage. *J Stroke Cerebrovasc Dis* 2011;20(6):489-93. doi: 10.1016/j.jstrokecerebrovasdis.2010.02.021
192. Wang KC, Tang SC, Lee JE, et al. Prognostic value of intrathecal heme oxygenase-1 concentration in patients with Fisher Grade III aneurysmal subarachnoid hemorrhage. *J Neurosurg* 2014;121(6):1388-93. doi: 10.3171/2014.7.JNS131704
193. Suzuki H, Kanamaru K, Tsunoda H, et al. Heme oxygenase-1 gene induction as an intrinsic regulation against delayed cerebral vasospasm in rats. *J Clin Invest* 1999;104(1):59-66. doi: 10.1172/JCI5357
194. Horky LL, Pluta RM, Boock RJ, et al. Role of ferrous iron chelator 2,2'-dipyridyl in preventing delayed vasospasm in a primate model of subarachnoid hemorrhage. *J Neurosurg* 1998;88(2):298-303. doi: 10.3171/jns.1998.88.2.0298
195. Yu Y, Lin Z, Yin Y, et al. The ferric iron chelator 2,2'-dipyridyl attenuates basilar artery vasospasm and improves neurological function after subarachnoid hemorrhage in rabbits. *NeuroSci* 2014;35(9):1413-9. doi: 10.1007/s10072-014-1730-8
196. Arthur AS, Fergus AH, Lanzino G, et al. Systemic administration of the iron chelator deferoxamine attenuates subarachnoid hemorrhage-induced cerebral vasospasm in the rabbit. *Neurosurgery* 1997;41(6):1385-91; discussion 91-2.
197. Selim M. Deferoxamine mesylate: a new hope for intracerebral hemorrhage: from bench to clinical trials. *Stroke* 2009;40(3 Suppl):S90-1. doi: 10.1161/STROKEAHA.108.533125
198. Nakamura T, Keep RF, Hua Y, et al. Deferoxamine-induced attenuation of brain edema and neurological deficits in a rat model of intracerebral hemorrhage. *Neurosurg Focus* 2003;15(4):ECP4.
199. Cui HJ, He HY, Yang AL, et al. Efficacy of deferoxamine in animal models of intracerebral hemorrhage: a systematic review and stratified meta-analysis. *PLoS One* 2015;10(5):e0127256. doi: 10.1371/journal.pone.0127256
200. Hishikawa T, Ono S, Ogawa T, et al. Effects of deferoxamine-activated hypoxia-inducible factor-1 on the brainstem after subarachnoid hemorrhage in rats. *Neurosurgery* 2008;62(1):232-40; discussion 40-1. doi: 10.1227/01.NEU.0000311082.88766.33
201. LeBlanc RH, 3rd, Chen R, Selim MH, et al. Heme oxygenase-1-mediated neuroprotection in subarachnoid hemorrhage via intracerebroventricular deferoxamine. *J Neuroinflammation* 2016;13(1):244. doi: 10.1186/s12974-016-0709-1
202. Yu ZQ, Jia Y, Chen G. Possible involvement of cathepsin B/D and caspase-3 in deferoxamine-related neuroprotection of early brain injury after subarachnoid haemorrhage in rats. *Neuropathol Appl Neurobiol* 2014;40(3):270-83. doi: 10.1111/nan.12091
203. Li Y, Yang H, Ni W, et al. Effects of deferoxamine on blood-brain barrier disruption after subarachnoid hemorrhage. *PLoS One* 2017;12(3):e0172784. doi: 10.1371/journal.pone.0172784
204. Schuller K, Buhler D, Plesnila N. A murine model of subarachnoid hemorrhage. *J Vis Exp* 2013(81):e50845. doi: 10.3791/50845

205. Calisaneller T, Lin C-L, Ukita N, et al. Blood Injection Subarachnoid Hemorrhage Mouse Model 2009.
206. Light M, Minor KH, DeWitt P, et al. Multiplex array proteomics detects increased MMP-8 in CSF after spinal cord injury. *J Neuroinflammation* 2012;9:122. doi: 10.1186/1742-2094-9-122
207. Kim TN, Goodwill PW, Chen Y, et al. Line-scanning particle image velocimetry: an optical approach for quantifying a wide range of blood flow speeds in live animals. *PLoS One* 2012;7(6):e38590. doi: 10.1371/journal.pone.0038590
208. Nakamura T, Kajimura M, Morikawa T, et al. Acute CO₂-independent vasodilatation of penetrating and pre-capillary arterioles in mouse cerebral parenchyma upon hypoxia revealed by a thinned-skull window method. *Acta Physiol (Oxf)* 2011;203(1):187-96. doi: 10.1111/j.1748-1716.2010.02212.x
209. Schwarzmaier SM, Kim SW, Trabold R, et al. Temporal profile of thrombogenesis in the cerebral microcirculation after traumatic brain injury in mice. *J Neurotrauma* 2010;27(1):121-30. doi: 10.1089/neu.2009.1114
210. Franciosi S, De Gasperi R, Dickstein DL, et al. Pepsin pretreatment allows collagen IV immunostaining of blood vessels in adult mouse brain. *J Neurosci Methods* 2007;163(1):76-82. doi: 10.1016/j.jneumeth.2007.02.020
211. Richard L, Sidman BK, Bijoy Misra, Stephen Senft. High Resolution Mouse Brain Atlas [Available from: <http://www.hms.harvard.edu/research/brain/atlas.html>].
212. Janowski M. Surgical Access to Cisterna Magna Using Concorde-Like Position for Cell Transplantation in Mice and CNS Dissection within Intact Dura for Evaluation of Cell Distribution. In: Janowski M, ed. *Experimental Neurosurgery in Animal Models*. New York, NY: Springer New York 2016:141-49.
213. Nehrkorn K. The Role of Pericytes in Microcirculatory Dysfunction After Subarachnoid Hemorrhage 2016.
214. Selim M, Yeatts S, Goldstein JN, et al. Safety and tolerability of deferoxamine mesylate in patients with acute intracerebral hemorrhage. *Stroke* 2011;42(11):3067-74. doi: 10.1161/STROKEAHA.111.617589
215. del Zoppo GJ, Schmid-Schonbein GW, Mori E, et al. Polymorphonuclear leukocytes occlude capillaries following middle cerebral artery occlusion and reperfusion in baboons. *Stroke* 1991;22(10):1276-83.
216. Tso MK, Macdonald RL. Acute microvascular changes after subarachnoid hemorrhage and transient global cerebral ischemia. *Stroke Res Treat* 2013;2013:425281. doi: 10.1155/2013/425281
217. Vatter H, Zimmermann M, Tesanovic V, et al. Cerebrovascular characterization of clazosentan, the first nonpeptide endothelin receptor antagonist clinically effective for the treatment of cerebral vasospasm. Part I: inhibitory effect on endothelin(A) receptor-mediated contraction. *J Neurosurg* 2005;102(6):1101-7. doi: 10.3171/jns.2005.102.6.1101
218. van Giersbergen PL, Dingemans J. Tolerability, pharmacokinetics, and pharmacodynamics of clazosentan, a parenteral endothelin receptor antagonist. *Eur J Clin Pharmacol* 2007;63(2):151-8. doi: 10.1007/s00228-006-0117-z
219. Lei Q, Li S, Zheng R, et al. Endothelin-1 expression and alterations of cerebral microcirculation after experimental subarachnoid hemorrhage. *Neuroradiology* 2015;57(1):63-70. doi: 10.1007/s00234-014-1435-y
220. Josko J, Hendryk S, Jedrejowska-Szypulka H, et al. Effect of endothelin-1 receptor antagonist BQ-123 on basilar artery diameter after subarachnoid hemorrhage (SAH) in rats. *J Physiol Pharmacol* 2000;51(2):241-9.
221. Liu H, Diemel A, Scholler K, et al. Microvasospasms After Experimental Subarachnoid Hemorrhage Do Not Depend on Endothelin A Receptors. *Stroke* 2018;49(3):693-99. doi: 10.1161/STROKEAHA.117.020028

222. Pisapia JM, Xu X, Kelly J, et al. Microthrombosis after experimental subarachnoid hemorrhage: time course and effect of red blood cell-bound thrombin-activated pro-urokinase and clazosentan. *Exp Neurol* 2012;233(1):357-63. doi: 10.1016/j.expneurol.2011.10.029
223. Chen G, Tariq A, Ai J, et al. Different effects of clazosentan on consequences of subarachnoid hemorrhage in rats. *Brain Res* 2011;1392:132-9. doi: 10.1016/j.brainres.2011.03.068
224. Terpolilli NA, Feiler S, Dienel A, et al. Nitric oxide inhalation reduces brain damage, prevents mortality, and improves neurological outcome after subarachnoid hemorrhage by resolving early pial microvasospasms. *J Cereb Blood Flow Metab* 2016;36(12):2096-107. doi: 10.1177/0271678X15605848
225. Rennels ML, Gregory TF, Blaumanis OR, et al. Evidence for a 'paravascular' fluid circulation in the mammalian central nervous system, provided by the rapid distribution of tracer protein throughout the brain from the subarachnoid space. *Brain Res* 1985;326(1):47-63.
226. Bacynski A, Xu M, Wang W, et al. The Paravascular Pathway for Brain Waste Clearance: Current Understanding, Significance and Controversy. *Front Neuroanat* 2017;11:101. doi: 10.3389/fnana.2017.00101
227. Iliff JJ, Wang M, Liao Y, et al. A paravascular pathway facilitates CSF flow through the brain parenchyma and the clearance of interstitial solutes, including amyloid beta. *Sci Transl Med* 2012;4(147):147ra11. doi: 10.1126/scitranslmed.3003748
228. Jessen NA, Munk AS, Lundgaard I, et al. The Glymphatic System: A Beginner's Guide. *Neurochem Res* 2015;40(12):2583-99. doi: 10.1007/s11064-015-1581-6
229. Luo C, Yao X, Li J, et al. Paravascular pathways contribute to vasculitis and neuroinflammation after subarachnoid hemorrhage independently of glymphatic control. *Cell Death Dis* 2016;7:e2160. doi: 10.1038/cddis.2016.63
230. Goulay R, Flament J, Gauberti M, et al. Subarachnoid Hemorrhage Severely Impairs Brain Parenchymal Cerebrospinal Fluid Circulation in Nonhuman Primate. *Stroke* 2017;48(8):2301-05. doi: 10.1161/STROKEAHA.117.017014
231. Sehba FA, Mostafa G, Knopman J, et al. Acute alterations in microvascular basal lamina after subarachnoid hemorrhage. *J Neurosurg* 2004;101(4):633-40. doi: 10.3171/jns.2004.101.4.0633
232. McConnell ED, Wei HS, Reitz KM, et al. Cerebral microcirculatory failure after subarachnoid hemorrhage is reversed by hyaluronidase. *J Cereb Blood Flow Metab* 2016;36(9):1537-52. doi: 10.1177/0271678X15608389
233. Provencio JJ, Fu X, Siu A, et al. CSF neutrophils are implicated in the development of vasospasm in subarachnoid hemorrhage. *Neurocrit Care* 2010;12(2):244-51. doi: 10.1007/s12028-009-9308-7
234. Satoh S, Yamamoto Y, Toshima Y, et al. Fasudil, a protein kinase inhibitor, prevents the development of endothelial injury and neutrophil infiltration in a two-haemorrhage canine subarachnoid model. *J Clin Neurosci* 1999;6(5):394-99. doi: 10.1054/jocn.1999.0089
235. Kamp MA, Dibue M, Sommer C, et al. Evaluation of a murine single-blood-injection SAH model. *PLoS One* 2014;9(12):e114946. doi: 10.1371/journal.pone.0114946
236. Hayman EG, Patel AP, James RF, et al. Heparin and Heparin-Derivatives in Post-Subarachnoid Hemorrhage Brain Injury: A Multimodal Therapy for a Multimodal Disease. *Molecules* 2017;22(5) doi: 10.3390/molecules22050724
237. Young E. The anti-inflammatory effects of heparin and related compounds. *Thromb Res* 2008;122(6):743-52. doi: 10.1016/j.thromres.2006.10.026
238. Amiconi G, Zolla L, Vecchini P, et al. The effect of macromolecular polyanions on the functional properties of human hemoglobin. *Eur J Biochem* 1977;76(2):339-43.
239. Ferrali M, Ciccoli L, Signorini C, et al. Iron release and erythrocyte damage in allyl alcohol intoxication in mice. *Biochem Pharmacol* 1990;40(7):1485-90.
240. Ayer RE, Zhang JH. Oxidative stress in subarachnoid haemorrhage: significance in acute brain injury and vasospasm. *Acta Neurochir Suppl* 2008;104:33-41.

241. Gomes JA, Selim M, Coteleur A, et al. Brain iron metabolism and brain injury following subarachnoid hemorrhage: iCeFISH-pilot (CSF iron in SAH). *Neurocrit Care* 2014;21(2):285-93. doi: 10.1007/s12028-014-9977-8
242. Suzuki H, Muramatsu M, Tanaka K, et al. Cerebrospinal fluid ferritin in chronic hydrocephalus after aneurysmal subarachnoid hemorrhage. *J Neurol* 2006;253(9):1170-6. doi: 10.1007/s00415-006-0184-1
243. Vollmer DG, Hongo K, Ogawa H, et al. A study of the effectiveness of the iron-chelating agent deferoxamine as vasospasm prophylaxis in a rabbit model of subarachnoid hemorrhage. *Neurosurgery* 1991;28(1):27-32.
244. Harada T, Mayberg MR. Inhibition of delayed arterial narrowing by the iron-chelating agent deferoxamine. *J Neurosurg* 1992;77(5):763-7. doi: 10.3171/jns.1992.77.5.0763
245. Christensen DW, Kisling R, Thompson J, et al. Deferoxamine toxicity in hepatoma and primary rat cortical brain cultures. *Hum Exp Toxicol* 2001;20(7):365-72. doi: 10.1191/096032701680350532
246. Ferrali M, Signorini C, Ciccoli L, et al. Iron release and membrane damage in erythrocytes exposed to oxidizing agents, phenylhydrazine, divicine and isouramil. *Biochem J* 1992;285 (Pt 1):295-301.
247. Fox JL. Intracranial vasospasm: a study with iron compounds. *Surg Neurol* 1979;11(5):363-8.

6. List of Abbreviations

2PM	Two-photon microscopy
aCSF	Artificial cerebrospinal fluid
BBB	Blood-brain barrier
CBF	Cerebral blood flow
CMI	Cisterna magna injection
CPP	Cerebral perfusion pressure
CSF	Cerebrospinal fluid
CT	Computed tomography
DAB	3,3'-Diaminobenzidine
DCI	Delayed cerebral ischemia
DFO	Deferoxamine
EBI	Early brain injury
ET	Endothelin
Et al.	Et alia
ET _A Receptor	Endothelin A receptor
FITC	Fluorescein isothiocyanate
Hb	Hemoglobin
HO	Heme oxygenase
ICAM	Intercellular adhesion molecule
ICP	Intracranial pressure
kDa	Kilo Dalton
MAPK	Mitogen-activated protein kinase
MCA	Middle cerebral artery
MMP	Matrix metalloproteinase
MRI	Magnetic resonance imaging
NF-κB	Nuclear factor kappa light chain enhancer of activated B-cells

NO	nitric oxide
PBS	Phosphate buffered saline
PVS	Paravascular space
SAH	Subarachnoid hemorrhage
TLR	Toll-like receptor
TMRM	Tetramethylrhodamine

7. Acknowledgements

First and foremost I want to thank my supervisor Prof. Nikolaus Plesnila for giving me the opportunity to join his group and do research here in ISD. Thanks for him to continuously offer me advice and encouragement. His great enthusiasm for scientific research inspired me throughout the past three years and will continue motivating me for the rest of my life. I would particularly thank my advisor Kathrin Nehrkorn. Thanks for always supporting and helping me whenever I was in need. It is two of you offered the great guidance and trained me in the scientific field.

I would also like to thank for my colleagues, especially the whole AG Plesnila group for the friendly and inspiring working atmosphere. I'm thankful to all the exploratory and inspiring talk and great time we had together. Special thanks for Uta and Burcu, who generously supported me in solving all kinds of problems in my project. I want to thank Nicole for giving me the opportunity to collaborate on her project. Thanks to Matilde, Sabrina, Carina, Irina, Yue, Farida, Susana, Chenchen and Mihail for giving help and advice on my experiments.

I am very grateful for the Chinese scholarship council to offer me the financial support and make it possible for me to study here. I would like to express my very sincere gratitude to Prof. Alexander Baethmann, who recommended me to Prof. Plesnila and opened the door to neuroscience for me.

My sincere thanks to Prof. Leda Dimou, thanks for being in my Thesis Advisory Committee and always being so nice and helpful in providing significant scientific input and improving my work.

I am also thankful to all the friends I got to know in Munich, Thanks for all the laughter we had, all the happy time we spent together.

I am thankful to my parents. They are always there for me and selflessly give me emotional and financial support. Thanks for the patience and sympathetic ear from all my friends. Even we are far away from each other, all the comfort and encouragement you gave kept me moving forwards.

Finally, I want to say thanks to my dear husband Li Deng, who come to Germany for me and has been doing the utmost to support me in the past two years. I want to thank him for his love and care.

8. Publication

Original Articles

1. The Relationship between Helicobacter pylori Infection and Open-Angle Glaucoma: A Meta-Analysis. Zeng J, **Liu H**, Liu X, Ding C. Invest Ophthalmol Vis Sci. 2015 Aug; 56(9):5238-45.
2. Comparison of the Effectiveness of Pars Plana Vitrectomy with and without Internal Limiting Membrane Peeling for Idiopathic Retinal Membrane Removal: A Meta-Analysis. **Liu H**, Zuo S, Ding C, Dai X, Zhu X. J Ophthalmol. 2015; 2015:974568.
3. Establishment of an experimental glaucoma animal model: A comparison of microbead injection with or without hydroxypropyl methylcellulose. **Liu H**, Ding C. Exp Ther Med. 2017 Sep; 14(3):1953-1960.
4. Microvasospasms After Experimental Subarachnoid Hemorrhage Do Not Depend on Endothelin A Receptors. **Liu H**, Dienel A, Schöller K, Schwarzmaier SM, Nehr Korn K, Plesnila N, Terpolilli NA. Stroke. 2018 Mar; 49(3):693-699

9. Curriculum Vitae

Hanhan Liu, born at the 1st of May 1989 in Changsha, Hunan, P.R.China

Education

1995-2001	Primary School Changsha, Hunan, P.R.China
2001-2004	Changjun Junior high school Changsha, Hunan, P.R.China
2004-2007	Changjun High school Changsha, Hunan, P.R.China
2007-2012	Bachelor of Clinical Medicine, Xiangya School of Medicine, Central South University Changsha, Hunan, P.R.China
2012-2015	Master of Clinical Medicine (Ophthalmology), Xiangya School of Medicine, Central South University Changsha, Hunan, P.R.China
Since 2015	Experimental doctoral thesis at the Institute for Stroke and Dementia Research (Director : Prof. Dr. Nikolaus Plesnila)

Clinical experiences

06/2011-07/2012	Internship, Clinical rotations at the Second Xiangya Hospital
11/2012-02/2014	Resident, Clinical rotations at the Second Xiangya Hospital
03/2014-07/2015	Resident, Ophthalmology department, the Second Xiangya Hospital

Scholarships and Awards

2007-2012	Third Prize of scholarship for four consecutive years
2008-2010	Vice Chairman of Youth Volunteers Association in Xiangya School of Medicine, Central South University
2009	Third prize in the Innovative Experimental Design Contest in Xiangya School of Medicine, Central South University

- 2009-2010 Lecturer of Psychological Association in Xiangya School of Medicine,
Central South University
- 2012-2015 Full Scholarship for three consecutive years
- 2013 Passed Exam of Medical Practitioners Qualification of People's
Republic of China
- 2015-2018 CSC Scholarship for 3-years doctoral study Third

Munich, 7th of May 2018

Affidavit

I, Liu hanhan, hereby confirm that my thesis entitled

The role of blood components in microcirculatory dysfunction after subarachnoid hemorrhage

is the result of my own work. I did not receive any help or support from commercial consultants. All sources and/or materials applied are listed and specified in the thesis.

Furthermore, I confirm that this thesis has not yet been submitted as part of another examination process neither in identical nor in similar form.

Place and date: Munich, 20.12.2018

Name: Hanhan Liu